

Responses and mechanisms of positive electron affinity molecules in the N2 mode of the thermionic ionization detector and the electron capture detector
by Christopher Stephen Jones

A thesis submitted in partial fulfillment of the requirements for the degree of Doctor of Philosophy in Chemistry
Montana State University
© Copyright by Christopher Stephen Jones (1989)

Abstract:
Very little knowledge has been acquired in the past on the mechanistic pathway by which molecules respond in the N2 mode of the thermionic ionization detector. An attempt is made here to elucidate the response mechanism of the detector. The basic response mechanisms are known for the electron capture detector, and an attempt is made to identify the certain mechanism by which selected molecules respond. The resonance electron capture rate constant has been believed to be temperature independent, and investigations of the temperature dependence of electron capture responses are presented.

Mechanisms for the N2 mode of the thermionic ionization detector have been proposed by examining the detector response to positive electron affinity molecules and by measurement of the ions produced by the detector. Electron capture mechanisms for selected molecules have been proposed by examining their temperature dependent responses in the electron capture detector and negative ion mass spectra of the samples. In studies of the resonance electron capture rate constant, the relative responses of selected positive electron affinity molecules and their temperature dependent responses were investigated.

Positive electron affinity did not guarantee large responses in the N2 mode thermionic ionization detector. High mass ions were measured following ionization of samples in the detector. Responses in the electron capture detector varied with temperature and electron affinity.

Results support a mechanism for the N2 mode of the thermionic ionization detector where a high mass ion is formed during decomposition of the sample and reaction with inorganic species. Resonance electron capture rate constants are not temperature independent, and electron mechanisms were elucidated. Electron capture responses do not bear a strict dependence on electron affinity.

RESPONSES AND MECHANISMS OF POSITIVE ELECTRON AFFINITY MOLECULES IN THE N_2 MODE OF THE THERMIONIC IONIZATION DETECTOR AND THE ELECTRON CAPTURE DETECTOR

by

Christopher Stephen Jones

A thesis submitted in partial fulfillment
of the requirements for the degree

of

Doctor of Philosophy

in

Chemistry

MONTANA STATE UNIVERSITY
Bozeman, Montana

November 1989

D378
J7125

APPROVAL

of a thesis submitted by

Christopher Stephen Jones

This thesis has been read by each member of the thesis committee and has been found to be satisfactory regarding content, English usage, format, citations, bibliographic style, and consistency, and is ready for submission to the College of Graduate Studies.

Oct 23, 1989 — Date

Eric Grimsrud — Chairperson, Graduate Committee

Approved for the Major Department

Oct 23, 1989 — Date

Edwin H. Abbot — Head, Major Department

Approved for the College of Graduate Studies

Nov. 9, 1989 — Date

Henry L Parsons — Graduate Dean

STATEMENT OF PERMISSION TO USE

In presenting this thesis in partial fulfillment of the requirements for a doctoral degree at Montana State University, I agree that the Library shall make it available to borrowers under rules of the Library. I further agree that copying of this thesis is allowable only for scholarly purposes, consistent with "fair use" as prescribed in the U.S. Copyright Law. Requests for extensive copying or reproduction of this thesis should be referred to University Microfilms International, 300 North Zeeb Road, Ann Arbor, Michigan 48106, to whom I have granted the "exclusive right to reproduce and distribute copies of the dissertation in and from microfilm and the right to reproduce and distribute by abstract in any format."

Signature Christopher S. Jones

Date 10/17/89

VITA

Christopher Stephen Jones was born January 10, 1961 in Monmouth, Illinois, the first child of Ronald L. and Maxine E. Jones. He lived in Ankeny, Iowa from 1966 to 1979, where he graduated from Ankeny High School. From 1979 to 1983 he resided in Indianola, Iowa, where he graduated from Simpson College. Since 1983 he has been enrolled in doctoral studies at Montana State University in Bozeman, Montana.

ACKNOWLEDGMENT

I would like to thank Dr. Eric Grimsrud, whose devotion to science gave me the opportunity to pursue an advanced degree. Thank you to all the members of Dr. Grimsrud's research group for putting up with me for the last four years.

TABLE OF CONTENTS

	Page
LIST OF TABLES	ix
LIST OF FIGURES	x
ABSTRACT	xiv
INTRODUCTION	1
Gas Chromatographic Detection	1
Thermionic Ionization Detection	2
Electron Capture Detection: Design and Operation	8
Electron Capture Response Mechanisms	14
RESEARCH OBJECTIVES	30
EXPERIMENTAL	32
Chromatographic Equipment	32
GC Detectors	33
ECMS Equipment and Conditions	41
APIMS Equipment and Conditions	43
Chromatographic Conditions	47
Sample Preparation	48
Data Collection and Processing	49
Computer Modeling	51
RESULTS AND DISCUSSION	54
TID-N_2 Responses of Substituted Nitrobenzenes	54
TID-N_2 - APIMS Measurements	66
TID-N_2 Candidate Response Mechanisms	71
Direct Electron Transfer to Analyte Molecule	71
Thermal Decomposition of Analyte Followed by Electron Attachment	78
Reaction of Analyte with Gas Phase Radicals Followed by Electron Attachment to Product(s)	82
Thermal Decomposition Followed by Polymerization and Electron Attachment	86

TABLE OF CONTENTS - Continued

Page

Thermal Decomposition Followed by Combination with Inorganic Species and Electron Attachment at the Gas-Solid Interface 88
Thermal Decomposition Followed by Electron Attachment and Association with Gas Phase Species Removed from Gas-Solid Interface 90
ECD Responses of the Substituted Nitrobenzenes . 95
Computer Simulations of ECD Response 101
ECD Response Mechanisms and Temperature Dependence of Substituted Nitrobenzenes and Azulene 107
ECD Responses to Quinones and Electron Affinity Dependence of Responses 125
Comparison of Detection Techniques 134

CONCLUSION 137

LITERATURE CITED 141

LIST OF TABLES

Table		Page
1.	Definitions for the Computer Model of Resonance Electron Capture.....	53
2.	TID-N_2 responses and effects of experimental parameters on responses to various positive electron affinity molecules.....	56
3.	Electron capture detector responses at two detector temperatures.....	99
4.	ECD_9 responses (response per mole in KHz-min x 10^{-9}) of 20 ng 1,4-benzoquinone (BQ), 32 ng 2-methyl-1,4-benzoquinone (MBQ) and 1 ng 1,4-naphthoquinone (NQ).....	127
5.	Maximum responses of resonance electron capture molecules and their calculated electron attachment rate constants.....	128

LIST OF FIGURES

Figure		Page
1.	Potential energy curves of the formation of a molecular negative ion for electron capture mechanism I	17
2.	Ln $KT^{3/2}$ versus 1/T plot showing temperature dependence and kinetic regions for electron capture mechanism I	19
3.	Potential energy curves for electron capture mechanism II	22
4.	Ln $KT^{3/2}$ versus 1/T plot showing temperature dependence and kinetic regions for electron capture mechanism II	24
5.	Potential energy curves for electron capture mechanism III	26
6.	Ln $KT^{3/2}$ versus 1/T plot showing temperature dependence and kinetic regions for electron capture mechanism III	27
7.	Potential energy curves for electron capture mechanism IV	29
8.	Schematic of a TID	34
9.	Configuration surrounding the thermionic ionization source	35
10.	Concentric Coaxial ECD	39
11.	Block diagram of electrical components of CCP-ECD	40
12.	Pneumatics for GC-ECD system	42
13.	Diagram of APIMS	44
14.	Ion source for APIMS	45

LIST OF FIGURES - Continued

Figure		Page
15.	Resonance ECD computer modeling flow chart.....	52
16.	TID-N_2 peak height responses to varied amounts of substituted nitrobenzenes.....	55
17.	Absolute TID-N_2 responses of five compounds and detector baseline current as a function of the detector block temperature.....	59
18.	Absolute TID-N_2 responses of five substituted nitrobenzenes and baseline current as a function of emitter heating current.....	61
19.	Absolute TID-N_2 responses of five substituted nitrobenzenes and baseline current as a function of emitter bias potential.....	63
20.	Negative ion responses to 350 ng o-nitrotoluene (GC retention time 4.4 minutes).....	68
21.	Total APIMS negative ion responses (m/e > 400) to 350 ng o-nitrotoluene, 383 ng m-nitrotoluene, 310 ng nitrobenzene, 230 ng o-fluoronitrobenzene, and 270 ng m-fluoronitrobenzene....	70
22.	Comparison of TID-N_2 molar responses with electron affinity values for substituted nitrobenzenes.....	73
23.	Comparison of absolute TID-N_2 responses of substituted nitrobenzenes and dinitrotoluenes with their relative molar ECD responses.....	77
24.	High temperature, negative ion electron capture mass spectra of nitrobenzene and three isomers of nitrotoluene.....	81
25.	ECD peak area responses to varied amounts of substituted nitrobenzenes at 200° C and 30 mL/min nitrogen.....	96

LIST OF FIGURES - Continued

Figure		Page
26.	ECD peak area responses to varied amounts of substituted nitrobenzenes at 300° C and 30 mL/min nitrogen	97
27.	Computer simulated data for the resonance electron capture process	103
28.	Computer simulated data for the resonance electron capture process	104
29.	Experimentally determined ECD temperature dependent response curve and computer generated curve to 50 ng azulene	106
30.	ECD temperature dependence response curve of 3.13 ng nitrobenzene	109
31.	Ln $KT^{3/2}$ versus 1/T plot for ECD response of nitrobenzene obtained experimentally by Wentworth and Chen (37)	110
32.	Ln $KT^{3/2}$ versus 1/T plot for ECD response of nitrobenzene, data obtained by author	112
33.	ECD temperature dependence curves for 100 pg o-nitrotoluene, 1 ng m-nitrotoluene, and 1 ng p-nitrotoluene	113
34.	ECD temperature dependence curves for 4.53 ng o-fluoronitrobenzene, 2.67 ng m-fluoro-nitrobenzene, and 3.76 ng p-fluoronitrobenzene	115
35.	Electron capture mass spectra of 4.53 ng of o-fluoronitrobenzene at 200° and 300°	117
36.	Electron capture mass spectra of 2.67 ng of m-fluoronitrobenzene at 200° and 300°	119

LIST OF FIGURES - Continued

Figure		Page
37.	Electron capture mass spectra of 3.76 ng of p-fluoronitrobenzene at 200° and 300°	121
38.	ECD temperature dependence response curve of 128 pg of p-bromonitrobenzene	123
39.	Electron capture mass spectra of 128 pg p-bromonitrobenzene at 200° C and 300° C	124
40.	Plot of calculated resonance electron capture rate constants versus molecular electron affinity	130
41.	ECD temperature dependence response curves for 20 ng BQ, 32 ng MBQ, and 1 ng NQ	131
42.	Electron capture mass spectra of 10 ng each BQ, MBQ, and NQ at 200° C	133

ABSTRACT

Very little knowledge has been acquired in the past on the mechanistic pathway by which molecules respond in the N_2 mode of the thermionic ionization detector. An attempt is made here to elucidate the response mechanism of the detector. The basic response mechanisms are known for the electron capture detector, and an attempt is made to identify the certain mechanism by which selected molecules respond. The resonance electron capture rate constant has been believed to be temperature independent, and investigations of the temperature dependence of electron capture responses are presented.

Mechanisms for the N_2 mode of the thermionic ionization detector have been proposed by examining the detector response to positive electron affinity molecules and by measurement of the ions produced by the detector. Electron capture mechanisms for selected molecules have been proposed by examining their temperature dependent responses in the electron capture detector and negative ion mass spectra of the samples. In studies of the resonance electron capture rate constant, the relative responses of selected positive electron affinity molecules and their temperature dependent responses were investigated.

Positive electron affinity did not guarantee large responses in the N_2 mode thermionic ionization detector. High mass ions were measured following ionization of samples in the detector. Responses in the electron capture detector varied with temperature and electron affinity.

Results support a mechanism for the N_2 mode of the thermionic ionization detector where a high mass ion is formed during decomposition of the sample and reaction with inorganic species. Resonance electron capture rate constants are not temperature independent, and electron mechanisms were elucidated. Electron capture responses do not bear a strict dependence on electron affinity.

INTRODUCTION

Gas Chromatographic Detection

The technique of gas chromatography (GC) was first demonstrated experimentally in the early 1950s (1). Since that time, the growth in applications of the procedure has been so great that the technique is now the most important and widely used of all the column chromatographic methods. An active area of research since the discovery of this technique has been the study of detection devices which respond to chemical compounds that elute from the gas chromatographic column. The function of a GC detector is to produce a measurable electrical signal by interaction with these compounds. In addition to signaling the moment of elution of a given compound, the detector provides the means by which the quantity of the chemical can be electronically measured and recorded.

Detection devices that produce an electrical signal by directly converting incoming compounds to gas phase ions have seen widespread success as GC detectors. Two devices that employ the formation of negative ions to produce a usable analytical signal are the N_2 mode of

the thermionic ionization detector (TID-N_2) and the electron capture detector (ECD). These are both selective GC detectors, responding only to compounds with molecular structures conducive to the formation of negative ions. The ECD has been especially popular for the selective detection of halogenated compounds, while the TID-N_2 has generally been used for the selective detection of nitrated and halogenated compounds. It was thought at the onset of this study that investigation of these two negative ionization techniques would produce converging results. Results, however, diverged somewhat, and the two techniques are quite distinct from one another.

Thermionic Ionization Detection

All methods of ionizing GC effluents involve the production of gas phase ions within the working volume of the GC detector by the application of energy in one form or another. In a TID, this energy is provided by a hot, solid surface known as the thermionic source. This thermionic emitter is positioned inside the detector housing so that samples eluting may impact the source surface, and any ionization produced is measured by an adjacent collector anode.

In 1964 Karmen and Giuffrida (2, 3, 4) demonstrated that a conventional flame ionization detector (FID) could be selective to halogen- and phosphorous-containing organic molecules if the flame was doped with an alkali salt. The thermionic source used in this study consisted of a wire mesh that had been treated with sodium hydroxide or sodium sulfate and subsequently heated in a hydrogen-air flame. Since that time, TIDs which use heated, alkali-impregnated sources have been widely used for the selective GC detection of nitrogen- and phosphorous-containing compounds (5-10). In these applications the thermionic source is heated either electrically in a reactive flameless atmosphere of hydrogen and air or by a hydrogen-air flame.

Many different thermionic emitter source compositions and configurations have been studied. These include the use of alkali reservoirs at the bottom (11) or above the top (12) of the flame, application of a rubidium silicate salt tip (10), a potassium chloride pellet (5), a cesium-ceramic cylinder with a nickel sub-layer (13), a rubidium silicate bead (7, 14, 15) and a rubidium-ceramic bead (8). Currently, all commercial TIDs are supplied with a thermionic emitter of one of the four following types:

(a) a homogenous alkali-glass bead formed on a loop of bare platinum wire (14);

(b) a ceramic cylinder core coated with an alkali salt activator and embedded with a heating coil (16);

(c) multiply-layered cylindrical ceramic with a conducting sub-layer of nickel-ceramic that covers a loop of nichrome heating wire and a surface layer of alkali-embedded ceramic (13, 17);

(d) a homogenous alkali-ceramic bead on a nichrome heating wire (8,9,18).

The sensitivity and selectivity of these nitrogen-phosphorous selective detectors depend upon the composition of the atmosphere surrounding the source, the source temperature, the hydrogen flow rate and the polarization voltage imposed upon the detector electrodes (9, 19, 20). Modern models generally employ thermionic sources composed of either a cesium- or rubidium-impregnated ceramic material. The ceramic sources are more resistant to melting than are the silicate sources, and the use of the higher molecular weight alkali metals allows a lower effective work function of the source surface to be established (8). The work function in this

case is defined as the energy required to transfer an electron from the source surface to the gas phase (21).

The selective response mechanism of the flameless TID to nitrogen- and phosphorous-containing organic compounds has been explained (8) in terms of a lowering of the effective work function of the thermionic surface due to the presence of electronegative species at the gas-solid interface. The response is thought to occur due to electron transfer from the low work function surface to highly electronegative radical species, possibly CN, NO_2 and PO_2, which are believed to be produced in the reactive gaseous boundary layer adjacent to the hot surface. It has been pointed out that this mechanism may not be operative for all the nitrogen-phosphorous selective detectors. In detectors where a flame is employed, it is fairly well established that the mechanism is a gas phase ionization process (22-24). The heated alkali impregnated source generates gas phase neutral alkali atoms, and the response is due to an electron transfer from the alkali atoms to the sample. These detectors are sometimes called alkali flame ionization detectors to distinguish them from the thermionic process, which is defined as the emission of electrical charge from a heated solid surface (25).

More recently, Patterson and coworkers (13, 26) have shown that a flameless TID can also be used for the selective detection of certain electronegative molecules in an inert atmosphere of nitrogen. Using a highly cesium-enriched ceramic thermionic source and a relatively low surface temperature of about 400^{o} to 600^{o} C, Patterson and coworkers observed selective responses to certain classes of molecules, such as the dinitrotoluenes. Optimization of response and selectivity for this mode (TID-N_2) requires a thermionic surface of very low work function (27), and this is accomplished by using a high cesium concentration in the source surface (28). Sub-picogram detection limits for these nitro-organics has been reported (27) for this mode of the TID, along with a very high specificity factor of 10^8 versus alkane hydrocarbons. Subsequent use of this detector for the specific analysis of nitrated polycyclic aromatic hydrocarbons in environmental samples has also been reported (29).

In this version of the TID, the analyte molecule itself appears to carry with it all of the ingredients necessary for occurrence of a surface-to-gas phase electron transfer. Beyond this general deduction, however, no more precise, descriptive evidence of the

surface ionization mechanism has been offered. Possible mechanisms by which the TID-N_2 mode responses might occur have been envisioned (28, 30). The first and simplest one is by direct electron transfer from the surface to the molecule to form a molecular negative ion as shown by Reaction 1.

$$e(\text{surface}) + M \longrightarrow M^- \qquad (1)$$

This possibility is a reasonable one in view of the fact that the compounds to which the nitrogen mode is known to respond have positive electron affinities (32). Another plausible mechanism, shown as Reaction 2,

$$M \longrightarrow N + X \xrightarrow{e \quad (\text{surface})} X^- \qquad (2)$$

is that the analyte molecule M is thermally decomposed on the hot surface of the thermionic source to form species N and X, one of which has a high electron affinity and abstracts an electron from the surface to form the negative ion X^-. This possibility is attractive if one considers species X in Reaction 2 to be NO_2. The NO_2 radical has a very high electron affinity (31, 32) and

specificity of response has been previously demonstrated to nitroaromatic hydrocarbons (13, 26, 29). An additional possibility is worthy of consideration since it is thought to be operative in the nitrogen-phosphorous mode of the TID. That is, gas phase radicals at the gas-solid interface might chemically alter the analyte molecule so as to again form an intermediate species X, which abstracts a surface electron as shown in Reaction 3.

$$M + R^{\cdot} \longrightarrow N + X \xrightarrow{e\ (surface)} X^{-} \qquad (3)$$

While the presence of reactive radical species, $R^{\cdot}$, might seem unlikely in an atmosphere of pure nitrogen, it is nonetheless possible due to either the presence of impurities in the nitrogen or due to the generation of reactive radical species from the analyte itself.

Electron Capture Detection: Design and Operation

Gas phase electron capture reactions have played a very central role in environmental analysis and analytical chemistry for nearly three decades. These reactions have been used for trace analysis in GC since Lovelock described the first ECD in 1958 (33). Currently the ECD

and the FID constitute the most widely used detection devices for gas chromatography. Following the introduction of this GC detector, it was soon recognized that the device was very sensitive and selective to certain groups of compounds, namely those that contain structures strongly conducive to the formation of negative ions. Many of these compounds are of environmental importance, and the ECD quickly became a useful tool for environmental analyses (34), even though the detector was very temperamental and the basic processes occurring within the cell were poorly understood. Today the detector remains a very important tool for the selective detection of pesticides in the environment (66), halocarbon aerosols in the atmosphere (67, 68), toxic chemicals in the workplace and disposal sites (69), drugs in human beings (70) and biologically active compounds in physiological fluids (70).

Like the TID-N_2, the ECD functions by producing negative ions. The energy necessary for this ionization is derived from beta particles emitted by a radioactive source. The ECD is unusual among ionization detectors in that a high level of ionization is present within the cell even in the absence of analyte molecules (27). It is also unique in that it functions by redistributing electric

charges between different types of ionized species instead of changing the total amount of electric charges within the detector (27). The beta particles emanating from the radioactive source in the ECD cell collide with carrier gas molecules, resulting in the formation of secondary electrons, positive ions and radical species within the atmosphere of the detector cell. The secondary electrons are thermalized by further collisions with carrier gas molecules. By applying a potential difference across two electrodes in the cell, the thermal electrons can be collected and a current measured. When electron capturing analyte molecules elute into the detector cell, they react with the thermalized electrons present to produce negative ions and therefore reduce the population of these thermal electrons. This removal of electrons from the atmosphere of the electron capture cell is the basis of an electrical signal indicative of the analyte molecule.

Lovelock's first ECD (33) contained an ionization chamber with a tritium radioactive beta emitter and two electrodes that measured the current within the cell at a small constant potential, hence the term DC-ECD. The responses to different concentrations of sample were very non-linear and responses to different molecules were unpredictable. In 1963 Lovelock (35) used 10% methane in

argon as the carrier gas and the pulse sampling technique to eliminate much of the anomalous behavior observed in the original model of the ECD. The presence of methane in the detector cell aided in the deactivation of metastables by inelastic collisions, enhanced the thermalization of the secondary electrons and nullified deleterious electron mobility effects by increasing the drift velocity of the electrons. The application of a momentary, recurrent voltage pulse to collect the electrons affected behavior of the detector in several ways. In the DC mode of the ECD, Lovelock (35) observed that anomalous responses were due to space charge potentials that had arisen from the separation of the positive and negative charges in the detector cell. Anomalous responses in the DC-ECD also were attributed to contact potentials arising from contamination of cell surfaces, high applied voltages, and unpredictable electron energies. By applying voltage pulses, one can restrict the electron capture reactions to a field free atmosphere in the period between the pulses. This eliminates the effects of space charges and contact potentials that are the root of much of the anomalous behavior in the DC-ECD. Application of the voltage pulses, 0.5 to 1.0 μsec width and 100 to 1000 μsec period, eliminates the contribution to cell current from

the collection of negative ions because the width of the voltage pulse is of insufficient duration to draw these relatively immobile ions to the anode. The pulsed mode ECD also produces a much more stable baseline and this allows a wider range of chromatographic conditions to be employed. Still, after all the improvements that were realized with the introduction of this fixed frequency pulsed (FFP) detector, a linear response factor was available for only 10% of the dynamic range of the device.

From a better understanding of the chemical and physical phenomena taking place in the ECD, investigators were able to improve detector designs and signal processing. Kinetic studies and models of Wentworth, et. al. (36) and Wentworth and Chen (37) in the 1960s showing that events in FFP-ECD were a series of competitive kinetically controlled reactions led to a new method of signal processing that produced a linear region 90% of the dynamic range of the detector. Previous methods of obtaining an analytical signal used the difference in the cell current with and without analyte present as the response. The new method of using the decrease in cell current divided by the instantaneous cell current led to a much more cooperative device. Operation of this mode required very clean conditions so a high

standing current with long pulse periods could be achieved.

The replacement of tritium with ^{63}Ni as the source of beta radiation (38) considerably broadened the scope of the ECD. The ^{63}Ni allows operation at much higher temperatures than the tritium beta emitter and lengthened the list of compounds which could be analyzed with the ECD.

In 1971 a new method of signal processing for the ECD was introduced (39). In this new mode of detector, the cell current is held constant and equal to a reference current by varying the frequency of voltage pulses. When an electron capturing analyte molecule enters the cell, the population of electrons decreases and the frequency of pulsing increases. This change in frequency is used as the response to an electron capturing molecule, the change being proportional to the amount of the compound. This constant current pulsed ECD (CCP-ECD) was shown to exhibit linearity with sample concentration up to 99% of the dynamic range of the detector. This mode of signal processing is most commonly used in the commercial ECDs today.

In the commercial models of the ECDs being employed presently, one of two detector geometries is usually

applied. One design is the coaxial ECD, first developed by Simmonds, et. al. (38). The anode of this detector is positioned concentrically within the ECD cell. Positive voltage wave forms are applied to the anode to collect the thermalized electrons within the detector cell. This cell design was employed in the collection of the electron capture data in this study. The other detector geometry that is very successfully used is the displaced coaxial ECD reported by Patterson (40). In this detector configuration, the anode is upstream from the actual detector cell. A narrow pulse of 0.64 μsec width collects the electrons from the cell of 0.3 cc volume counter to the carrier gas flow. The advantages of this configuration are the tolerability to detector contamination and its large linear dynamic range (40). The detector provides a linear response to many compounds until electron density is reduced to 0.005 of its original magnitude.

Electron Capture Response Mechanisms

The first electron attachment response mechanisms were postulated in the kinetic studies of Wentworth and coworkers (36, 37, 41) for a FFP-ECD. The first of the

mechanisms proposed, designated as mechanism I, is depicted in Reaction 4.

$$AB + e \longrightarrow AB^- \qquad (4)$$

This process is commonly known today as resonance electron capture. The rate constants for the forward electron capture reaction and the reverse detachment process are denoted by k_1 and k_{-1} respectively. The molecular anion formed for this process, depending upon a number of physical and chemical properties, may be stable, or may detach to reform the original analyte molecule and electron as depicted in Reaction 4. If stable it will react further by recombination with positive ions as shown by Reaction 5

$$AB^- + P^+ \longrightarrow \text{Neutrals} \qquad (5)$$

where k_+ is the recombination rate constant, or it may dissociate according to Reaction 6

$$AB^- \longrightarrow A + B^- \qquad (6)$$

where k_2 is the dissociation rate constant. The potential energy curve for the formation of a stable molecular ion is shown in Figure 1. This figure portrays the case where the electron affinity of the analyte molecule AB is greater than zero. Molecules that undergo the process are usually large systems, often conjugated and containing electron attracting functionalities, allowing distribution of excess energy among many internal degrees of freedom. The rate constants for this process can be as high as 10^{-7} cc mol^{-1} sec^{-1} (62) but vary greatly from compound to compound. This accounts for the high sensitivity and selectivity of electron capture detection. If the electron affinity is less than zero, a Franck-Condon transition leads to an unstable molecular anion which may disappear by autodetachment, or, if above the dissociation limit, may dissociate to $A^{\cdot} + B^{-}$. Based on these competitive kinetic relationships, Wentworth and Becker (42) derived the relationship shown in Equation 7

$$\ln KT^{3/2} = \ln A + \ln \frac{k+}{k_e} + \frac{EA}{RT} \qquad (7)$$

between a molecule's electron affinity and its ECD response where A is composed of fundamental constants, k_+ and k_e are the recombination rate constants for a

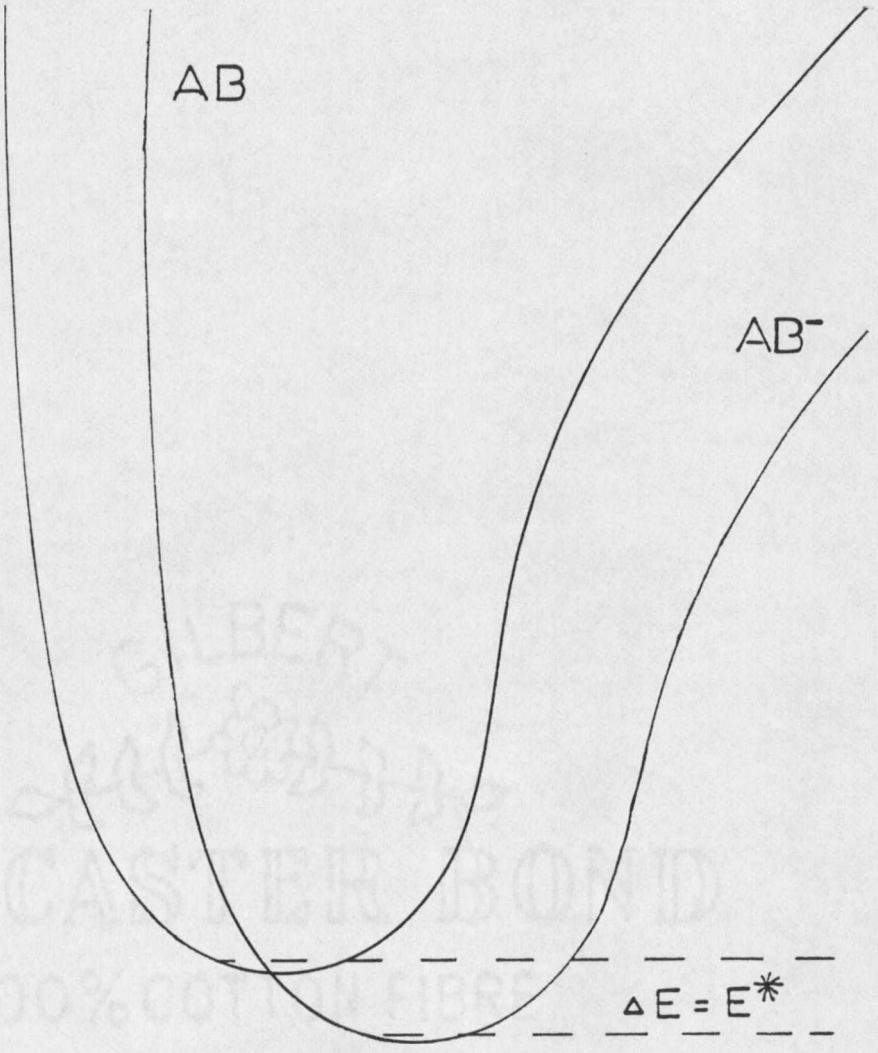


Figure 1. Potential energy curves of the formation of a molecular negative ion for electron capture mechanism I.

negative ion and an electron, respectively, K is the electron capture coefficient, and EA is the electron affinity of the analyte molecule. From this equation a plot of ln $KT^{3/2}$ versus 1/T indicates temperature dependence and kinetic regions of the electron capture process. A graph of this sort for mechanism I is shown in Figure 2. There are two regions in this graph, the alpha (α) region and the beta (β) region. The beta region corresponds to the kinetic relationship shown in Equation 8

$$k_+ > k_{-1} > k_2 \qquad (8)$$

for mechanism I. In this region the electron capture process was proposed to be nearly temperature independent for molecules which responded via mechanism I. This was indeed observed experimentally by Wentworth and Chen (37, 43) for about 40-50 compounds, principally aromatic molecules, over a temperature range of 80^{o} to 250^{o} C. The alpha region of Figure 2 corresponds to the kinetic relationship shown in Equation 9

$$k_{-1} > k_+ > k_2 \qquad (9)$$

for mechanism I. The detachment rate constant is fast and

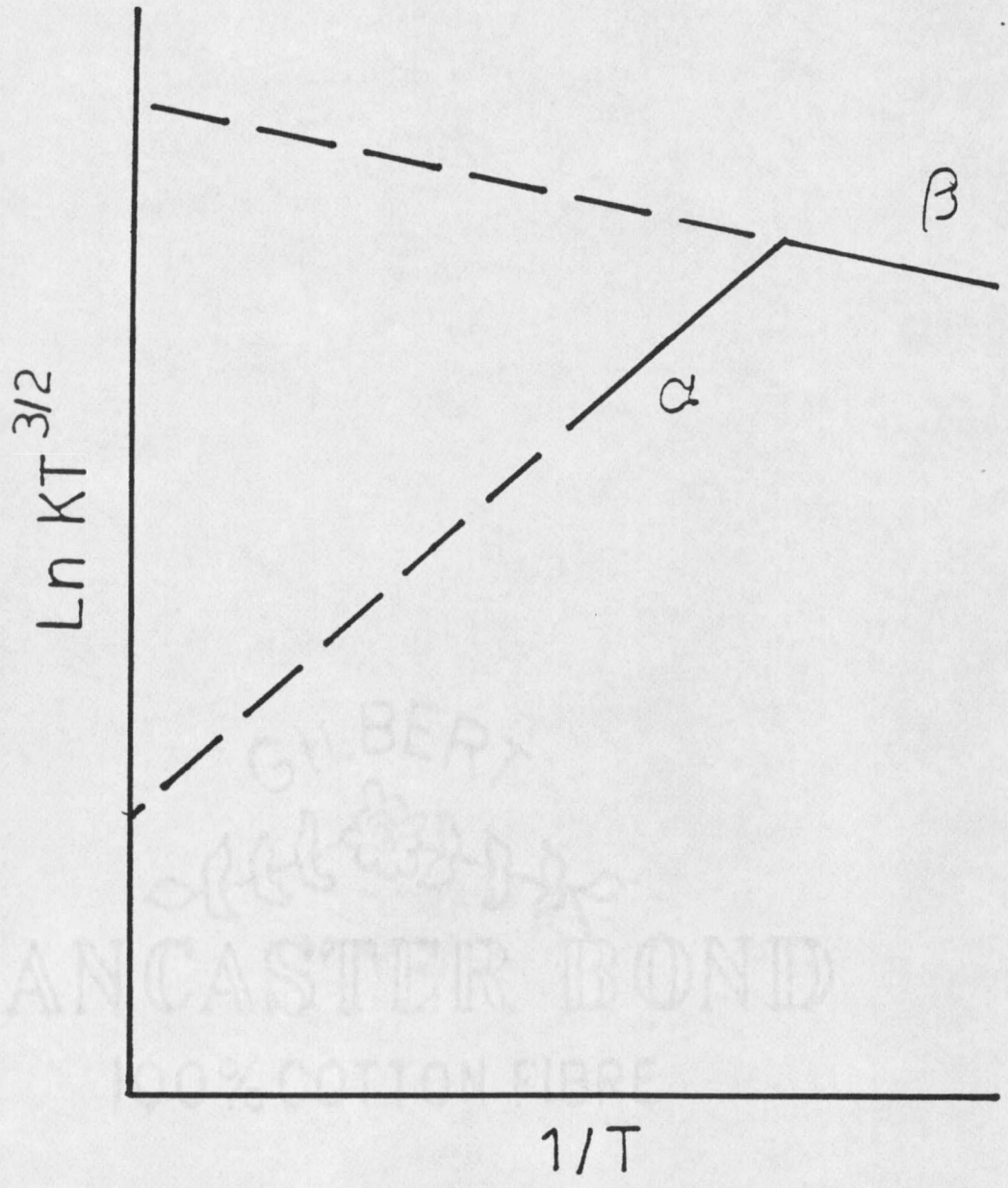


Figure 2. Ln $KT^{3/2}$ versus 1/T plot showing temperature dependence and kinetic regions for electron capture mechanism I.

is increasing with temperature, therefore causing the electron capture response to decrease. Again, this behavior was experimentally observed (44) for a number of compounds. These compounds generally have low electron affinities and the negative ions formed from them cannot hang on to the electron at the higher temperatures. Wentworth and Chen's (43) conclusions on the FFP-ECD response of molecules which respond via mechanism I were:

(a) If the electron affinity of the analyte molecule is greater than 18.5 kcal/mol, the data will be in the beta region and the response magnitude will be regulated by the thermal electron attachment rate constant, which is thought to be temperature independent.

(b) If the electron affinity of the analyte molecule is between 9 and 18.5 kcal/mol, the data will indicate an alpha and beta region. At high detector temperatures the response will decrease with increasing temperature, the slope of the decrease being dependent upon the electron affinity.

(c) If the electron affinity of the analyte molecule is below 9 kcal/mol, the data will exhibit only

an alpha region with a decreasing response as temperature increases.

It should be noted that one molecule that did not behave according to these conclusions was nitrogen dioxide (NO_2). This molecule has a high electron affinity (31, 32) and a low electron attachment rate constant (71). The electron affinity is above 18.5 kcal/mol; nevertheless, the data has an alpha region.

The second mechanism proposed by Wentworth and coworkers (36, 37, 41), designated mechanism II, is depicted in Equation 10,

$$AB + e \longrightarrow A + B^- \qquad (10)$$

where k_3 is the rate constant for the process. This is a single bimolecular electron attachment step leading immediately to dissociation via the dissociative potential energy curve depicted in Figure 3. The negative ion B^- can undergo recombination with positive ions as shown by Reaction 11,

$$B^- + P^+ \longrightarrow \text{Neutrals} \qquad (11)$$

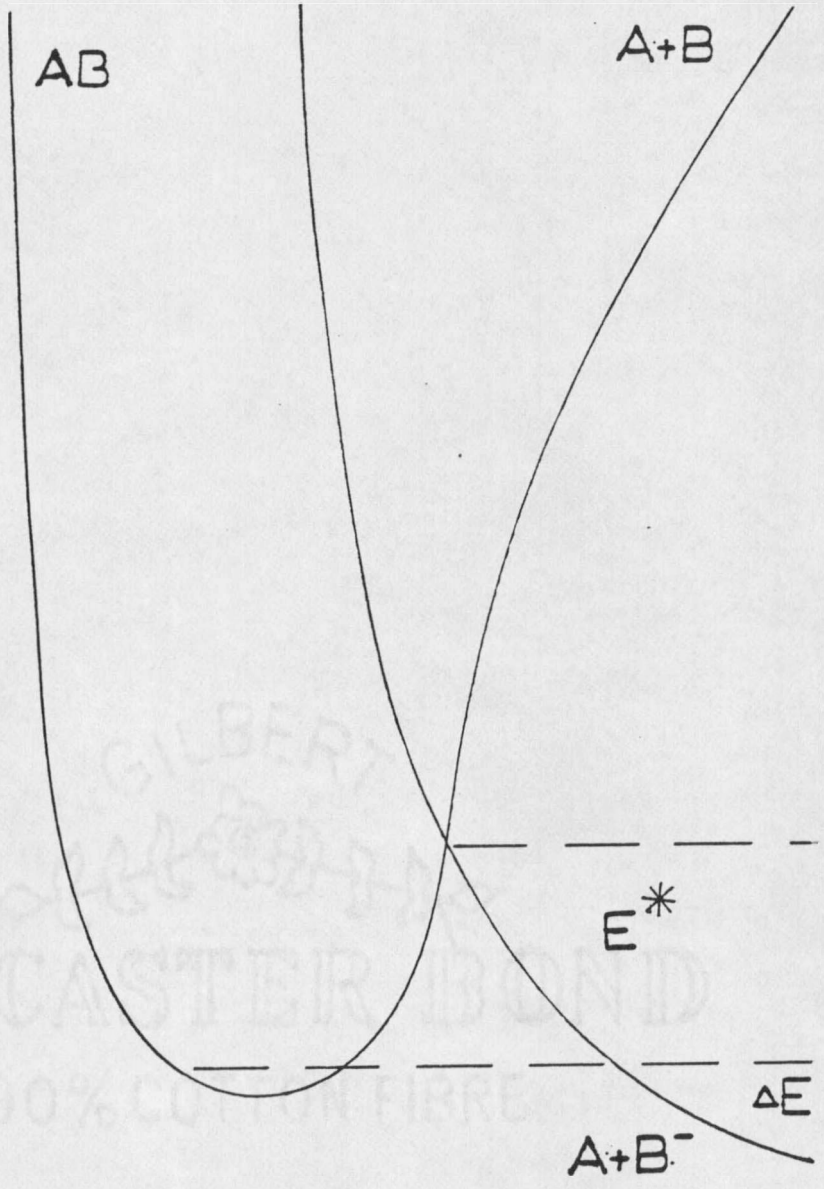


Figure 3. Potential energy curves for electron capture mechanism II.

where k_+ is the recombination rate constant for the process. This electron attachment response mechanism is commonly known as dissociative electron capture. This mechanism is favored at higher temperatures, as the ln $KT^{3/2}$ versus 1/T plot in Figure 4 depicts. The beta region of Figure 4 corresponds to the kinetic relationship shown in Equation 12.

$$k_+ > k_{-1} > k_2 \qquad (12)$$

The horizontal region of Figure 4 corresponds to energies of insufficient magnitude for dissociative electron attachment to occur. Compounds that undergo dissociative electron attachment commonly are aliphatic and aromatic molecules which contain electronegative functionalities, especially halogens, the result being a halogen negative ion and a radical. It should be noted that many molecules can respond via mechanism I and mechanism II, depending upon the temperature (37).

The third mechanism proposed by Wentworth and coworkers, designated mechanism III, is shown in Reaction 13.

$$AB + e^- \longrightarrow AB^- \longrightarrow A + B^- \qquad (13)$$

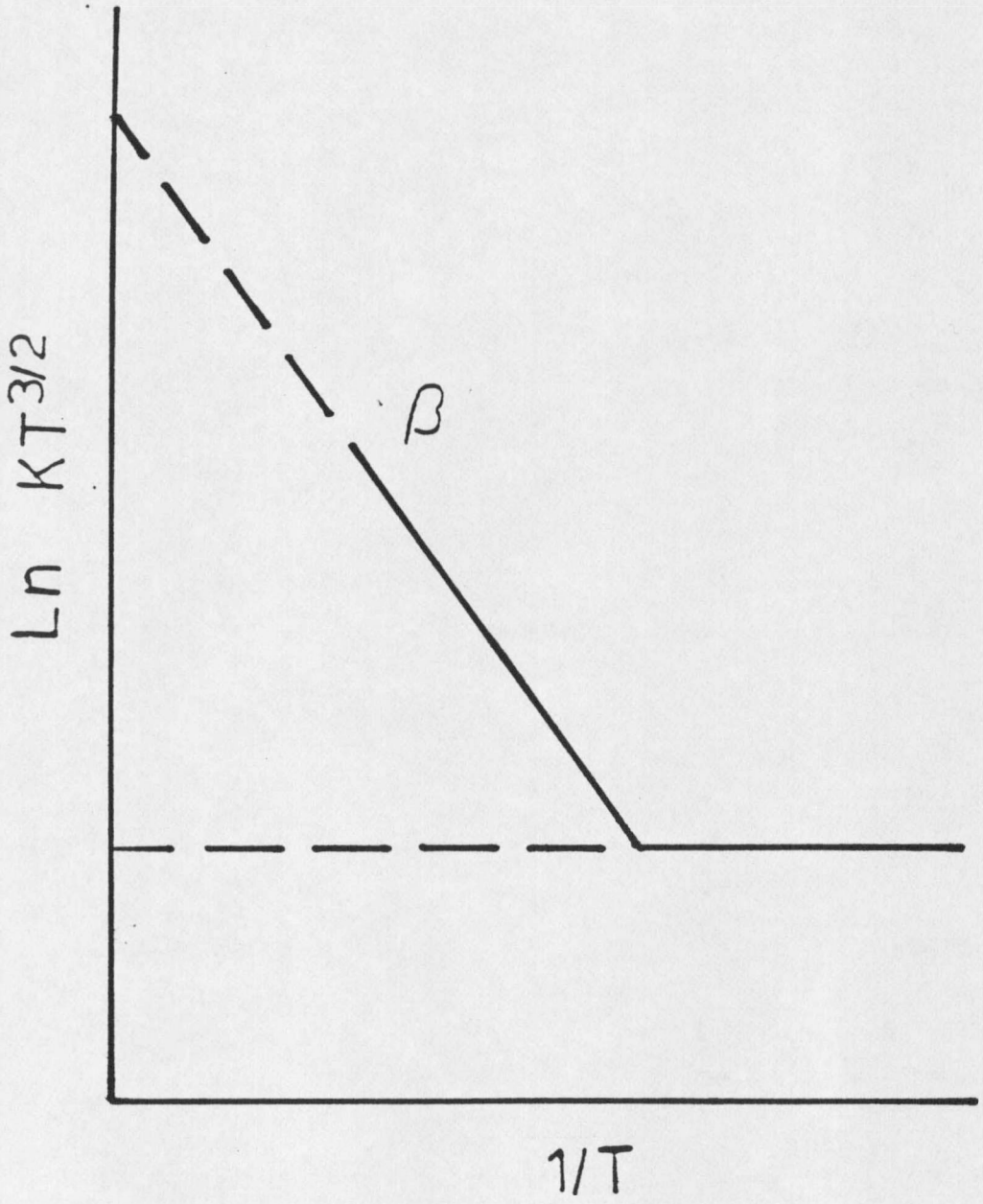


Figure 4. Ln $KT^{3/2}$ versus 1/T plot showing temperature dependence and kinetic regions for electron capture mechanism II.

This is a two step dissociative process whereby the formation of a molecular negative ion is followed by a dissociative step which proceeds via the dissociative potential energy curve shown in Figure 5. The ln $KT^{3/2}$ versus 1/T plot shown in Figure 6 indicates three temperature dependence and kinetic regions. The gamma (γ) region corresponds to the kinetic relationship in Equation 14,

$$k_{-1} > k_2 > k_+ \tag{14}$$

the alpha region to Equation 15,

$$k_{-1} > k_+ > k_2 \tag{15}$$

and the beta region to Equation 16.

$$k_+ > k_{-1} > k_2 \tag{16}$$

The fourth and final mechanism proposed by Wentworth and coworkers is very similar to mechanism III. The difference is that mechanism IV involves the formation of a molecular negative ion followed by dissociation via the

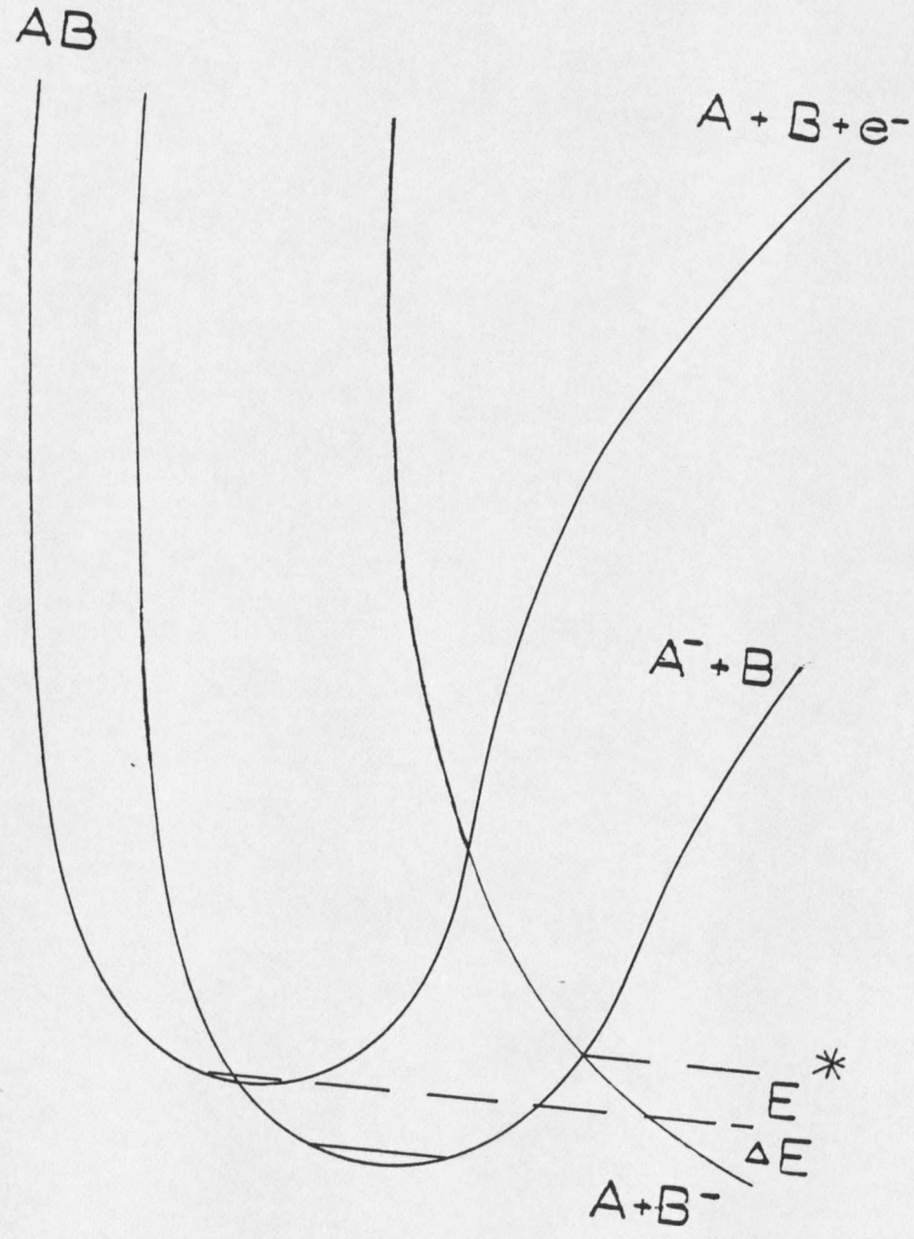


Figure 5. Potential energy curves for electron capture mechanism III.

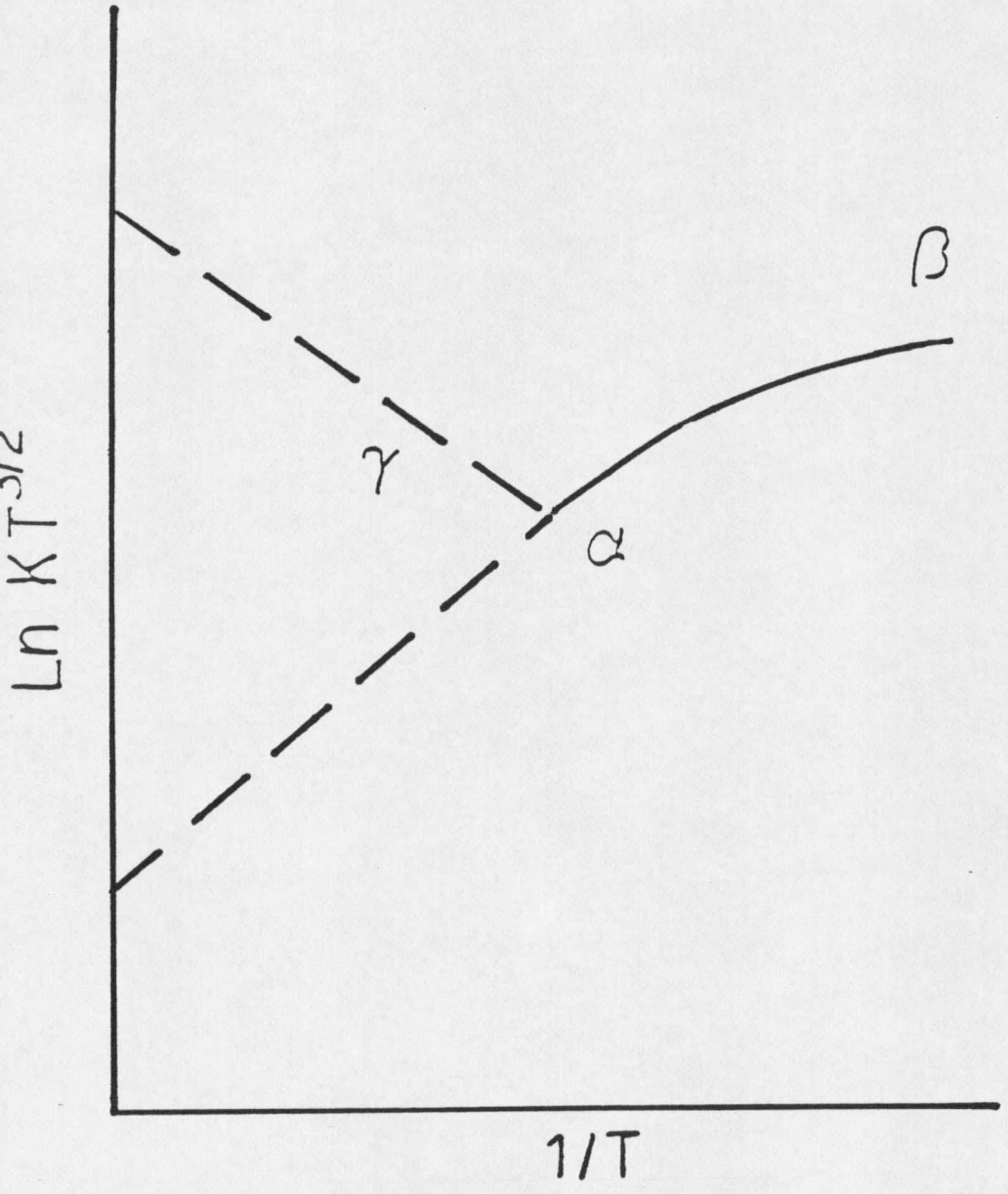


Figure 6. Ln $KT^{3/2}$ versus 1/T plot showing temperature dependence and kinetic regions for electron capture mechanism III.

same potential energy curve. This is depicted in Figure 7. The temperature dependent kinetic regions are identical to those of mechanism III.

It should again be noted that the device that was employed when these mechanisms were proposed was a FFP-ECD suitable for fundamental physical measurements. Wentworth and Chen (37) did point out, however, that this detector was sufficiently similar to those used for analytical work that their measurements could be applied to problems of analytical importance.

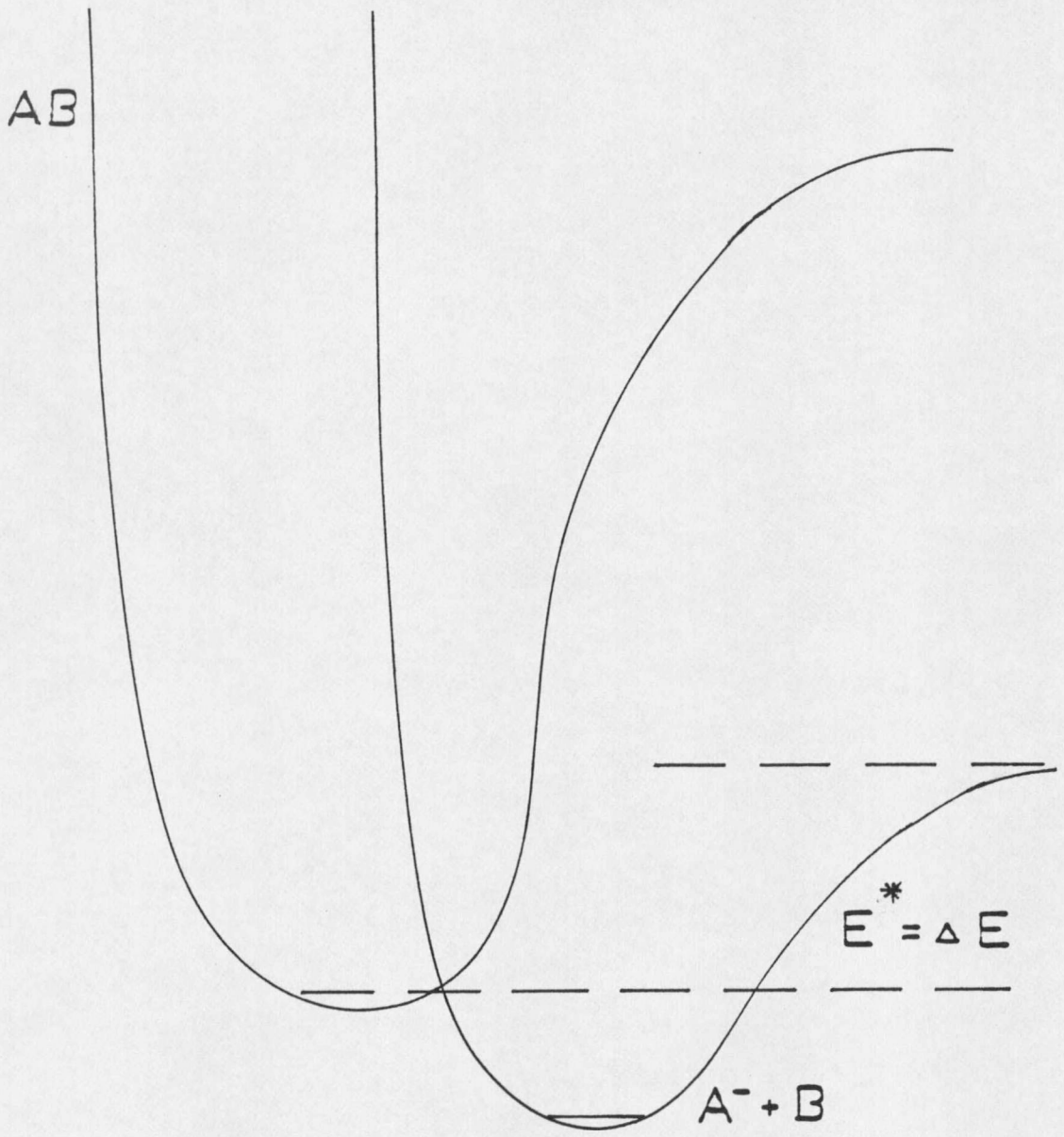


Figure 7. Potential energy curves for electron capture mechanism IV.

RESEARCH OBJECTIVES

The primary goal of this study was to elucidate the response mechanisms of selected positive electron affinity molecules, most of which are substituted nitrobenzenes, in TID-N_2 and the ECD. Both of these analytically important GC detectors are selective to molecules whose structures are conducive to the formation of negative ions.

Very little is known about the basic processes and, hence, response mechanisms that are occurring during the formation of negatively charged species at the surface of the heated, alkali embedded source of a TID-N_2. An attempt was made here, using the TID-N_2 responses of the aforementioned compounds and mass spectrometric measurements obtained with a TID-N_2 emitter employed as the ion source, to shed light on the basic processes occurring in this GC detector and to identify the negatively charged species that are being formed at the gas-solid interface. Investigations of the parameters affecting detector response, including source bias voltage, source heating current, detector temperature and detector atmosphere composition were performed not only to facilitate elucidation of response mechanisms, but also to optimize the usefulness of analyte signals.

While electron capture response mechanisms have been thoroughly investigated in the past, many of the details concerning the basic processes occurring within the ECD remain a mystery. An attempt was made here to shed light on two factors which affect ECD response: the electron affinity of the analyte molecule and the temperature dependence of the electron capture rate constants. Again, the compounds used to study these factors are positive electron affinity molecules, many of them substituted nitrobenzenes. Studies addressing the possibility that molecules may respond via more than one electron capture mechanism, depending upon the temperature, are also described.

The final objective is to compare the analytical usefulness of the two detection methods.

EXPERIMENTAL

Chromatographic Equipment

The TID data reported in this study were obtained with a Varian Aerograph 3700 GC on which the detector was mounted.

The ECD data were obtained using a Hewlett Packard 5890 GC.

A Hewlett Packard fused silica wide-bore capillary column (10 m x 0.53 mm inside diameter) with 50% phenylmethyl silicon stationary phase was used in both gas chromatographs. The end of this column was threaded through a transfer line in each instrument and into the base of the respective detector so that exposure of the sample to metallic surfaces was minimized.

For the electron capture mass spectrometry (ECMS) experiments, the samples were introduced into the mass spectrometer (MS) via a Varian 3700 GC. The chromatographic column used in this instrument was a J & W Scientific fused silica capillary column (30 m x 0.25 mm inside diameter) with 5% phenyl and 95% methyl as the stationary phase.

Samples were introduced into the atmospheric pressure ionization mass spectrometer (APIMS) via a Gow-Mac Model

750 GC. The column used in this instrument was the same wide-bore capillary column previously described.

GC Detectors

The TID-N_2 was purchased from Detector Engineering and Technology, Walnut Creek, California. It has been described previously by Patterson (13, 26). Figure 8 is a schematic of this detector. Its heart is the cylindrical thermionic source, positioned on the axis of a cylindrical collector electrode. Figure 9 is a detailed sketch of the detector configuration surrounding the source. The source consisted of multiply-layered cylindrical ceramic with a sub-layer of electrically-conducting nickel-ceramic and a surface layer of cesium-impregnated ceramic. The source, which can withstand very high temperatures, was electrically heated by a power supply obtained from the detector manufacturer. The nickel-ceramic sublayer provided protection to the heating wire from corrosive attack by materials present in the surface coating layer and allowed electrical charge lost at the surface during the ionization process to be replaced by a charge migration through the body of the source. The detector tower in which the source was enclosed was heated to

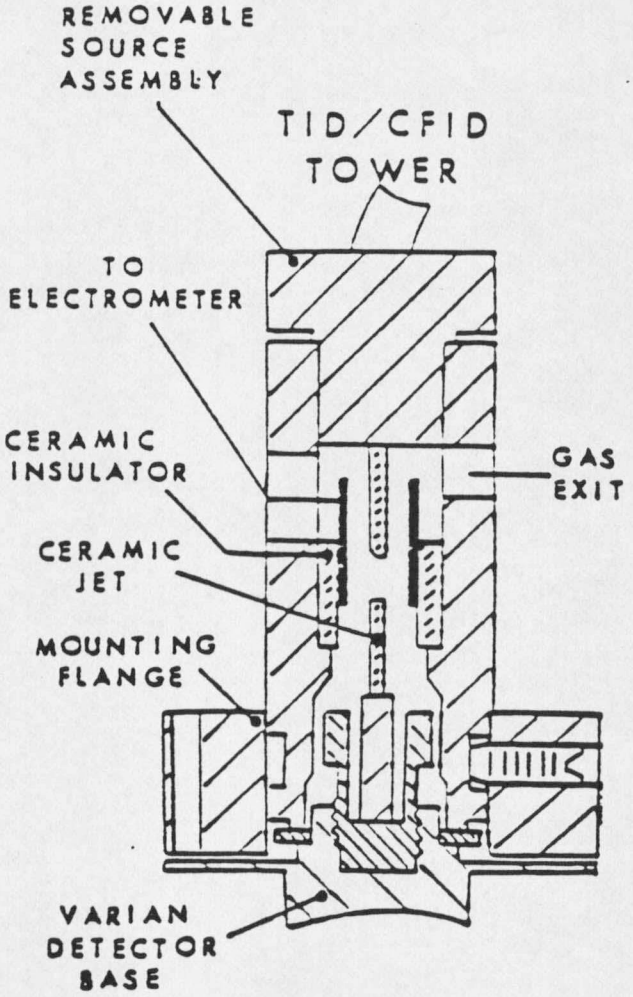


Figure 8. Schematic of a TID.

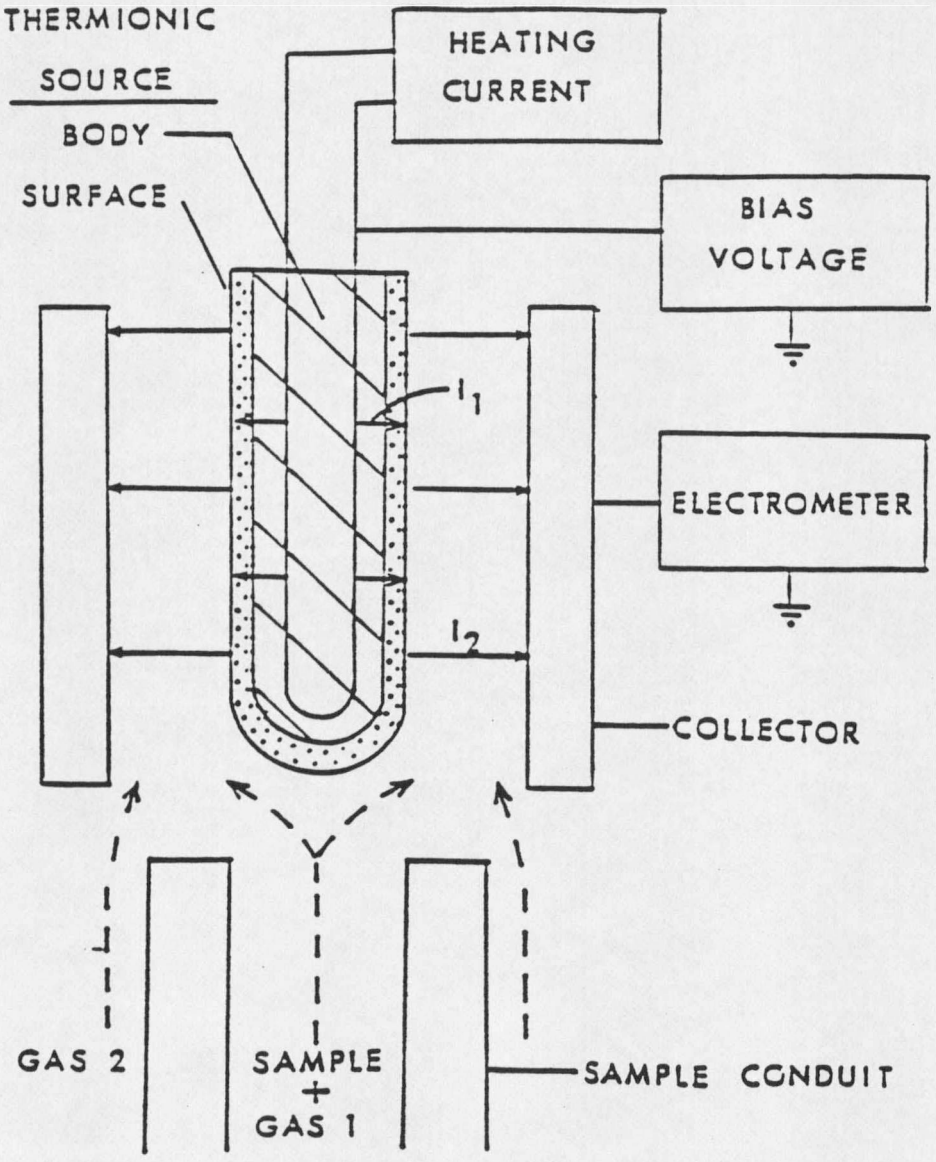


Figure 9. Configuration surrounding the thermionic ionization source.

temperatures of 270° to 370° C by the gas chromatograph. The source was biased at a negative voltage with respect to the surrounding collector electrode which was held as virtual ground potential. Negative ionization current was measured by an electrometer that was attached to the collector electrode. The detector was mounted on a FID base so that more than one type of gas could be supplied to the detector. The chromatographic effluent (10 mL/min) was mixed at the detector base with additional gas so that the total gas flow rate through the detector was 100 mL/min. This high gas flow rate through the detector provided a well-purged detector volume. The additional detector gas was usually nitrogen, purchased from Liquid Air Co., San Francisco, California, except in selected cases where one of the following gases was used: argon, carbon dioxide, nitrous oxide, methane, isobutane and 0.31% oxygen in nitrogen. The argon, carbon dioxide, and nitrous oxide were purchased from Chemetron Co., Chicago, Illinois. The methane and isobutane were obtained from Linde Co., Danbury, Connecticut. The specially prepared tank of 0.31% oxygen in nitrogen was purchased from Airco, Montvale, New Jersey. All gases except for the 0.31% oxygen in nitrogen were first passed through

oxygen-removing traps and a molecular sieve to remove water and particles entering the gas chromatograph. The 0.31% oxygen in nitrogen was passed through a molecular sieve only.

There are several characteristics of this mode of thermionic ionization detection operated in an inert atmosphere which make it distinct from the previously described nitrogen-phosphorous selective detector (5, 10). The first is the atmosphere surrounding the source. In the nitrogen-phosphorous selective detector, a hot, chemically reactive gas boundary layer surrounds the source. In this chemically reactive layer, reactive radical species such as $H^{\cdot}$, $O^{\cdot}$, and $HO^{\cdot}$ can be envisioned as arising from the hydrogen and air flows supplied to the detector. In the TID-N_2 mode of detection, a hot, inert atmosphere of nitrogen surrounds the source. In the TID-N_2 mode, the source is operated at temperatures of 400° to 600° C, while temperatures of 600° to 800° C are used with the nitrogen-phosphorous mode. The TID-N_2 source has a higher concentration of alkali (cesium) than does the nitrogen-phosphorous mode, resulting in a lower work function surface.

Figure 10 is a schematic of the Hewlett Packard ECD used in the experiments. Its concentric coaxial geometry has previously been discussed by Simmonds, et. al. (38) and by Grimsrud and Warden (45). The inside of the detector cell is lined with 10 mCi ^{63}Ni. The high energy electrons, or beta particles, which are emitted collide with the carrier gas molecules and produce about 500 secondary electrons per initial beta particle. The energy of these secondary electrons is reduced to the thermal range by further collisions. The resulting thermal electrons can be captured by analyte molecules. As a result the electron population in the detector is reduced. Positive voltage pulses applied to the anode collect the uncaptured electrons. The current measured is compared to a reference current and the interval of the pulses is adjusted to maintain a constant cell current, hence the name constant current pulsed ECD (CCP-ECD). Therefore, when an electron capturing analyte enters the detector cell, the pulse rate rises. This pulse rate is then converted to a voltage which is related to the amount of electron capturing analyte. Figure 11 is a block diagram of the electrical components for this detector.

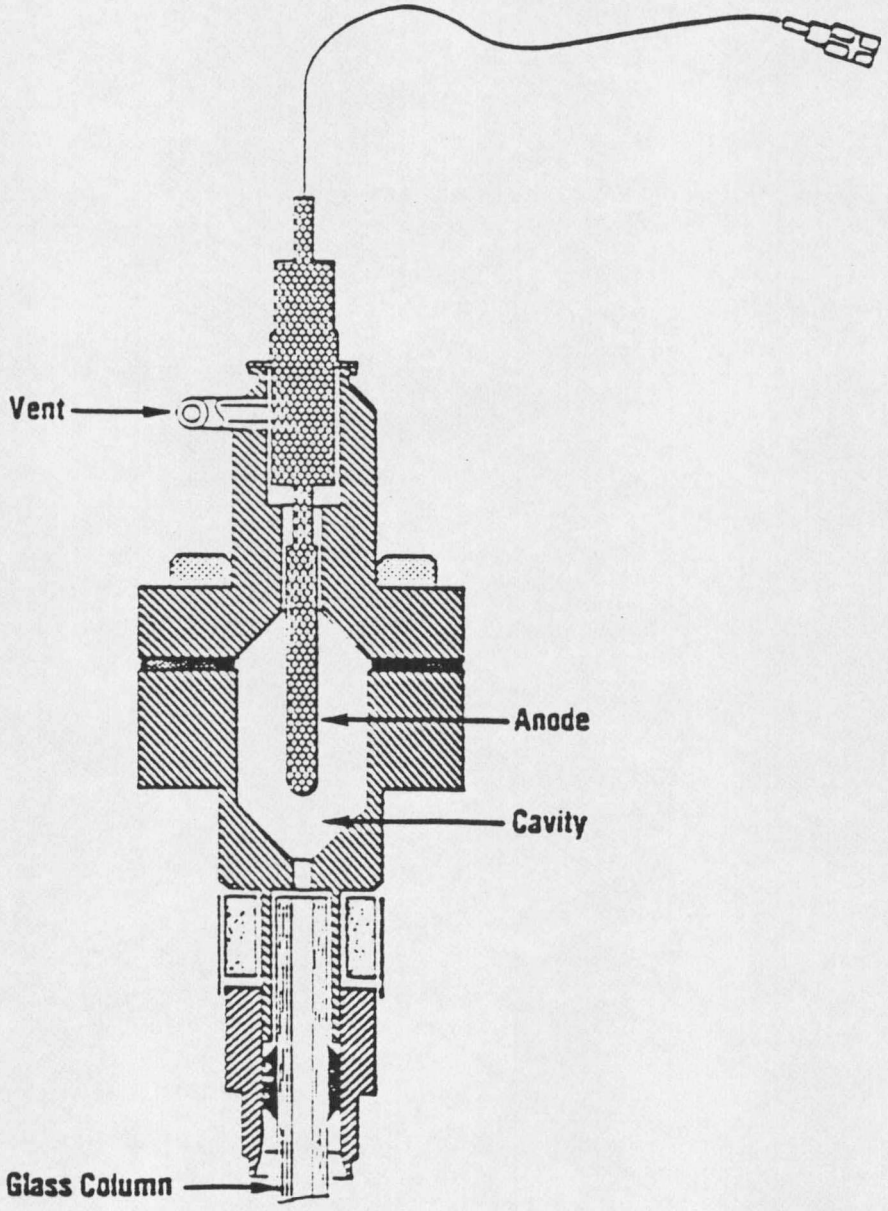


Figure 10. Concentric Coaxial ECD.

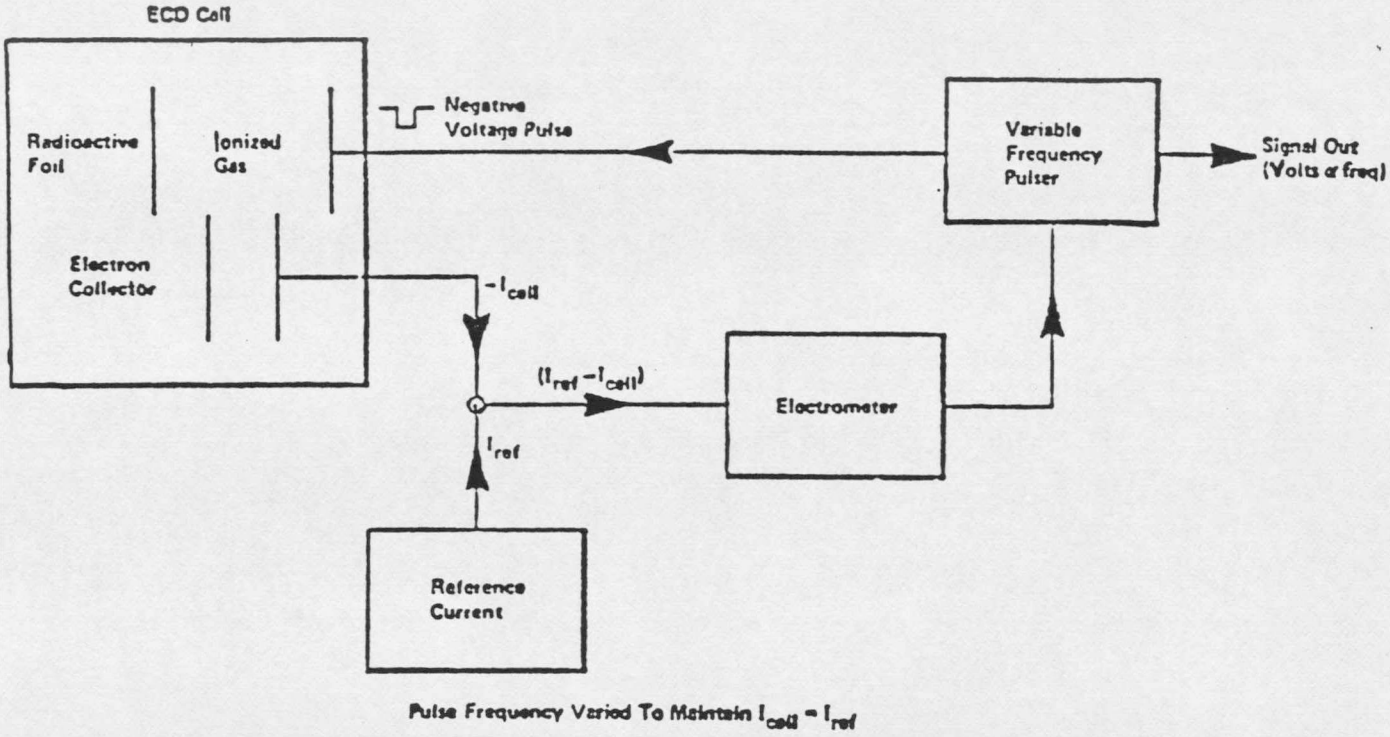


Figure 11. Block diagram of electrical components of CCP-ECD.

The detector was heated by the gas chromatograph to temperatures of 80° to 350° C. To prevent peak tailing and to optimize detector performance, 20 mL/min nitrogen was mixed with the column effluent (10 mL/min) at the detector base. These gases were first passed through oxygen-removing traps and through a molecular sieve before entering the gas chromatograph. A diagram of the pneumatics of the system is shown in Figure 12.

ECMS Equipment And Conditions

All electron capture mass spectra reported here were obtained with a VG Instruments model 7070E-HF MS. This is a double sector, medium resolution instrument. The ion source was operated at temperatures between 200° and 300° C, the temperature being determined by a thermocouple attached to the ion source block. The capillary chromatographic column was threaded through the GC-MS interface to the entrance port of the ion source. Methane, which was used as the reagent gas, was introduced into the ion source through a different port. The pressure of the methane in the ion source, measured by a MKS model 270B capacitive manometer, was 0.3 torr. The ion repeller voltage was held at -1 V. The emission

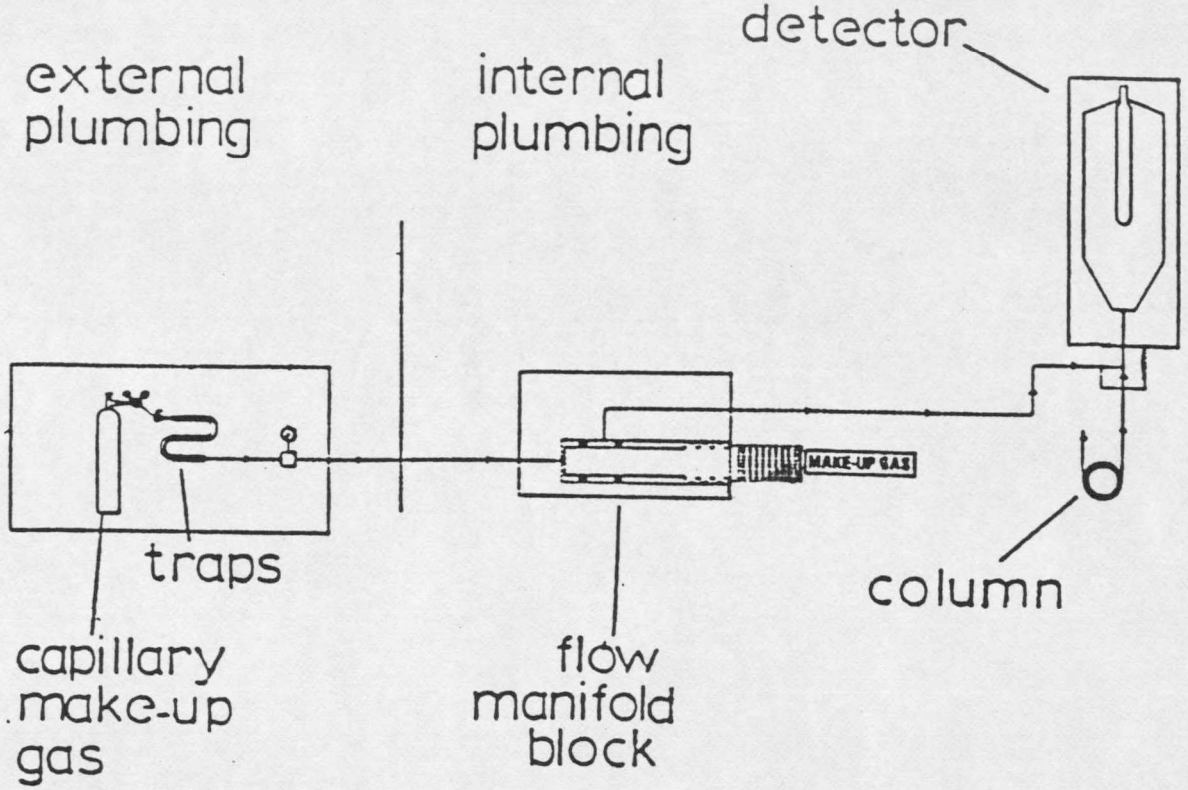


Figure 12. Pneumatics for GC-ECD system.

current typically was 2 mA. Electron energy was maintained at 150 eV. The mass spectrum was scanned exponentially down at a rate of 5 sec/decade. Mass resolution was typically 1000.

APIMS Equipment and Conditions

A homebuilt APIMS was used to measure the ions being formed by the TID-N_2. The instrument has been described in detail previously (46, 47) and is diagrammed in Figure 13. A specialized ion source, constructed specifically for this study, is shown in Figure 14. Its housing was designed so that a commercially available TID-N_2 source offered by Detector Engineering and Technology could be bolted onto the flange of the existing APIMS. The nitrogen carrier gas emerging from the GC was mixed with additional nitrogen makeup gas and was passed through the ion source with a total flow rate of 30 mL/min. The chromatographic column was threaded through transfer lines to the entrance port of the ion source to minimize exposure of the analyte to metallic surfaces. The housing of the ion source was maintained at 250^{o} C. The source was heated in the usual way with the associated power supply. A heater current of 2.5 A and a bias voltage of -5 V were applied to the source. The grounded walls of

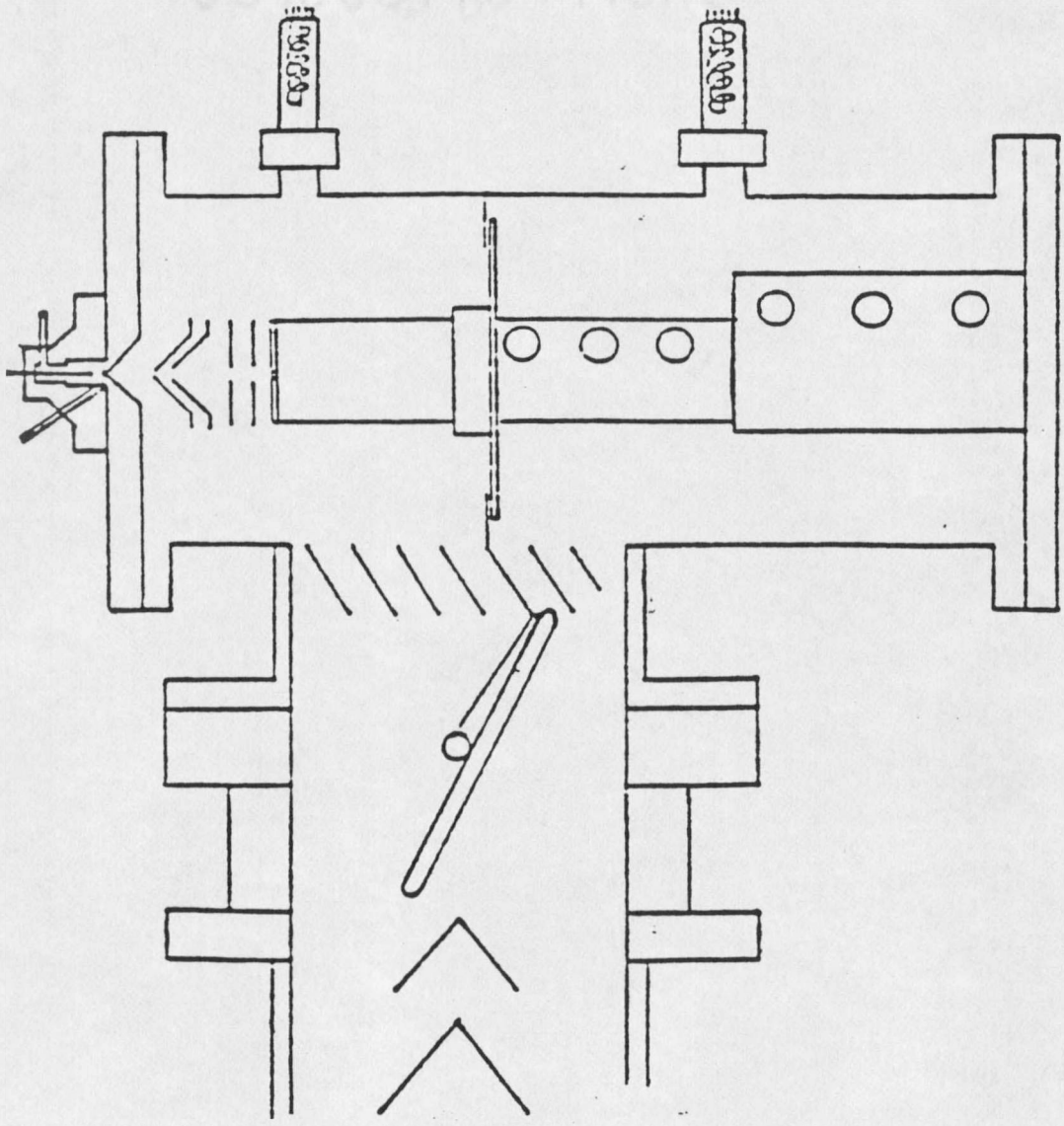


Figure 13. Diagram of APIMS.

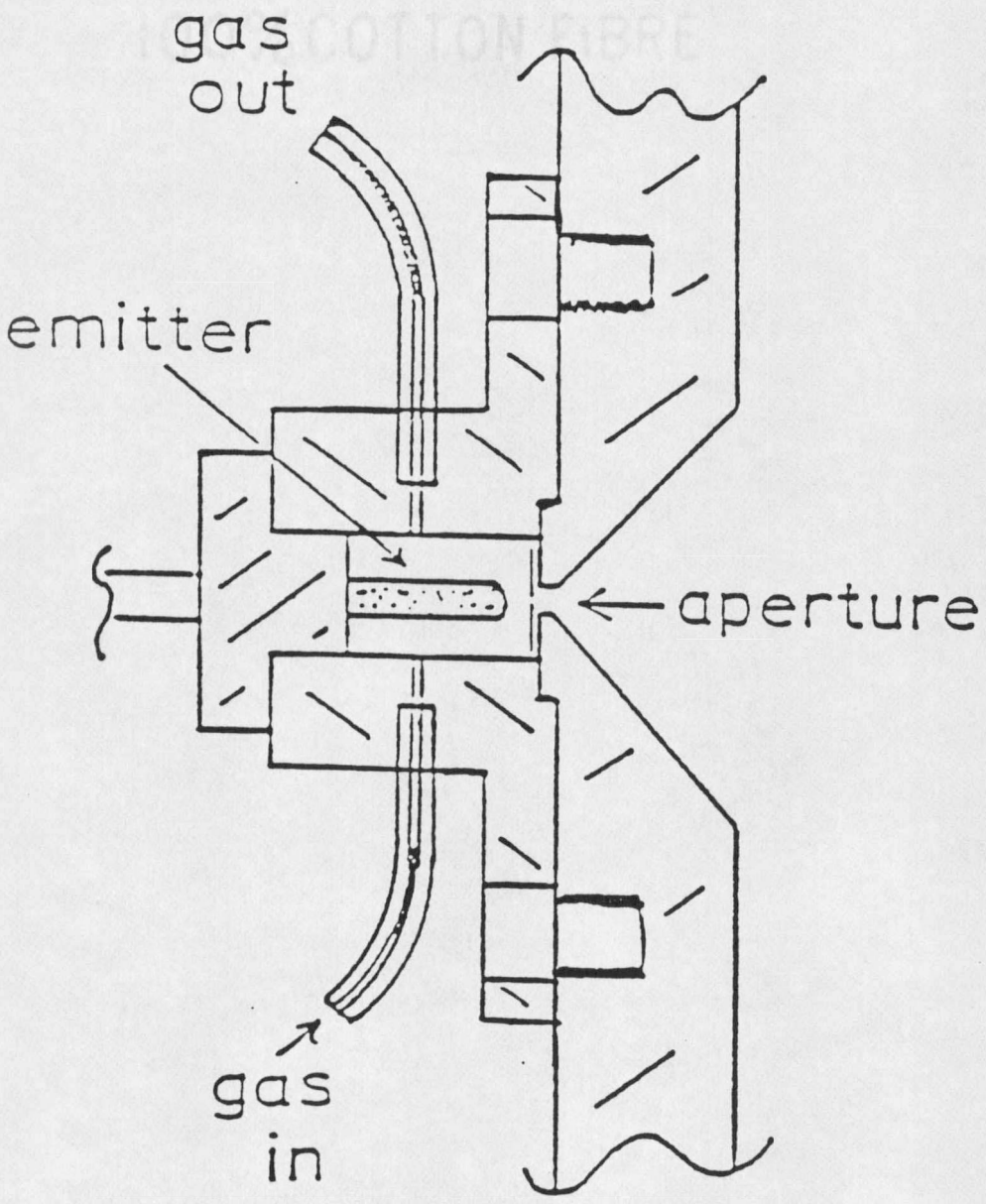


Figure 14. Ion source for APIMS.

the ion source serve as the anode to which a negatively charged species will migrate. Rather than measuring the current associated with these negative charge carriers, as is done with the TID-N_2, this instrument detects the negative ions which are directed toward and pass through a 20 m aperture which connects the atmospheric pressure ion source with the vacuum envelope of a quadrupole mass spectrometer. The quadrupole rods are biased to +24 V so as to attract negative ions from the ion source which is at ground potential. The upper mass range of the quadrupole filter was 500 amu when operated either in the single ion or scan mode. In the total ion mode (DC component to quadrupole rods is then set to zero) all ions of mass greater than any selected threshold value from 20 to 500 amu are allowed to pass to the detector. Detection of negative ions was accomplished by the ion counting method (48) using a channeltron 4309 electron multiplier (Galileo Corp., Sturbridge, Massachusetts) which is capacitively coupled to a counting preamplifier and rate meter.

Chromatographic Conditions

For the TID-N_2, ECD and APIMS experiments 1 μL splitless injections were used to introduce the sample onto the column. The column carrier gas was always nitrogen. The injection port was maintained at 200° C and the column operated isothermally at various temperatures. The chromatographic retention times of all compounds were first established using an FID. This detector gives a response proportional to the number of carbon and hydrogen atoms in the molecule (49). Column temperatures required for the convenient elution of the compounds studied ranged from 75° to 180° C. Only one compound was analyzed at a time, therefore no multicomponent chromatographic runs were performed. Sufficient resolution between the solvent and analyte peaks was always insured. Injection reproducibility measured as peak area was routinely better than $\pm$ 10%.

For the ECMS experiments, 1 μL split injections were used to introduce the sample onto the capillary column. The column carrier gas used was always helium. The injection port was maintained at 250° C. The column was temperature programmed from an initial temperature of

50° C to a final temperature of 220° C. The oven was held at the initial temperature for four minutes, after which the temperature was raised at a rate of 10° C/min.

Sample Preparation

Most of the compounds in this study were purchased from commercial suppliers. The following chemicals were obtained from Aldrich Chemical Company, Milwaukee, Wisconsin: 2,3-dinitrotoluene; 2,4-dinitrotoluene; 2,6-dinitrotoluene; 3,4-dinitrotoluene; α, α, α-m-trifluoronitrotoluene; o-bromonitrobenzene; m-bromonitrobenzene; p-bromonitrobenzene; 2,4-dichloronitrobenzene; 3,4-dichloronitrobenzene; 2,3,4-trichloronitrobenzene; 2,3,5-trichloronitrobenzene; 2,3,4,5-tetrachloronitrobenzene; 2,3,5,6-tetrachloronitrobenzene; 1,2,3,4-tetrachlorobenzene; pentachlorobenzene; hexachlorobenzene; p-chloronitrobenzene; o-fluoronitrobenzene; m-fluoronitrobenzene; p-fluoronitrobenzene; o-dinitrobenzene, m-dinitrobenzene; p-dinitrobenzene; 2-methyl-p-benzoquinone; and 2,3,5,6-tetrafluoro-p-benzoquinone. The following chemicals were obtained from Chem Service, Media, Pennsylvania: 1,4-naphthoquinone; o-nitrotoluene; m-nitrotoluene; p-nitrotoluene; and o-chloronitrobenzene.

J. T. Baker Chemical Co., Phillipsburg, New Jersey, was the supplier of p-benzoquinone and azulene. m-Chloronitrobenzene and nitrobenzene were purchased from Eastman Kodak Co., Rochester, New York. Paul Kebarle of the University of Alberta, Edmonton, Alberta, Canada donated o-cyanonitrobenzene, m-cyanonitrobenzene, p-cyanonitrobenzene, m-nitroanisole and p-nitroanisole.

A standard stock solution of each compound was made by dissolving a weighed sample (10 to 50 mg) in 10 mL of either benzene or toluene, both HPLC grade. The benzene was purchased from EM Science, Cherry Hill, New Jersey and the toluene was obtained from J. T. Baker Chemical Co., Phillipsburg, New Jersey. The concentration of these stock solutions was therefore between $1X10^{-6}$ and $5x10^{-6}$ g/μL. Successive 1:10 dilutions were made so that standard solution concentrations of 10^{-6} g/μL to 10^{-12} g/μL were available for each compound.

Data Collection and Processing

The TID-N_2 data reported in this study were collected with a Servogor 330 strip chart recorder. Molar responses were calculated from peak areas of the respective chromatographic peaks. Areas were determined by cutting and weighing the peaks.

The data collection and processing for the ECD experiments were performed in a quite different manner. A Cyborg model 91A ISAAC analog-to-digital interfacing system linked an Apple II+ computer with the Hewlett Packard gas chromatograph. This hardware, along with DYSC Appligration II software purchased from Dynamic Solutions Corporation, Pasadena, California, allowed data aquisition and analysis to be performed on the chromatographic runs. The computer program can perform operations such as peak area and peak height analysis, retention time determination, baseline subtraction and other processes beneficial to analyzing a chromatographic run.

For the ECMS experiments, a Digital pdp 8/a computer system was interfaced to the VG MS. With this system, the necessary mass spectrometric parameters were set, the chromatographic runs monitored, and the mass spectra analyzed.

The data for the APIMS experiments were collected on a Houston Instruments Omniscribe strip chart recorder.

Computer Modeling

Simulated resonance ECD responses were generated by a computer program written by Dr. E. P. Grimsrud and run on an Apple II+ personal computer. A flow chart of the program is shown in Figure 15 and the definitions of the terms in the flow chart are shown in Table 1. The detector parameters in the program were set to levels appropriate for the Hewlett Packard CCP-ECD and held constant for all simulation experiments. The standing current was set at 1×10^{10} electrons/sec (1.60 mA), the sample interval at 2 msec and the positive ion density - recombination rate product at 500 sec^{-1}.

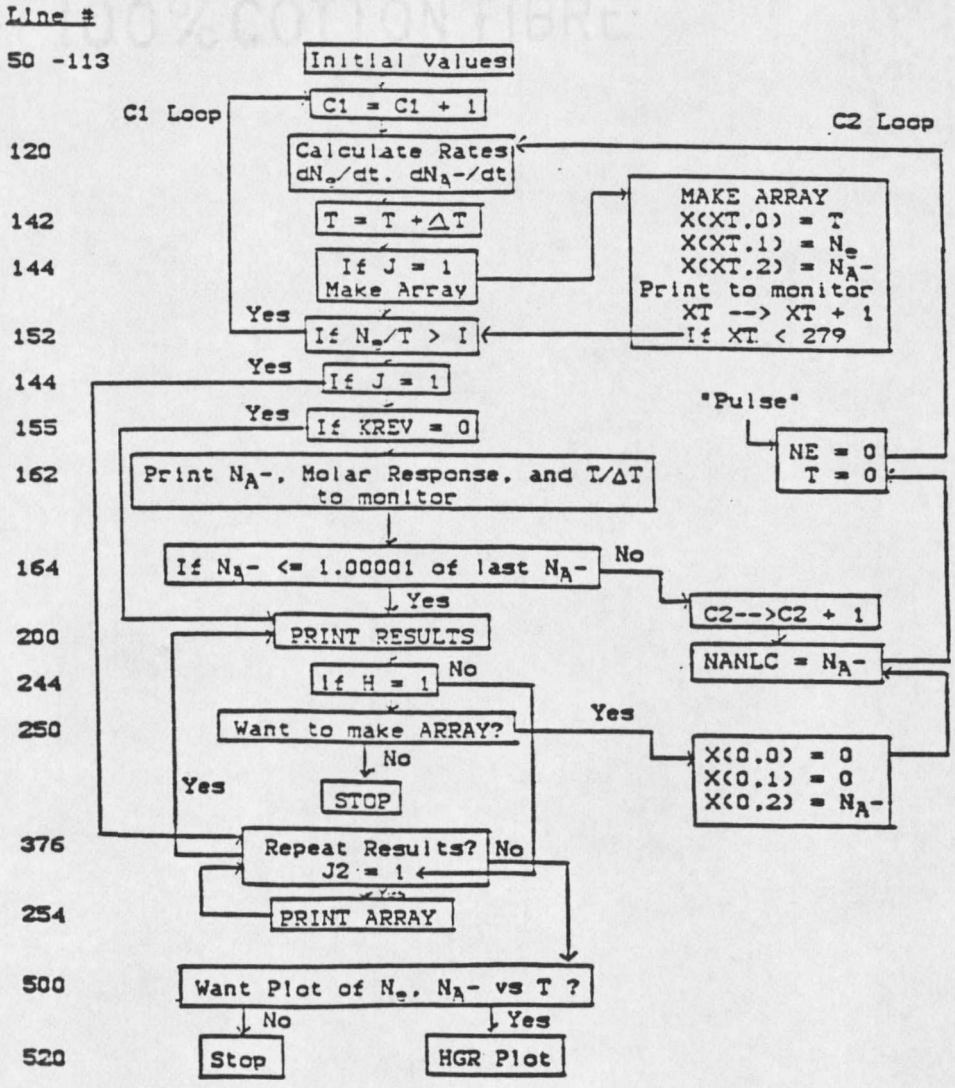


Figure 15. Resonance ECD computer modeling flow chart.

Table 1. Definitions for the Computer Model of Resonance Electron Capture.

TERM	VARIABLE NAME	UNITS
[ETCL][a]	ETHCL	molecules/cc
R_2	KETHCL	$cc^{-1} * sec^{-1}$
Standing Current	I	electrons/sec
k_1	K1	$cc^{-1} * sec^{-1}$
k_{-1}	KREV	$cc^{-1} * sec^{-1}$
R_1	XRECOMB	sec^{-1}
R_3	WRECOMB	sec^{-1}
Baseline frequency	FO	sec^{-1}
[Sample][a]	NSAMPLE	molecules/cc
Smallest time unit for integration	INCT	seconds
N_A-	NNEGA	molecules/cc
N_A- last Cl loop	NANLC	molecules/cc
N_e-	NE	molecules/cc
dN_e-/dt	RE	rate of change
dN_A-/dt	RANEG	rate of change

[a] Concentration or population in detector volume

RESULTS AND DISCUSSION

TID-N_2 Responses of Substituted Nitrobenzenes

The responses of 36 compounds were determined in a TID-N_2 over a wide range of concentrations and detector conditions. Peak height calibration curves determined using two different levels of source heating current, 2.30 A and 2.10 A, are shown in Figure 16. Generally, a region of near-linear molar response was observed only for the first decade or two of concentration change above the lowest detectable concentration. The molar responses to most substances increased or decreased significantly with further increases in sample concentrations. A few compounds, however, exhibited quite linear behavior over a wide range of concentrations.

The peak area responses observed for the lowest concentration of each compound in Figure 16 at 2.30 A are listed in Table 2 as the absolute response (C/mol) of that substance. All the compounds but one (perfluorobenzoquinone) are substituted nitrobenzenes. The electron affinities of all the mono-substituted nitrobenzenes have recently been measured (32) and are listed in Table 2. The compounds for which the electron affinities are not

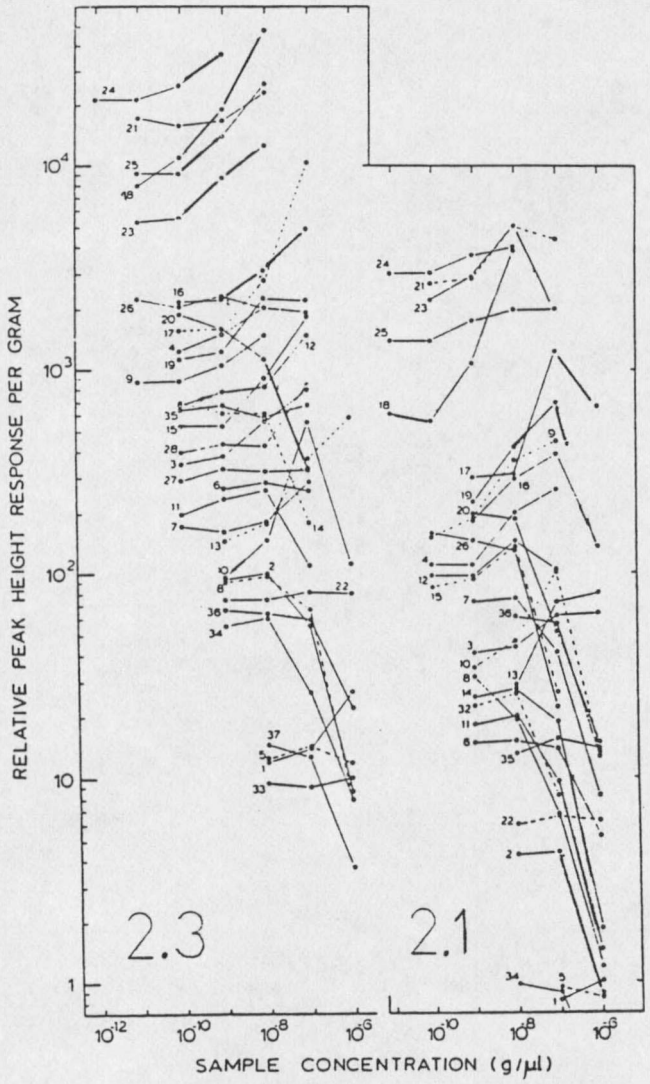


Figure 16. TID-N_2 peak height responses to varied amounts of substituted nitrobenzenes. The compound associated with each calibration curve is indicated by the number assigned in Table 2. Detector conditions are: temperature, 320° C; gas flow, 100 mL/min nitrogen; bias voltage, -45 V; source heating current, 2.30 A and 2.10 A.

Table 2. TID-N_2 responses and effects of experimental parameters on responses to various positive electron affinity molecules.

*Compound**	*EA*** (kcal/mol)	*Absolute molar response**** (C/mol)	*Detection limit (pg)*	*Effect§ of detector temp.*	*Effect§§ of heater current*	*Effect§§§ of bias voltage*	*Different detector gases†*					
							0.3% O_2	*90% CO_2*	*90% N_2O*	*15% CH_4*	*15% Isobutane*	*90% Ar*
1 NB	22.1	$2.2 \cdot 10^{-4}$	$12 \cdot 10^3$	4.2	8.4	2.3	0.37	0.80	0.77	0.18	0.10	6.1
2 *m*-CH_3ONB	22.7	$5.5 \cdot 10^{-3}$	780	4.9	7.4	2.8	0.59	0.73	0.43	0.32	0.24	4.6
3 *p*-CH_3ONB	19.6	0.08	125	4.5	14	2.5	0.57	0.88	0.20	0.45	0.31	4.0
4 *o*-CH_3NB	20.0	0.29	65	2.6	4.0	2.7	0.53	1.06	0.36	0.75	0.58	2.3
5 *m*-CH_3NB	21.4	$1.1 \cdot 10^{-3}$	$4 \cdot 10^3$	4.3	8.9	2.6	0.36	0.73	0.43	0.35	0.11	3.7
6 *p*-CH_3NB	20.5	0.03	250	4.4	5.0	2.8	0.50	0.75	0.41	0.71	0.59	3.2
7 *o*-FNB	23.5	0.11	115	3.2	2.2	2.7	0.72	1.54	0.54	1.1	0.76	1.3
8 *m*-FNB	27.5	0.018	165	4.9	9.3	2.4	0.40	0.73	0.32	0.65	0.45	1.9
9 *p*-FNB	24.3	0.51	65	3.75	4.0	2.7	0.80	1.50	0.32	1.00	0.71	1.5
10 *o*-ClNB	25.0	0.018	470	3.4	2.1	2.6	0.41	1.1	0.32	0.50	0.47	1.5
11 *m*-ClNB	28.1	0.018	340	5.5	6.3	2.2	0.52	0.77	0.33	0.62	0.52	1.70
12 *p*-ClNB	27.5	0.060	105	5.2	4.9	2.7	0.67	0.90	0.30	0.59	0.41	1.50
13 *o*-BrNB	25.5	0.043	260	3.7	4.6	2.5	0.82	1.00	0.50	0.35	0.45	1.8
14 *m*-BrNB	28.8	0.035	140	3.3	3.9	2.8	0.75	0.92	0.40	0.47	0.45	1.56
15 *p*-BrNB	28.3	0.13	150	5.0	3.8	2.9	0.67	0.88	0.27	0.49	0.33	1.3
16 *o*-CNNB	35.1	0.39	25	4.2	4.2	2.9	0.51	0.88	0.25	0.40	0.35	2.1
17 *m*-CNNB	34.1	0.49	14	4.8	5.6	2.7	0.34	0.84	0.19	0.55	0.52	1.8
18 *p*-CNNB	38.1	1.4	9	4.0	4.1	2.7	0.27	0.78	0.12	0.57	0.57	1.7

* B = Benzene; NB = nitrobenzene; DNT = dinitrotoluene.

** Electron affinity values taken from ref. 12.

*** Determined from peak areas using following conditions: detector temperature, 320°C; emitter heater current, 2.30 A; flow-rate, 100 ml/min nitrogen.

§ Ratio of molar response observed at 370°C to that at 270°C; emitter heating current, 2.1 A.

§§ Ratio of molar response observed with heater current 2.4 A to that with 2.1 A; detector temperature, 320°C.

§§§ Ratio of molar responses observed using bias potentials of −45 and −15 V applied to the emittor; detector temperature, 320°C; emitter heating current, 2.3 A.

† These detector gases were mixed at the base of the detector with nitrogen so that the total detector gas flow-rate was 100 ml/min. Values listed are ratio of responses relative to responses in nitrogen gas.

†† I_X/I_{N_2}.

Table 2. (cont'd) TID-N_2 responses and effects of experimental parameters on responses to various positive electron affinity molecules.

*Compound**	*EA*** (kcal/mol)*	*Absolute molar response**** (C/mol)*	*Detection limit (pg)*	*Effect§ of detector temp.*	*Effect§§ of heater current*	*Effect§§§ of bias voltage*	*Different detector gases†*					
							0.3% O_2	*90% CO_2*	*90% N_2O*	*15% CH_4*	*15% Iso-butane*	*90% Ar*
19 *o*-NO_2NB	36.2	0.32	10	3.6	2.0	2.8	0.60	1.3	0.36	0.74	0.67	1.7
20 *m*-NO_2NB	36.2	0.23	6	4.3	6.6	3.0	0.51	0.61	0.24	0.51	0.43	1.9
21 *p*-NO_2NB	43.6	3.9	3	1.9	3.6	2.5	0.85	1.2	0.30	0.87	0.65	1.6
22 *m*-CF_3NB	30.9	0.011	200	3.1	4.3	2.5	0.42	0.62	0.27	0.44	0.33	1.7
23 2,3-DNT		4.4	8	3.4	3.3	2.7	1.27	0.55	0.37	0.60	0.49	1.56
24 2,4-DNT		23	2	4.5	4.2	2.7	1.3	0.64	0.50	0.69	0.59	1.7
25 2,6-DNT		6.5	7	3.3	2.9	2.6	0.42	0.75	0.22	0.44	0.35	2.0
26 3,4-DNT		1.6	50	4.4	3.2	2.7	0.83	1.00	0.59	0.67	0.50	1.5
27 2,4-Cl_2NB		0.18	90	3.0	3.1	1.9	0.72	0.86	0.58	0.65	0.45	2.1
28 3,4-Cl_2NB		0.21	130	2.7	3.2	3.1	0.96	0.77	0.75	0.56	0.38	2.1
29 2,3,4-Cl_3NB		0.28	90	3.6	3.2	3.0	0.93	0.60	0.83	0.37	0.37	3.2
30 2,3,5-Cl_3NB		0.30	120	3.6	4.3	2.6	0.73	0.77	0.76	0.36	0.34	3.0
31 2,3,4,5-Cl_4NB		0.33	200	2.5	3.5	2.7	1.08	0.79	1.15	0.44	0.44	3.3
32 2,3,5,6-Cl_4NB		0.27	170	2.9	5.0	2.5	0.75	0.84	1.25	0.30	0.28	5.6
33 1,2,3,4-Cl_4B		$3.2 \cdot 10^{-3}$	$8 \cdot 10^3$	4.4	5.1	2.6	1.08	0.87	1.3	0.48	0.55	2.0
34 Cl_5B		0.037	720	3.7	4.5	2.86	1.12	0.84	0.92	0.40	0.44	2.02
35 Cl_6B		0.38	60	3.1	2.2	2.5	0.88	1.1	0.56	0.71	0.75	1.26
36 Perfluorobenzo-quinone	60.2	0.15	$1 \cdot 10^3$	2.6	3.7	2.6	0.56	0.75	0.47	0.54	0.54	4.0
Baseline current††							0.46	1.9	1.1	0.74	0.55	8.8

* B = Benzene; NB = nitrobenzene; DNT = dinitrotoluene.

** Electron affinity values taken from ref. 12.

*** Determined from peak areas using following conditions: detector temperature, 320°C; emitter heater current, 2.30 A; flow-rate, 100 ml/min nitrogen.

§ Ratio of molar response observed at 370°C to that at 270°C; emitter heating current, 2.1 A.

§§ Ratio of molar response observed with heater current 2.4 A to that with 2.1 A; detector temperature, 320°C.

§§§ Ratio of molar responses observed using bias potentials of −45 and −15 V applied to the emittor; detector temperature, 320°C; emitter heating current, 2.3 A.

† These detector gases were mixed at the base of the detector with nitrogen so that the total detector gas flow-rate was 100 ml/min. Values listed are ratio of responses relative to responses in nitrogen gas.

†† I_X/I_{N_2}.

known contain a high degree of electronegative functionality and most certainly have positive electron affinities. As shown in Table 2, compounds with multiple nitro groups respond very strongly in the detector, supporting prior studies (13, 26, 29) that this is a nitro-selective detector. Also listed in Table 2 are the observed detection limits at which the response to each compound was about five times the noise level. Picogram levels of the most strongly responding compounds could be routinely detected.

The effect of temperature of the detector housing on the response to each compound was determined over the range of 270° to 370° C. Typical results are shown in Figure 17 for five compounds. The absolute response to all compounds is increased by temperature in an almost linear manner as shown. It is possible, therefore, to describe the temperature dependence of response for each compound by the ratio of responses at 370° and 270° C. This is done in the fourth column of data of Table 2. The result is that the relative responses of almost all of the compounds are increased in a similar manner, about three to five times, by this 100° C temperature increase. Also shown in Figure 17 is the baseline current observed at various detector temperatures. The baseline current rises

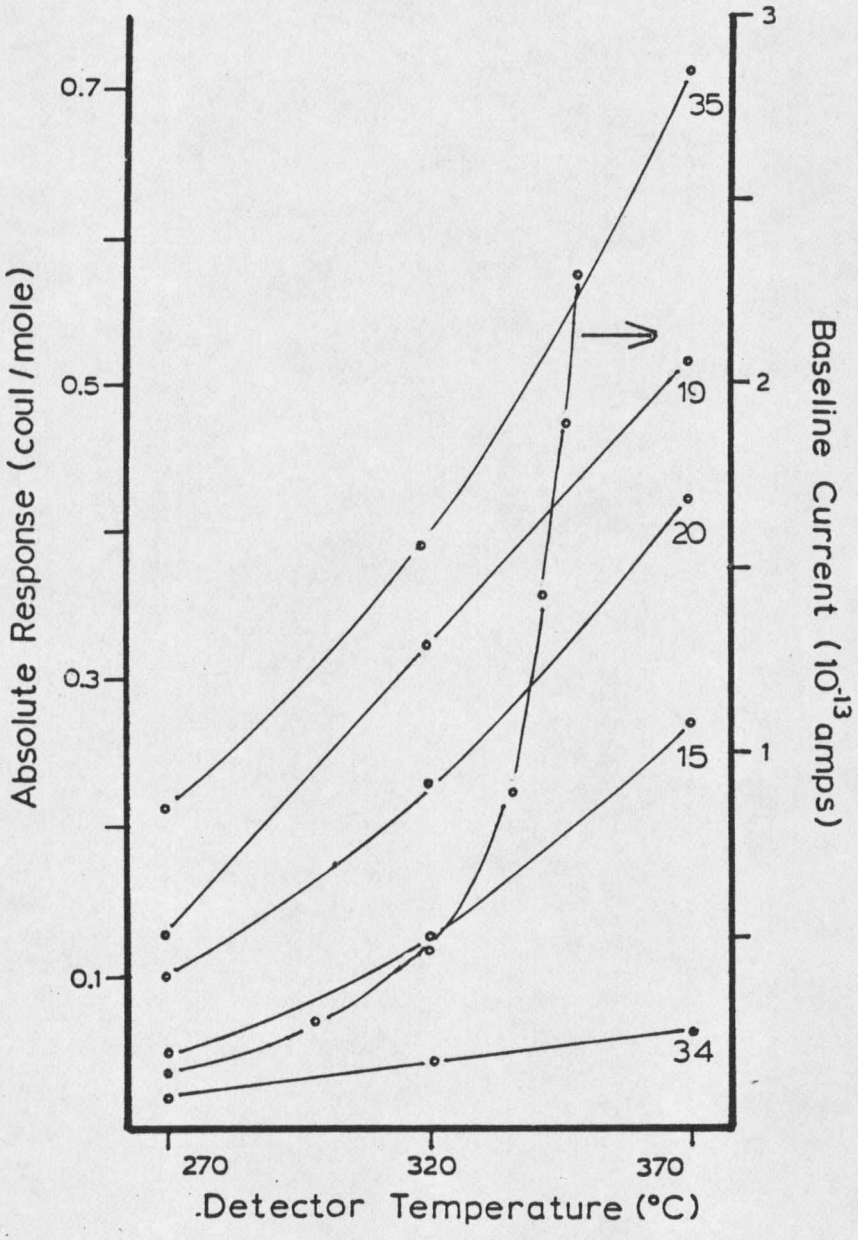


Figure 17. Absolute TID-N_2 responses of five compounds and detector baseline current as a function of the detector block temperature. Source heater current, 2.10 A; bias voltage, -45 V. Hexachlorobenzene = 35; o-dinitrobenzene = 19; m-dinitrobenzene = 20; p-bromonitrobenzene = 15; pentachlorobenzene = 34.

proportionately with responses between 270° and 320° C and then increases more sharply than relative responses at higher detector temperatures. Maximum signal-to-noise responses to all compounds, therefore, were observed in the 270° to 320° C temperature range.

The effect of heating current supplied to the source emitter was also determined for each component from heating current (I) = 2.1 to 2.4 A. Typical results are shown in Figure 18. Again, a near linear positive dependence of response on heater current was observed for all compounds. This dependence for each compound is expressed in Table 2 as the ratio of responses observed at 2.40 and 2.10 A heating current. For this variable a somewhat wider range of response dependencies is observed than was noted for variations in detector temperature. Response amplifications from about 2 to 8 are observed for most of the compounds by this 0.3 A increase in source current. As a general rule, the responses of the more weakly responding compounds were enhanced to a greater degree by the increase in heating current than were the responses of strongly responding compounds. Also shown in Figure 18 is the effect of source heating current on the baseline current. For this detector the relative increase in baseline current is roughly equal to relative response

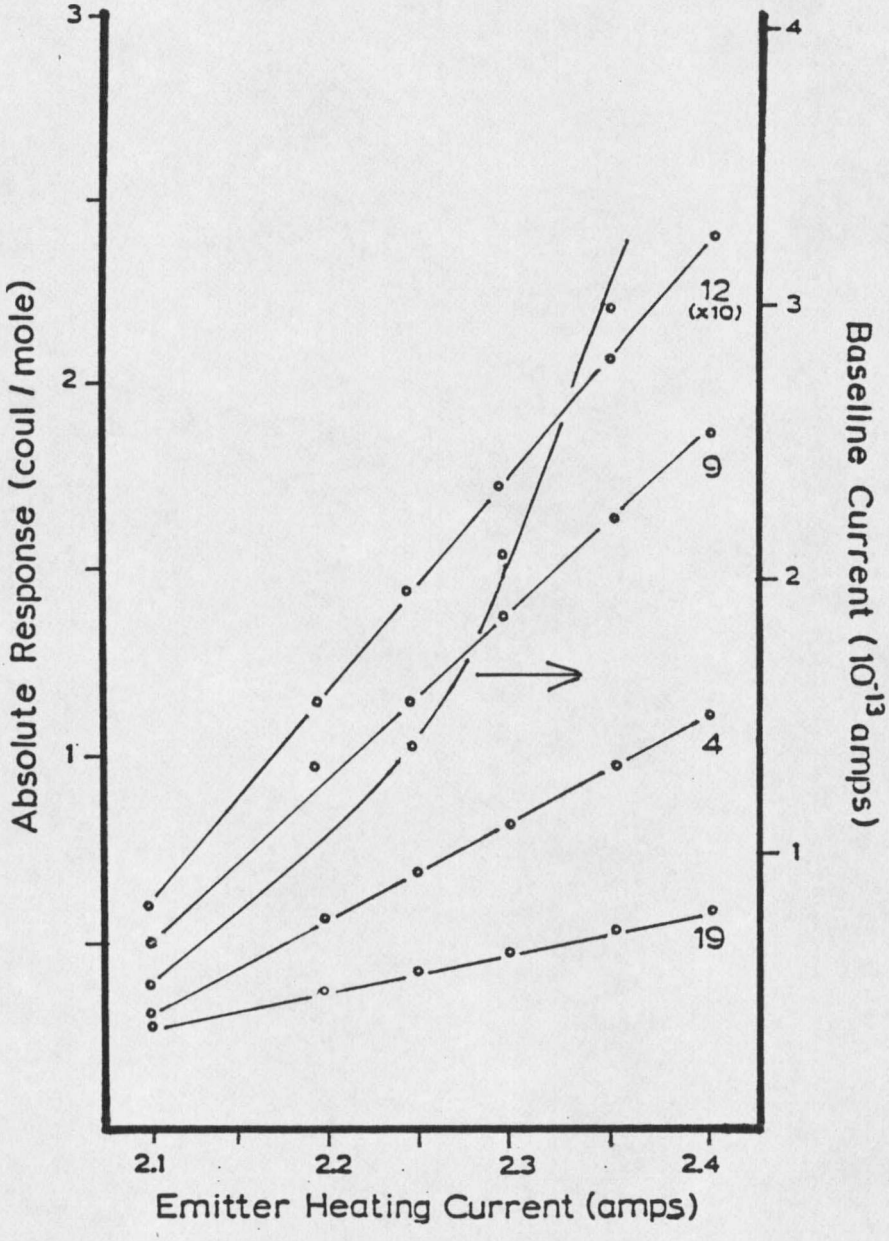


Figure 18. Absolute TID-N_2 responses of five substituted nitrobenzenes and baseline current as a function of emitter heating current. Detector temperature, 320° C; bias voltage, -45 V. p-Chloronitrobenzene = 12; p-fluoronitrobenzene = 9; o-nitrotoluene = 4; o-dinitrobenzene = 19.

increases up to about 2.25 A, after which the baseline current and associated noise level increase more sharply than do molar responses to analyte molecules.

The effect of variation in the bias voltage, from -5 to -45 V applied to the central emitter source, on responses is shown in Figure 19 for several arbitrarily selected cases. The obvious result here is that responses are continuously and linearly increased by an increasingly negative bias voltage. For all compounds the ratios of responses observed with bias voltages of -45 and -15 V are listed in Table 2. Most of these fall within the narrow range of 2.5 to 3.0, which is nearly equal to the voltage ratios. It is significant that these results differ distinctly from those of analogous experiments with the TID operated in the nitrogen-phosphorous selective mode (8), where a saturation level of response to analyte was observed with only -12 V applied to the emitter in a source of similar dimensions. In Figure 19 the baseline current is also shown to vary linearly with bias voltage. Since this plot approaches a non-zero origin, however, the ratio of response to baseline current is somewhat superior with the use of the greater bias voltage. This clearly physical effect, which is relatively insensitive to the chemical differences occurring among

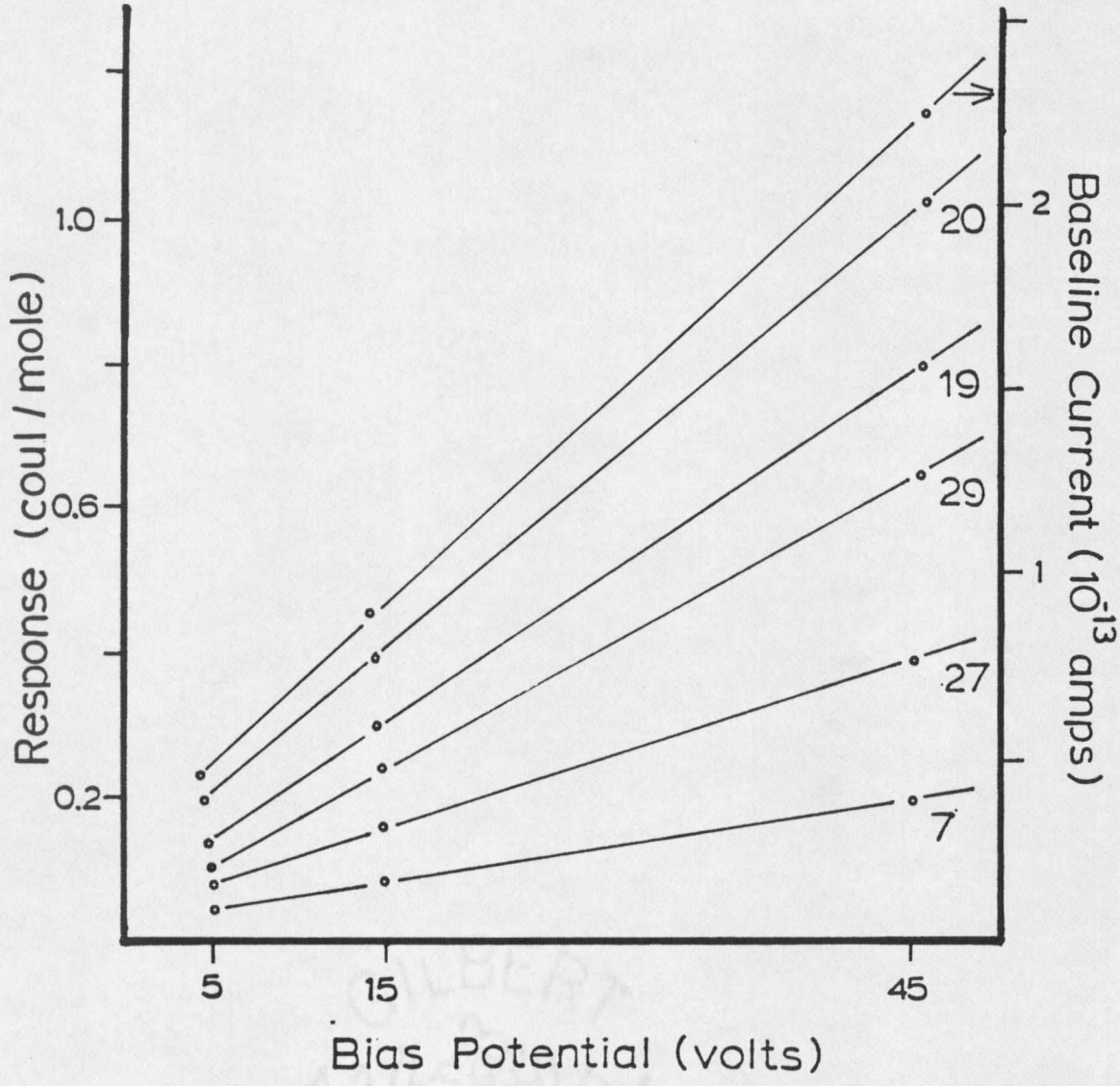


Figure 19. Absolute TID-N_2 responses of five substituted nitrobenzenes[2] and baseline current as a function of emitter bias potential. Source heating current, 2.30 A; detector temperature, 320° C; m-Dinitrobenzene = 20; o-dinitrobenzene = 19; 2,3,4-trichloronitrobenzene = 29; 2,4-dichloronitrobenzene = 27; o-fluoronitrobenzene = 7.

the 36 compounds, was not anticipated. Expected was a saturation level of response with the application of -15 V or even -5 V since the field thereby induced was expected to be sufficient to collect essentially all gas phase negative ions. This expectation was supported by calculations of expected ion velocities in the direction of the anode relative to the linear velocity of ions due to ventilation through the cell. For example, for the following values of these experiments: bias voltage, 15 V; cathode-to-anode distance, 0.12 cm; total flow rate, 100 cc/min; cross sectional area of flow path 0.11 cm^2; and conservatively assuming the mobility of the ion in question in atmospheric pressure nitrogen to be at least 1.0 $cm^2 sec^{-1} V^{-1}$ (55); the radial velocity of ions along the applied field is predicted to be 125 cm/sec while the longitudinal velocity due to detector gas flow is only 15 cm/sec. Since the length of the detector is several times greater than the radial dimension, all negative ions are expected to be collected, if the applied field serves only to sweep negative ions to the anode. Since the experiments of Figure 19 indicate that the response is continuously proportional to relatively large applied electric fields, the probable explanation for this observation is that the rate of emission of negative ions

from the emitter surface is directly proportional to the electric field in that vicinity or that the field is somehow enhancing the ionization process.

Absolute responses to all compounds were also determined using altered detector gases. These included oxygen, carbon dioxide, argon, nitrous oxide, isobutane and methane mixed in various proportions into nitrogen. These results and accompanying affects on standing current are shown in the last six columns of Table 2. For all detector gases studied, relatively minor changes in signals were observed.

The TID operated in the nitrogen-phosphorous selective mode has always been known as very temperamental device. Variables such as electrode position (16), source heating current (8, 50), detector temperature (8), hydrogen flow rate (15), source composition (15, 50), irreversible loss of alkali from the emitter source (51), damage to the source by overheating (52), and buildup of deposits such as silicon dioxide on the source surface (52) can alter the sensitivity and selectivity on a day-to-day basis. For routine analysis with the nitrogen-phosphorous selective detector, it is crucial that detector variables be monitored carefully to insure valid results. For analyses with the TID-N_2, it is also

important to be aware of the relevant detector parameters to optimize responses, as is obvious from the previously presented data. Responses increase with detector tower and source temperature but a point is reached where the signal-to-noise begins to decrease. Both molar responses and signal-to-noise ratio levels are optimized with the use of high bias voltages. Although the use of argon consistently increases molar responses, the associated noise and baseline levels increase, leaving nitrogen as the detector gas of choice. Because the detector operates in an inert atmosphere of one type of gas only, responses are less dependent on the fine tuning of flow rates, and injection reproducibility was routinely better than $\pm$ 10%. Responses do decrease over time, indicating either a loss of the alkali from the surface of the source or contamination of the source surface. This response decrease is not drastic, however, and day-to-day analyses can be performed without significant losses in detectability.

TID-N_2 - APIMS Measurements

A specialized ion source, described in Experimental, was constructed for an APIMS so that ionizing conditions within it were identical to those existing within the

TID-N_2. The following compounds were selected for study here: nitrobenzene, the three isomers of nitrotoluene, and the three isomers of fluoronitrobenzene. A number of experiments were performed for each of these molecules in which detection of negative ions either by single ion monitoring or by mass scans from 10 to 500 amu was attempted as each molecule of interest eluted through the specialized ion source. In no experiments were ions in this mass range observed. It was specifically noted that in the very sensitive single ion mode, no negative ion signals were detected. Examples of these experiments are shown in the first two chromatograms of Figure 20 for the case of o-nitrotoluene.

When the quadrupole mass spectrometer was operated in the total ion mode, however, negative ion signals for the analyte molecules studied were in fact observed. Total negative ion signals for o-nitrotoluene are shown in the last three chromatograms of Figure 20 where the total negative ions have masses greater than 20, 200 and 400 amu respectively. Analogous results for all eight compounds studied were obtained, therefore no individual ions with masses between 10 and 500 amu were observed but total negative ion signals were. The highest cut-off level of 400 amu produced a signal of the same intensity as did the

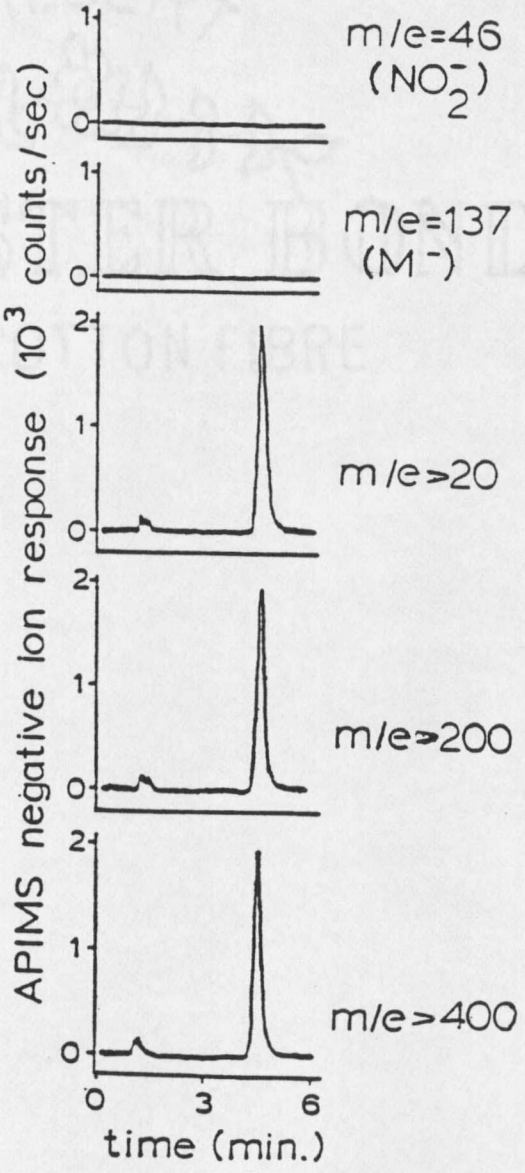


Figure 20. Negative ion responses to 350 ng o-nitrotoluene (GC retention time 4.4 minutes).

application of the low cut-off threshold of 20 amu. Figure 21 shows five total ion signals of five different molecules which were obtained in rapid succession so that the instrument sensitivity was reasonably constant during the period of analysis. The sample concentrations are relatively uniform and the signals exhibit the relative tendency of the analyte molecules to generate negative ions. It is shown that the signal for the ortho isomer of nitrotoluene is much larger than that of the meta isomer and nitrobenzene, while the ortho and meta isomers of fluoronitrobenzene produce responses of intermediate magnitude. This correlates with the TID-N_2 data previously shown in Table 2 for the five compounds. The TID-N_2 responses of o-nitrotoluene, o-fluoronitrobenzene, m-fluoronitrobenzene, m-nitrotoluene and nitrobenzene were found to be 0.29, 0.11, 0.02, 0.001 and 0.0002 C/mol respectively. Therefore the order of negative ion responses observed in Figure 21 is identical to responses recorded with an actual TID-N_2. This observation provides evidence that the negative ion chemistry observed by the APIMS is also responsible for the signals observed in an actual TID-N_2.

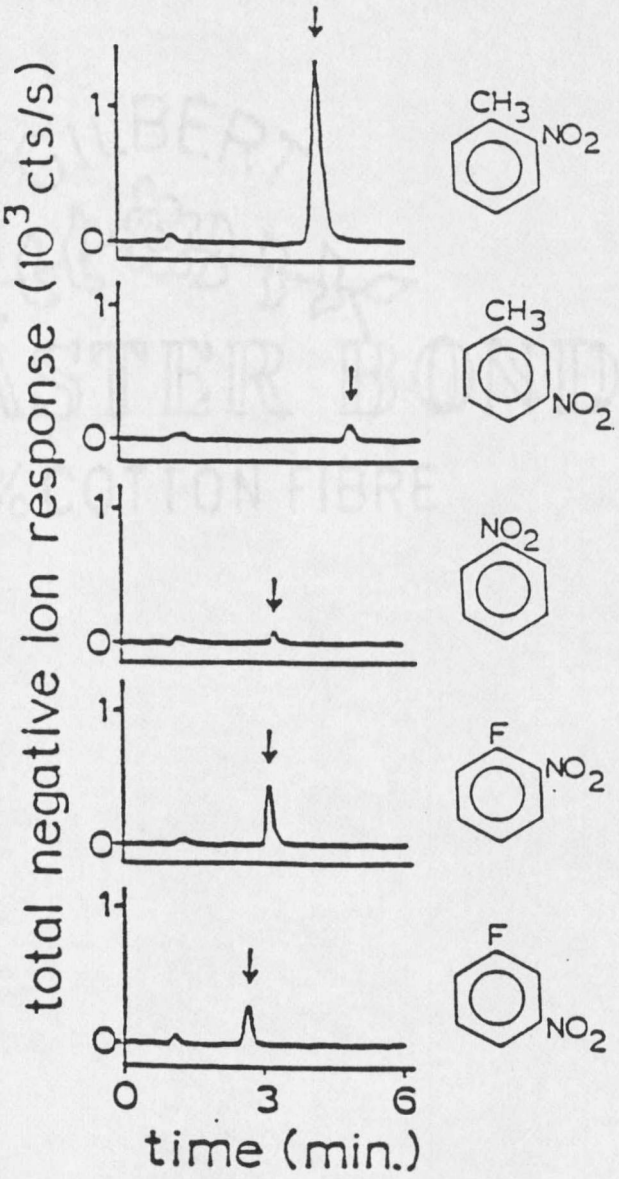


Figure 21. Total APIMS negative ion responses (m/e > 400) to 350 ng o-nitrotoluene, 383 ng m-nitrotoluene, 310 ng nitrobenzene, 230 ng o-fluoronitrobenzene, and 270 ng m-fluoronitrobenzene. The arrow in each chromatogram indicates the known retention times of the above substances.

TID-N_2 Candidate Response Mechanisms

Direct Electron Transfer to Analyte Molecule

The first candidate response mechanism to be considered for the N_2 mode of the TID is a simple, reversible electron transfer from the low work function surface to the analyte molecule as was shown in Introduction as Reaction 1. If the response mechanism does involve a reversible electron transfer to form a gas phase molecular negative ion, the responses might be expected to bear a predictable dependence on the electron affinity of the analyte. More specifically, the observed current response to a molecule, M, might then be given by Equation 17,

$$I = AT^2 \exp [-(W-EA_m)/RT] \qquad (17)$$

which is a variation of Richardson's equation (21) for the limiting magnitude of current by thermionic emission, which assumes that all negative charges formed at the surface-gas interface are rapidly swept to the anode by an applied electric field. In this equation, W is the work function for thermionic emission of an electron from a heated surface at temperature T, EA_m is the electron

affinity of M, and A is a constant for a given surface. Therefore, if this mechanism is operative, the relative responses observed within a closely related group of molecules such as the substituted nitrobenzenes might be expected to increase exponentially with increased electron affinity. As has been mentioned, the electron affinity values for all of the mono-substituted nitrobenzenes shown in Table 2 have recently been measured (32) and are listed in the table. In Figure 22, the logarithm of the TID-N_2 absolute response to each substituted nitrobenzene is plotted as a function of EA_m. If Equation 17 applies to this system, a straight line of positive slope is expected. This figure indicates, however, that over the entire group of substituted nitrobenzenes, the observed relative responses do not bear a strict exponential dependence on the electron affinity. Therefore direct, reversible electron transfer to the analyte molecule and the factor of molecular electron affinity does not alone explain the responses of all of the substituted nitrobenzenes. If the data in Figure 22 is considered in parts, one set of isomers at a time, select portions of the data might be taken to suggest that reversible, direct electron transfer to form a molecular negative ion may be partially involved or that it may be one of several

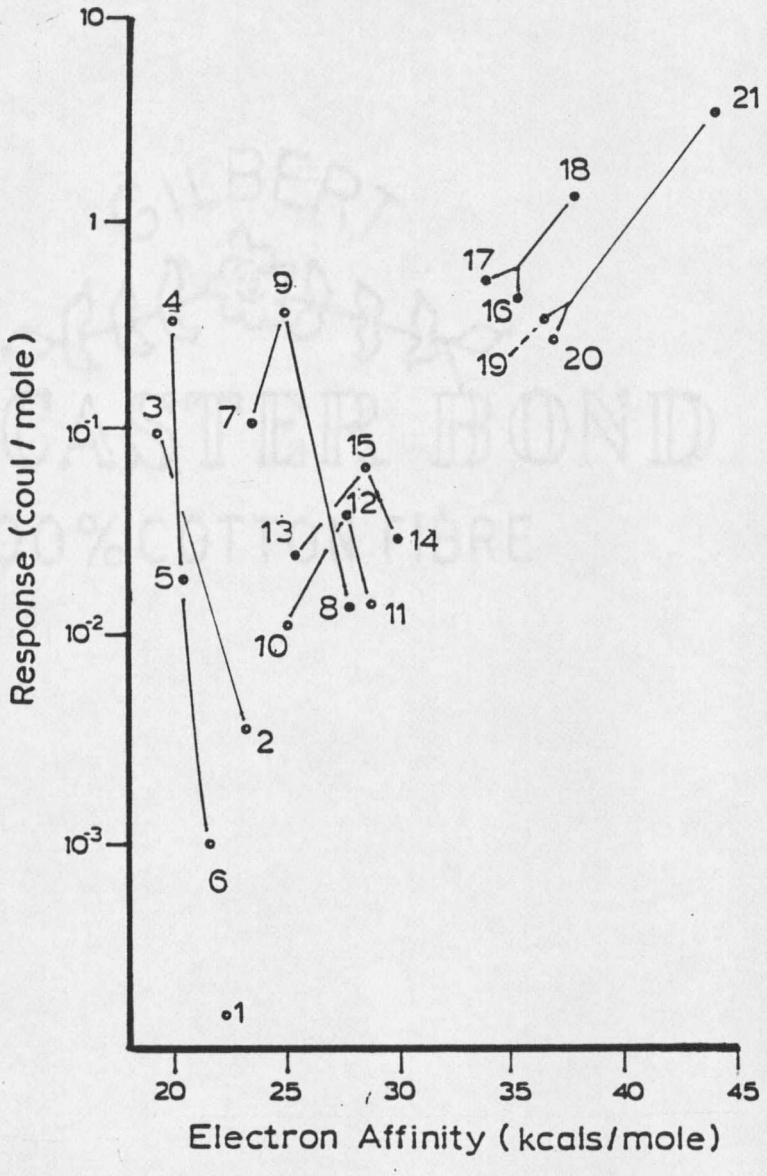


Figure 22. Comparison of TID-N_2 molar responses with electron affinity values for substituted nitrobenzenes. Nitrobenzene = 1; m, p-nitroanisole = 2, 3, respectively; o, m, p-nitrotoluene = 4, 5, 6; o, m, p-fluoronitrobenzene = 7, 8, 9; o, m, p-chloronitrobenzene = 10, 11, 12; o, m, p-bromonitrobenzene = 13, 14, 15; o, m, p-cyanonitrobenzene = 16, 17, 18; o, m, p-dinitrobenzene = 19, 20, 21.

mechanisms involved. For example, the cyanonitrobenzenes and the dinitrobenzenes have the highest electron affinities and they do, indeed, have responses which are as great or greater than the rest. Moreover, within each of these compound types, the isomeric variations of response appear to correlate reasonably well with electron affinity; that is the para isomers of cyanonitrobenzene and dinitrobenzene have distinctly larger responses and electron affinity values than the meta and ortho isomers. It can also be seen that unsubstituted nitrobenzene has the lowest molar response observed and also has one of the lowest electron affinity values. On the other hand, the nitrotoluenes and nitroanisoles both exhibit a distinct reverse response dependence on electron affinity. Also, within each isomeric group of halogenated nitrobenzenes, the relative TID-N_2 responses do not correlate with their electron affinity values. For these halogenated compounds the para isomers always have the greatest response even though the meta isomers have the highest electron affinity values.

An additional argument against the importance of electron affinity on response is provided by perfluorobenzoquinone. Its electron affinity is very high, 60.2 kcal/mol (32). Yet its TID-N_2 response is

lower than about half of the responses of the substituted nitrobenzenes shown in Figure 22. Also, one might have expected that successive additions of chlorine on dichloronitrobenzene to form trichloronitrobenzene and tetrachloronitrobenzene would have significantly increased the electron affinity and, therefore, the TID-N_2 response, if reversible, direct electron transfer to the analyte molecule is operative. As shown in Table 2, however, the molar responses of the di- to tetra-chlorinated nitrobenzenes are almost constant. Additionally, Equation 17 predicts that the responses of compounds which have low electron affinity values will have greater temperature dependence than those of higher electron affinity. Again, inspection of the data in Table 2 under the two headings concerning detector temperature and source heating current provide no convincing support for this expectation.

Finally, the results of the TID-N_2-APIMS experiments indicate that no molecular ions are being formed at the gas-solid interface of the thermionic emitter. Neither single ion monitoring nor scanning experiments revealed the existence of M^- species for any of the molecules studied.

From the above considerations of electron affinities and responses, it appears that if reversible, electron transfer to form a molecular negative ion is involved at all in the TID-N_2, it is definitely not the only mechanism involved nor is it a dominant one in many instances. If it can be assumed that only one mechanism is operative in the TID-N_2, that mechanism does not appear to be reversible, direct electron transfer to the analyte molecule.

The TID-N_2 is related to the ECD by virtue of the fact that both provide selective responses to molecules by the formation of negative ions. It is interesting, therefore, to compare the relative responses obtained with each in order to see if any additional similarities of mechanism are suggested. Relative ECD responses were also measured and a comparison is made for the substituted nitrobenzenes and dinitrotoluenes in Figure 23. From this comparison it appears that absolutely no correlation exists between the rates of electron capture to the substituted nitrobenzenes on a heated, low work function surface and in a gaseous medium. Also compared were the ECD and TID-N_2 responses of other molecules not shown in Figure 23, and with these, also, little correlation of response magnitudes was observed. It is not necessarily

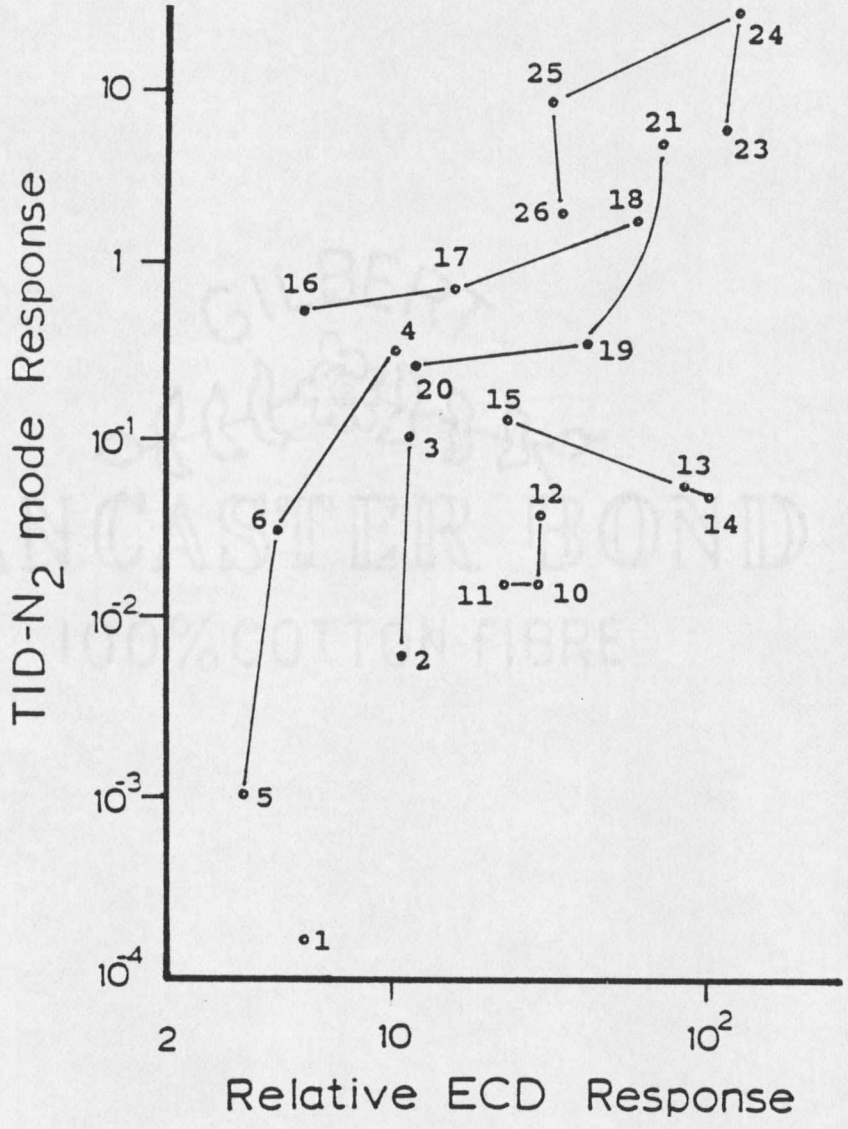


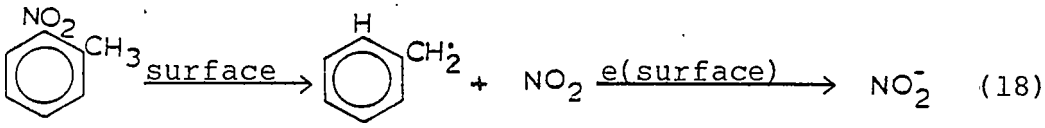
Figure 23. Comparison of absolute TID-N_2 responses of substituted nitrobenzenes and dinitrotoluenes with their relative molar ECD responses. Nitrobenzene = 1; m, p-nitroanisole = 2, 3; respectively; o, m, p-nitrotoluene = 4, 5, 6; o, m, p-chloronitrobenzene = 10, 11, 12; o, m, p-bromonitrobenzene = 13, 14, 15; o, m, p-cyanonitrobenzene = 16, 17, 18; o, m, p-dinitrobenzene = 19, 20, 21; 2,3-, 2,4-, 2,6-, and 3,4-dinitrotoluene = 23, 24, 25, 26.

surprising that no correlation between ECD and TID-N_2 responses exist, unless the expected mechanism for the TID-N_2 involves gas phase electron capture near the low work function surface. This possibility, which would constitute a slight alteration of direct electron transfer to an analyte molecule, appears also not to be operative.

Thermal Decomposition of Analyte Followed by Electron Attachment

The second candidate response mechanism involves thermal decomposition of the analyte at the gas-solid interface followed by an electron transfer to one of the decomposition products, as was shown as Reaction 2 in Introduction. This possibility is difficult to prove conclusively because little is known of the possible elementary steps in this process. As mentioned earlier, however, it is an attractive alternative because if nitrogen dioxide is formed by such a surface or temperature assisted decomposition, electron transfer to it would be facilitated by its very high electron affinity of 53 kcal/mol (31, 32). Another inviting feature of this mechanism is that it offers the following plausible explanation for the anomalous relative responses of the nitrotoluene isomers and nitrobenzene, previously shown in Figure 22. The ortho isomer responds ten times more

strongly than the second-most strongly responding p-nitrotoluene. This might be explained by Reaction 18,

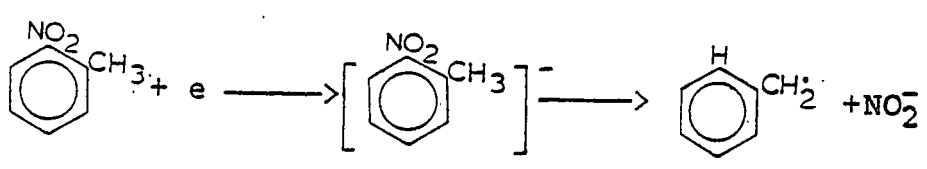


(18)

in which a benzyl rather than a phenyl radical is formed by hydrogen atom transfer to the reaction site from the adjacent methyl group. The formation of a benzyl rather than a phenyl radical decreases the energy of the decomposition by 23 kcal/mol as deduced from benzyl versus phenyl C-H bond strengths (53). The same type of radical stabilization is possible with the meta and para isomers of nitrotoluene during their decomposition on the hot surface, but the decomposition of these molecules would not occur as rapidly due to the increased distance between their methyl group and the reaction site. With nitrobenzene, no such assistance by a methyl group is possible as the molecule comes in close contact with the surface. According to this model, its initial decomposition to nitrogen dioxide requires the formation of a higher energy phenyl radical, and, therefore, is not as fast at a given temperature of the surface. In Table 2, the relative responses of four dinitrotoluenes are also reported. Again, it is noted that the one isomer

among these which does not have a nitro group adjacent to a methyl group, 3,4-dinitrotoluene, also has the lowest TID-N_2 response.

In considering the above and other mechanistic proposals, it is interesting to note the high temperature negative ion spectra shown in Figure 24 of the nitrotoluenes and nitrobenzene which result from gas phase electron capture at 300° C. Ions due to the species M^-, $(M-O)^-$, and NO_2^- are observed for all four compounds. At 200° C only the M^- ion is formed in significant abundance for all four compounds. The distinct feature of the spectra in Figure 24 is the intensity of the NO_2^- ion at m/e=46 is greatly increased by temperature only for the ortho isomer, so that at 300° C, it becomes the base peak in the spectrum of o-nitrotoluene. The cause for this may be closely related to the mechanism just proposed for the surface ionization of the nitrotoluenes except that in gas phase electron capture, the decomposition step would be expected to follow, rather than precede, the ionization step, as shown in Reaction 19.



(19)

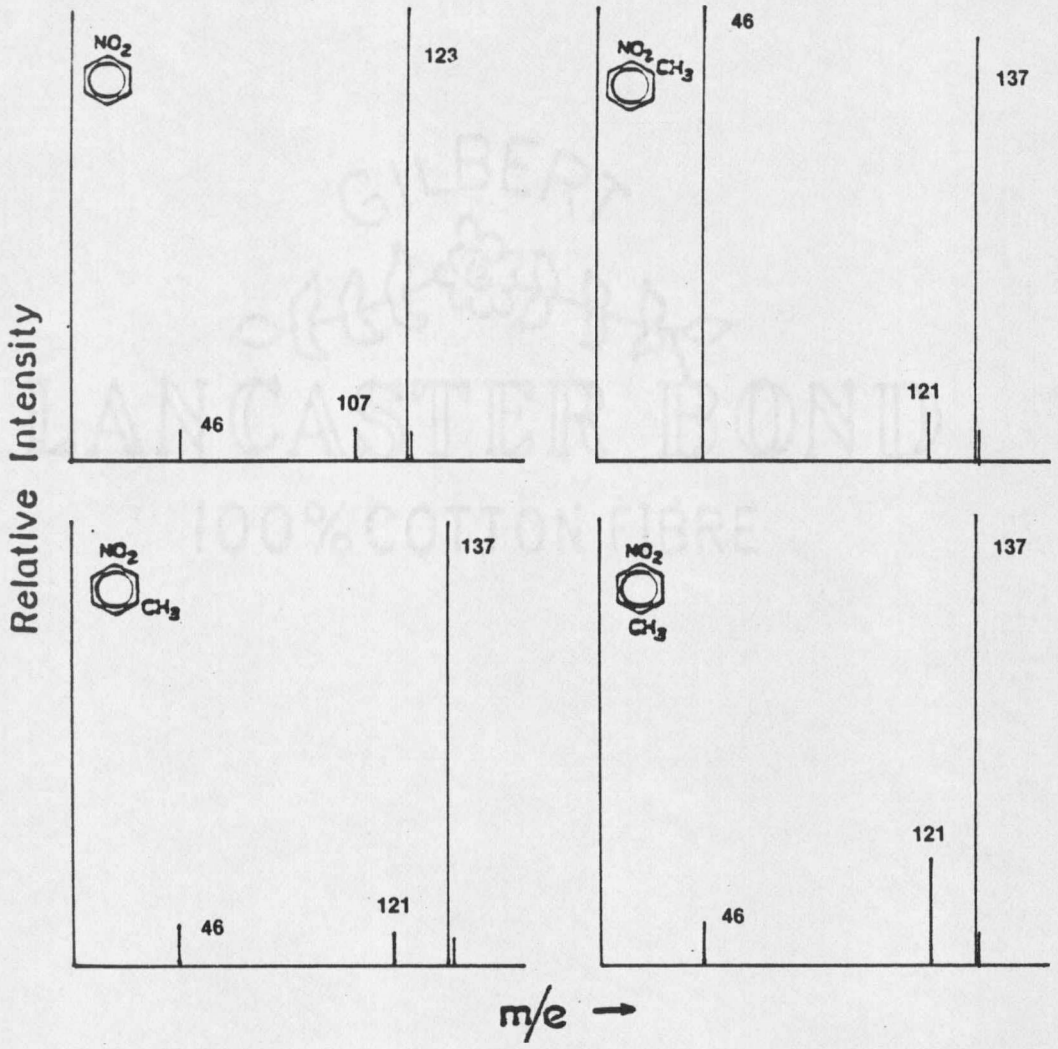


Figure 24. High temperature, negative ion electron capture mass spectra of nitrobenzene and three isomers of nitrotoluene. Ion source gas, 0.3 torr methane; source temperature, 300° C; sample introduction by capillary GC.

In this case the second step may again be facilitated by an adjacent methyl group which permits a benzyl rather than a phenyl radical to be formed. Moreover, in the gas phase it may be possible to form the more stable benzyl radical only for the ortho isomer. That is, without the assistance of a surface, phenyl radicals probably are formed in the production of NO_2^- from the meta and para isomers of nitrotoluene, as they must be in the case of nitrobenzene. This may explain why, in Figure 24, the relative rates of NO_2^- production for m- and p-nitrotoluene and nitrobenzene appear to be equal.

Evidence against this mechanism is presented by the TID-N_2-APIMS experiments. No negative ions of mass 46 (NO_2^-) were observed for any of the compounds studied. This does not exclude the possibility that NO_2^- ions are indeed formed, however, and are undergoing ion-molecule interactions following their formation. The possibility of this occurring is discussed later.

Reaction of Analyte with Gas Phase Radicals Followed by Electron Attachment to Product(s)

This mechanism, shown as Reaction 3 in Introduction, is considered here because of its acknowledged importance in the nitrogen-phosphorous selective mode of the TID. In

this candidate response mechanism, the analyte is decomposed by reactions with reactive species, R, which are continuously formed at the gas-solid interface by the decomposition of either permanent components of the detector gas or from the analyte itself. If the detector gas is a very stable molecule, such as nitrogen, or is an atomic gas, such as argon, any reactive species present would have to be formed from either carrier gas impurities or the analyte.

In order to examine the potential participation of detector gas in the TID-N_2, the responses to all compounds were measured using a variety of different detector gases. The results of these experiments, which included detector gases 0.30% oxygen, 90% carbon dioxide, 90% argon, 90% nitrous oxide, 15% isobutane and 15% methane in nitrogen, are reported in Table 2. The most striking feature of these data is that these wide variations in detector gas cause only relatively minor alterations of the absolute responses. With the exception of argon, the vast majority of responses fall within factors of about 0.4 to 1.0 of the responses observed with nitrogen. If reactive species were important, as suggested for this mechanism, one might have expected their production rates, as well as their destruction

rates, to have been very different in these varied detector gases. The conclusion, therefore, is that this mechanism is not generally operative at concentration levels near the detection limits. It remains possible, however, that for higher concentration levels of certain compounds, this mechanism may be operative where the reactive intermediate species is produced by the destruction of the analyte molecule itself. This may provide a clue as to why, in several cases shown in Figure 16, the molar responses increase with increasing concentrations of sample. This trend was particularly apparent, for example, for all isomers of cyano-nitrobenzene.

The use of 90% argon as detector gas caused consistently greater responses, ranging from 1.3 to 4 times that in pure nitrogen. Also, as was previously mentioned, the baseline emission current was significantly higher with the use of argon. This result may be more easily explained in terms of physical rather than chemical effects of the detector gas if one assumes that the detailed nature of the emitter source surface and its work function, W, can be altered slightly by the nature of its surrounding gas. Argon, being the most chemically inert of the gases used, interacts least with the cesium

enriched surface and may allow the lowest effective work function to be established. Another possible physical explanation of the variations of responses with different detector gases has been considered; that due to their differences in thermal conductivities which, in turn, might cause differences in the temperature of the emitter surface. The thermal conductivities are: nitrogen, 65.7; oxygen, 68.2; carbon dioxide 43.8; argon, 45.5; nitrous oxide, 46.1; isobutane, 44.2; and methane, 89.3 units (54) at 49^{o} C. While this factor could explain why responses and baseline are greater in argon due to its lower thermal conductivity than that of nitrogen, and an expected hotter surface, it does not explain the lower responses observed in carbon dioxide, nitrous oxide, and isobutane. For carbon dioxide, nitrous oxide, isobutane, and probably methane, it appears that chemical modification of the source surface and an accompanying increase in the effective work function is the cause of the slightly lowered responses observed in these detector gases.

Thermal Decomposition Followed by Polymerization and Electron Attachment

As was previously mentioned, a specialized ion source for an APIMS was constructed to simulate ionizing conditions within a TID-N_2 detector. In the single ion mode, potentially expected ions of the type NO_2 or of the molecular anion type for each compound were continuously monitored during the chromatographic elution but were never observed. Scanning of the mass spectrum from 10 to 500 amu did not produce signals either, but operation of the mass spectrometer in the total ion mode resulted in measurable signals for all the compounds studied. These results were shown in Figures 20 and 21. The clear indication of these experiments is that no negative ions of mass less than 500 amu are formed in the TID-N_2. With this in mind, the fourth candidate response mechanism is considered, thermal decomposition of the analyte molecule, M, followed by initiation by one of the products of a polymerization reaction with several (n) other analyte molecules to form some large species XM_n which then attaches an electron, as shown in Reaction 20.

$$M \longrightarrow N + X \xrightarrow{nM} XM_n \xrightarrow{e(surface)} XM_n \qquad (20)$$

This appears possible due to the previous mass spectral data discussed and the probability that this large species may have a considerable number of degrees of freedom and could easily accommodate an electron. If this mechanism is operative, the TID-N_2 molar responses might be expected to have very complex concentration dependencies. The molar responses might be expected to depend on a complex relationship such as the n+1 power of the analyte concentration since n+1 sample molecules are combined into the terminal negative ion. The previously shown concentration curves in Figure 16, however, indicate that complex concentration dependencies are not necessarily the rule. The TID-N_2 detector responses to some compounds were indeed shown to be non-linear, but the nature of diversions from linearity are not consistent with Reaction 20. Also, molar responses to some compounds are often very linear and linearity near the detection limits is observed for nearly all the analytes.

Thermal Decomposition Followed by Combination with Inorganic Species and Electron Attachment at the Gas Solid Interface

Use of the APIMS for the measurement of ions produced by the TID-N_2 created a problem immediately. When the heating current was applied to the emitter source, the aperture between the ion source and the vacuum envelope was consistently and continuously coated and eventually plugged. This phenomenon was readily noted by observation of a steady decrease in manifold and foreline pressures within the MS and by the steady decrease in mass spectral signals which accompany the process. Experiments were performed as quickly as possible once heating of the source commenced. After a few hours of use, the aperture was virtually clogged and no signals were observable until it was replaced. With this observation in mind, a fifth candidate response mechanism is considered, that being thermal decomposition of the sample, M, followed by a combination of a decomposition product, X, with an inorganic species, I, and an electron attachment to the terminal species XI, as shown in Reaction 21,

$$M \longrightarrow N + X \xrightarrow{I} XI \xrightarrow{e(surface)} XI^{-} \qquad (21)$$

where the combination step precedes attachment. The addition of an electronegative species X (possibly NO_2 when M is a substituted nitrobenzene) to an inorganic species may facilitate the transport of a surface electron to a species XI at the gas solid interface. This mechanism seems more plausible than the fourth candidate response mechanism which involved polymerization with other analyte molecules because the responses would not have a complex concentration dependence. The approximately linear responses displayed in Figure 16 could be explained since the large majority of the mass of the negative ion formed originates from the source surface and not the analyte molecules. Additionally, it was obvious that material was continuously being emitted from the heated emitter source. The role of decomposition species, X, therefore, may not be to cause the emission of a neutral species from the cesium-embedded ceramic surface, but to facilitate the attachment of an electron to the terminal species of which it is a part.

Thermal Decomposition Followed by Electron Attachment and Association with Gas Phase Species Removed From Gas-Solid Interface

The sixth and last candidate response mechanism is a more trivial interpretation of the observations reported in this study. Possibly the thermal decomposition of the analyte molecule does indeed determine the TID-N_2 response magnitudes and that the high mass ions observed here are formed in the gas phase by ion-molecule reactions of the smaller negative ion X^- with species removed from the gas-solid interface (G) as X^- migrates to the collector electrode, as shown in Reaction 22.

$$M \longrightarrow N + X \xrightarrow{e(surface)} X^- \xrightarrow{G} XG^- \qquad (22)$$

If the species X^- is indeed NO_2 this negative ion would provide a particularly good center for clustering by a nitrobenzene molecule (47). If negative ions of masses greater than 500 amu are to be formed by this mechanism, incorporation of many analyte molecules would be required. The formation constants for multiple clustering will be very small (47), however, at the temperatures at which the ion source was operated and the formation of very large

mass negative ions by clustering with analyte molecules will not occur. If, however, the clustering species is a large inorganic character emitted from the heated source, a single clustering could provide the necessary mass to result in an ion greater than 500 amu. This mechanism is distinct from the fifth candidate mechanism in that the attachment of an electron precedes, rather than follows, the association step. Furthermore, the sixth mechanism involves reaction with an inorganic species in the gas phase, rather than at the gas-solid interface. The decomposition of the analyte, however, could be the rate limiting process for both of the last two proposed mechanisms. Both of these mechanisms are attractive for many reasons. Firstly, they take into account the aperture plugging phenomenon. Secondly, these mechanisms are an extension of the second mechanism and are consistent with the supporting evidence thereof. Therefore, the anomalous responses of nitrobenzene and the nitrotoluenes shown in Figure 22, the abundance of the NO_2 ion in the high temperature negative ion spectra (Figure 24) of said molecules, and the explanations for each, are in agreement with these mechanisms. Thirdly, both mechanisms offer an explanation for the APIMS experiments that indicate the formation of ions of at

least mass 500 amu. Finally, there is evidence in the literature of organic species combining with inorganic species to form large ions. Shteinboc (56) reported that heavy ions can be the products of the combustion of nitrogen-containing organic compounds. These heavy ions can combine with cesium species to form even heavier ions. Allison and coworkers (57) have also reported ions of the type $(M+K)^+$, where M is a molecular analyte species and K is a potassium atom, in an MS where a potassium thermionic emitter is used as the ion source. Whether these phenomena have any connection with the observations described here remains to be seen.

A variation of this theme, and certainly a plausible one, is that species X^- is undergoing an electron transfer reaction with species G to form a high mass negative ion, as shown in Reaction 23.

$$X^- + G \longrightarrow X + G^- \qquad (23)$$

The thermal decomposition of the analyte would still be the rate limiting process for this variation. The experiments performed here with the available equipment and the data obtained tend to support thermal decomposition of the analyte followed by association with

an inorganic species either in the gas phase or at the gas solid interface, with ionization occurring sometime after the decomposition of the analyte. In order to explore the mechanistic and operating principles of the TID-N_2 further, additional experiments as described here, but with use of an MS of higher mass range and with collisional activation, MS-MS (48) capabilities are required.

One final point on this subject is worthy of additional discussion. That is the previously shown (Figure 19) TID-N_2 response dependence on the source bias voltage. As was previously indicated, all responses are continuously and linearly increased by an increasingly negative bias voltage. If the applied field serves only to transport negative ions to the anode, a saturation of response should be observed at field magnitudes much less than the maximum applied -45V, based on calculations. The mobility of the ions in question are determined by the Langevin equation (72) shown as Equation 24,

$$\mu_o = 13.876/(\gamma\, m_r)^{1/2} \quad cm^2/V\ sec \qquad (24)$$

where μ_o is the reduced mobility, γ is the polarizability

of the carrier gas molecules in A^3 and m_r is the reduced mass of the ion and a carrier gas molecule in g/mol. Since the mass of the carrier gas molecule (N_2) is light (28 amu) compared to the mass of the negative charge carrier (>500 amu), the reduced mass converges on the mass of the carrier gas molecule. The mobility is inversely proportional to the reduced mass as shown by Equation 24. Considering these relationships, the mobilities of ions of mass 10,000 amu and greater should be great enough to be swept to the anode by an applied voltage as small as -15V. Furthermore, it has been experimentally observed (55) that once the mass of an ion reaches the 100 amu level, ion mobilities remain essentially constant. Obviously the applied field has some role other than sweeping ions to the anode. Considering the previously discussed mechanisms, one possibility is that the field is facilitating the emission of ions, in a linear manner, from the source surface. The fifth mechanism proposes the formation of a heavy mass ion at the surface of the source, while the sixth mechanism involves formation of a small mass ion at the surface. If the field does assist in the emission of ions from the surface, this would lend credence to mechanisms that involved formation of an ion directly at the source

surface. The final possibility is that the field is assisting the ionization process itself. At any rate, further elucidation of the field's role may lead to a more precise description of the mechanism.

ECD Responses of the Substituted Nitrobenzenes

The responses of the same 36 compounds that were examined in the TID-N_2 were also determined, along with azulene, in an ECD over a wide range of concentrations. Selected peak area calibration curves determined using two different detector temperatures, 200° C and 300° C, are shown in Figures 25 and 26. The degree of linearity varies greatly from compound to compound, some analytes exhibiting quite linear behavior while others behaving quite non-linearly. Very strongly responding compounds, such as the bromonitrobenzenes and the polychlorinated nitrobenzenes, often have upward curving calibration curves. This phenomenon has been previously addressed (58-61) and explained as follows. When a low concentration sample enters the cell, a substantial fraction of the analyte is destroyed by the electron capture reaction because of the large electron capture rate constant and electron density. For small analyte

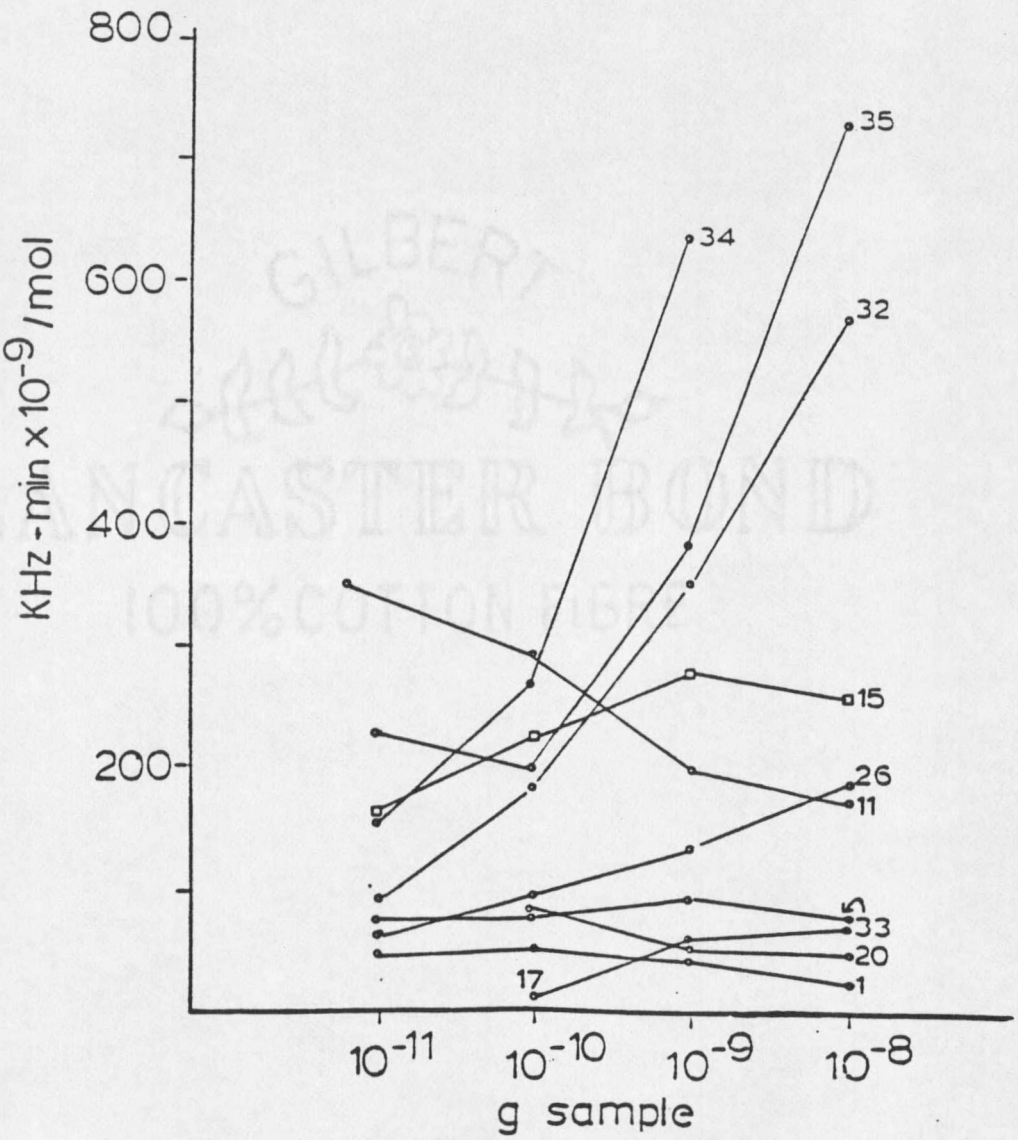


Figure 25. ECD peak area responses to varied amounts of substituted nitrobenzenes at 200° C and 30 mL/min nitrogen. The compound associated with each calibration curve is indicated by the number assigned in Table 3.

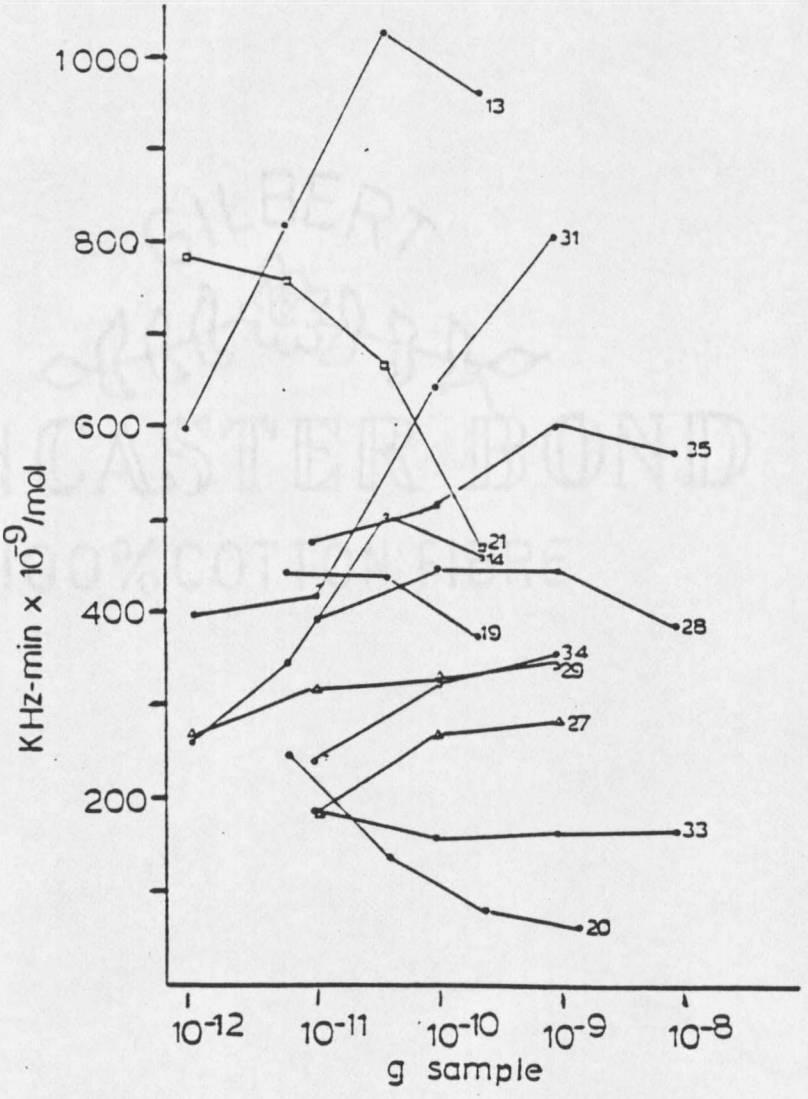


Figure 26. ECD peak area responses to varied amounts of substituted nitrobenzenes at 300° C and 30 mL/min nitrogen. The compound associated with each calibration curve is indicated by the number assigned in Table 3.

concentrations a linear response is observed as long as the electron density remains large and constant, resulting in like fractions of the analyte molecules to be reacted with over this small concentration range. When sample sizes increase, however, a smaller population of electrons reacts with a successively smaller portion of the analyte molecules entering the cell. In the CCP-ECD, the device used for these experiments, the signal is proportional to the instantaneous concentration of the analyte within the detector. The response cannot, therefore, also be linearly related to analyte concentration over the entire dynamic range of the detector.

The peak area responses observed for the lowest concentration of each compound in Figures 25 and 26, in addition to several other compounds, at the two detector temperatures are listed in Table 3 as the absolute response ([KHz-min mol^{-1}] X 10^{-9}) of that substance. The known electron affinities are again listed in Table 3. Also listed in Table 3 are the observed detection limits at which the response to each analyte was approximately five times the noise level. It is obvious from these detection limits that the ECD is superior to the TID-N_2 for the absolute detection of this group of molecules. These compounds are classic ECD analytes, containing large

Table 3. Electron capture detector responses at two detector temperatures.

Compound*	Electron Affinity** (K cal mol^{-1})	Detection Limit 200° (pg)	Absolute Molar Response*** 200°	Absolute Molar Response 300°	Effect**** of Temperature
1. NB	22.1	5	43.0	21.6	0.50
2. m-OCH_3B	22.7	4	57.5	35.9	0.62
3. p-OCH_3NB	19.6	9	13.8	77.1	5.59
4. o-CH_3NB	20.0	5	52.5	7.25	0.14
5. m-CH_3NB	21.4	5	66.4	14.8	0.22
6. p-CH_3NB	20.5	20	29.1	4.65	0.16
7. o-FNB	23.5	3	149	99.7	0.67
8. m-FNB	27.5	6	52.6	66.1	1.26
9. p-FNB	24.3	2.5	82.6	91.9	1.11
10. o-ClNB	25.0	2	97	152	1.57
11. m-ClNB	28.1	0.5	317	374	1.18
12. p-ClNB	27.5	1	182	306	1.68
13. o-BrNB	25.5	1	100	584	5.84
14. m-BrNB	28.8	0.5	288	253	0.88
15. p-BrNB	28.3	1	158	316	2.00
16. o-CNNB	35.1	30	10.4	104	10.0
17. m-CNNB	34.1	15	36.0	79.5	2.20
18. p-CNNB	38.1	3	119	544	4.57
19. o-NO_2NB	36.2	2	272	440	1.62
20. m-NO_2NB	36.2	3.5	82.9	242	2.92
21. p-NO_2NB	43.6	1.5	456	769	1.69
22. m-CF_3NB	30.9	0.5	190	428	2.25
23. 2,3-DNT		2.5	225	289	1.28
24. 2,4-DNT		10	52.9	149	2.82
25. 2,6-DNT		1.5	385	393	1.02
26. 3,4-DNT		7	106	207	1.95
27. 2,4-Cl_2NB		4	36.7	180	4.90
28. 3,4-Cl_2NB		2	56.5	386	6.83
29. 2,3,4-Cl_3NB		3	72.6	399	5.50
30. 2,3,5-Cl_3NB		3	43.2	265	6.13
31. 2,3,4,5-Cl_4NB		4	230	384	1.67
32. 2,3,5,6-Cl_4NB		4	91	248	2.73
33. 1,2,3,4-Cl_4B		3	74.2	186	2.51
34. Cl_5B		2.5	150	234	1.56
35. Cl_6B		5	228	462	2.03
36. Perfluoro benzoquinone	60.2	30	3.73	18.6	4.99
37. Azulene	17.3	30	7.92	0.388	0.049

*B = benzene; NB = nitrobenzene; DNT - dinitrotoluene
**Electron Affinity Values taken from ref. 32
***Peak Areas in (KHz-min mol^{-1}) x 10^{-9}
****Ratio of Absolute Molar Response at 300° to that at 200°

pi systems and electronegative functionalities. The responses, however, vary less from compound to compound than do the TID-N_2 responses. This observation shows that the ECD is the less selective detection device, responding to high electron affinity molecules in general, as opposed to the TID-N_2 which is especially sensitive to molecules with multiple nitro groups.

The effect of temperature of the detector housing on the responses to each compound over the range of 200° to 300° C is listed in the sixth column of Table 3. Most of the compounds have responses that increase significantly with temperature, while a few decrease. Molecules whose responses decreased with increasing temperature usually contained a relatively small degree of electronegative functionality, such as the nitrotoluenes. The dependence of response on the detector temperature will be discussed in more detail later.

Computer Simulations of ECD Response

The first ECD response mechanism that was discussed in Introduction was a resonance electron capture process forming a molecular negative ion. This mechanism was designated mechanism I. Experimental data obtained with the CCP-ECD were compared with simulated data generated by a computer program that modeled the resonance ECD response as a function of a number of different parameters. These parameters included the forward electron capture rate constant (k_1) and the detachment rate constant (k_{-1}). The detachment rate constant is a function of electron affinity and temperature, and was calculated using Equation 25 (65)

$$k_{-1}\ (s^{-1}) = \frac{k_1\ 2.07\ X\ 10^{16} T^{3/2}}{\exp[EA_m/RT]} \qquad (25)$$

where EA_m is the electron affinity of the analyte molecule. The entropy change for the ionization process was assumed to be zero, and the forward electron capture rate constant was assumed to be temperature independent.

Shown in Figure 27 is data generated for several different forward rate constants at a constant electron affinity of 20 kcal/mol. It is obvious that the responses at low temperatures are proportional to the magnitude of the forward rate constant. The program predicts that detachment to reform the analyte molecule and electron does not commence until the 200° C temperature level is reached for a molecule of electron affinity of 20 kcal/mol. At temperatures below 200° C, the response is constant with temperature, therefore the imagined negative ions are not detaching the electron. Since the forward electron capture rate constant is assumed to be constant with temperature, simulated responses will not change as long as the detachment rate constant is negligible. Figure 28 depicts simulated data for several different electron affinity molecules at a constant forward electron capture rate constant of 1×10^{-9} cc molecule^{-1}. The maximum simulated response for each of the different electron affinity molecules is the same. The temperature where simulated responses begin to decrease, however, is dependent upon the electron affinities. This correlates with the fact that the detachment rate constants are dependent upon the electron affinity of the molecule and the temperature. The program predicts that once the

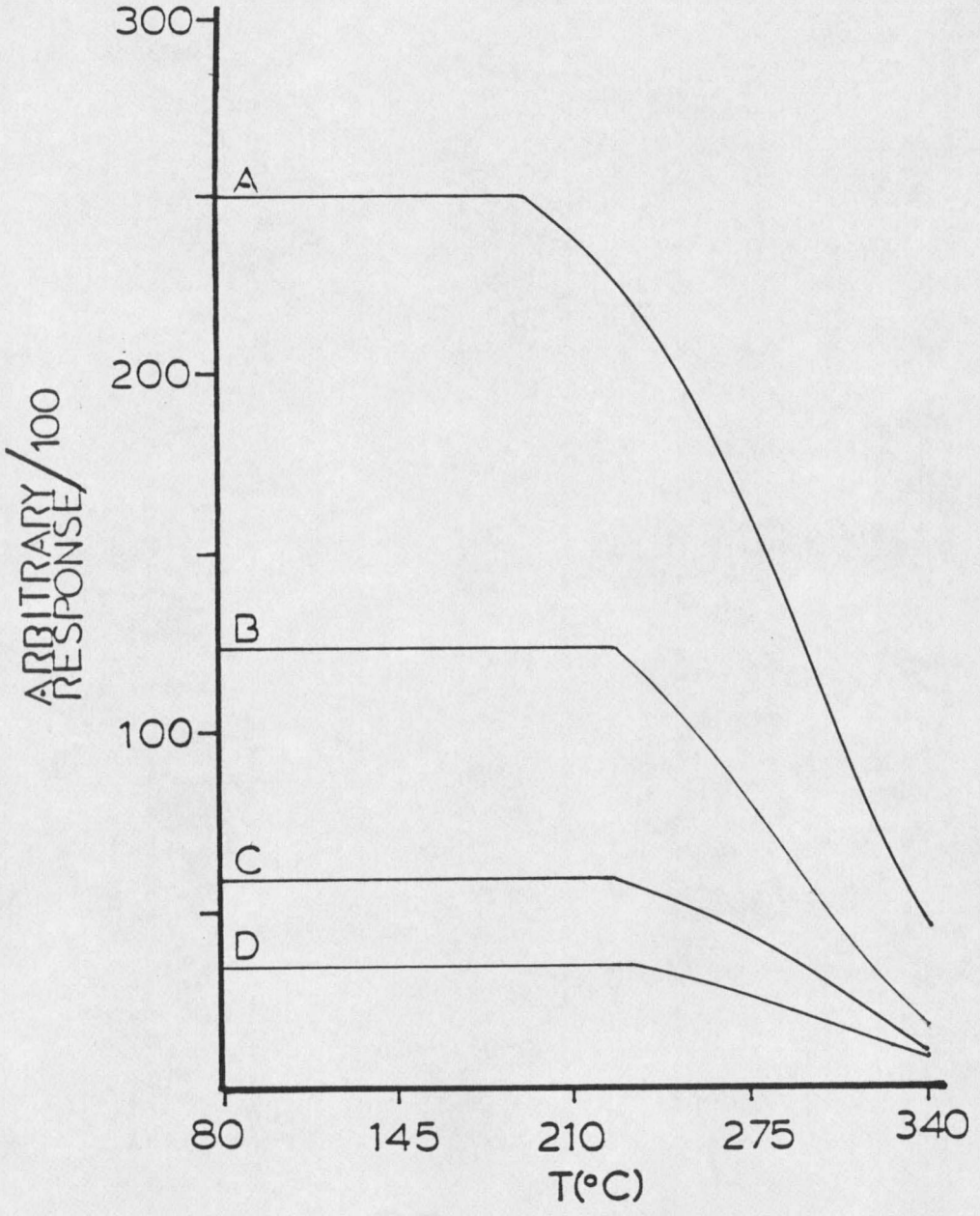


Figure 27. Computer simulated data for the resonance electron capture process. Electron affinity = 20 kcal/mol. Forward attachment rate constants = 1×10^{-7} cc mol^{-1} sec^{-1} (A); 5×10^{-8} (B); 2.5×10^{-8} (C); and 1.25×10^{-8} (D).

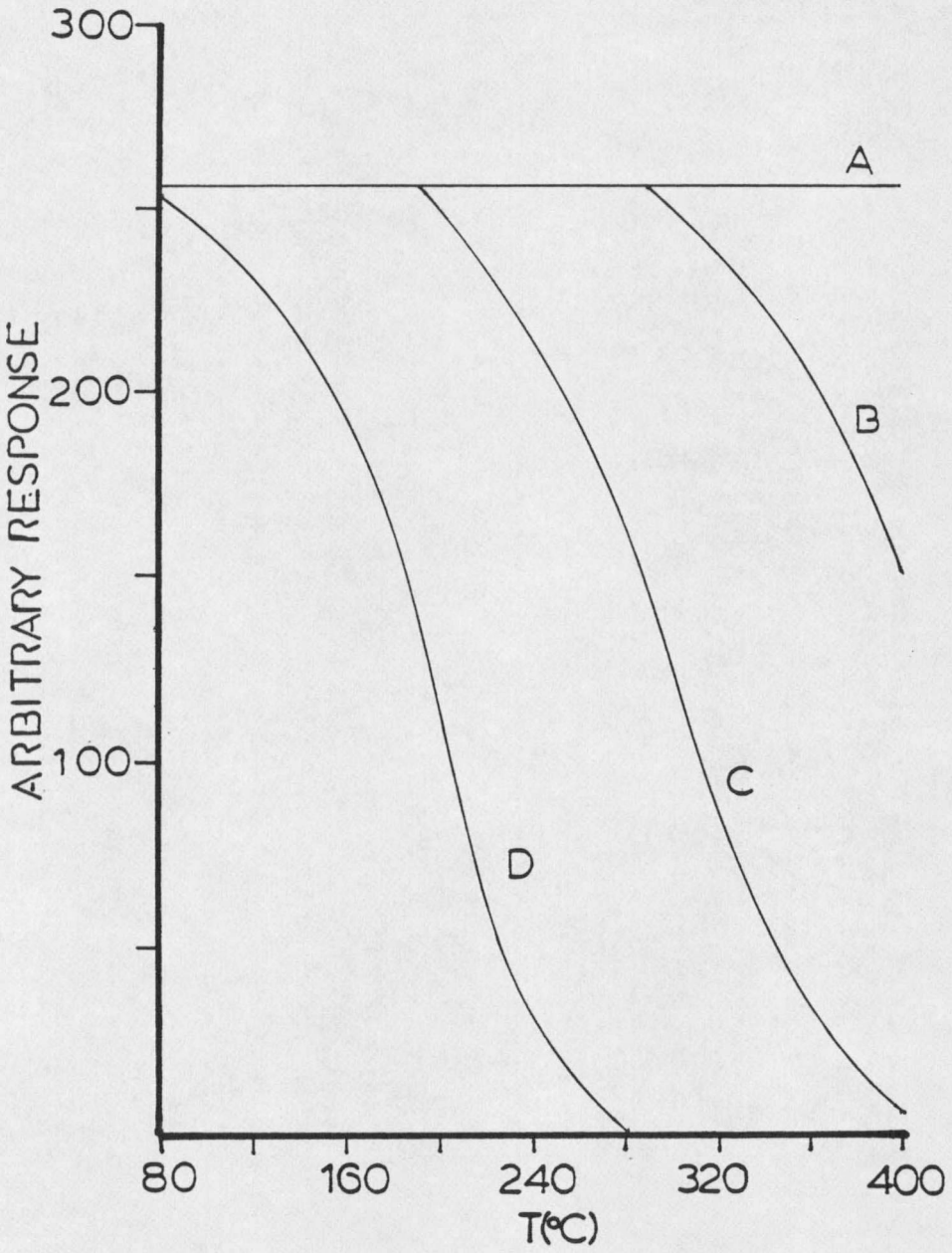


Figure 28. Computer simulated data for the resonance electron capture process. Forward attachment rate = 1 x 10^{-9} cc mol^{-1} sec^{-1}. Electron affinity = 30 kcal/mol (A); 25 (B); 20 (C); and 15 (D).

electron affinity of the molecule reaches a level of 30 kcal/mol, detachment should not be a significant factor throughout the working temperature range of the CCP-ECD, and decreases in response with increasing temperature should not occur.

Comparisons were made between data generated by the computer program and data obtained with the actual CCP-ECD. Figure 29 shows both the experimentally obtained data from a CCP-ECD and the simulated responses for the molecule azulene. One can see that the computer program predicts the actual decrease in response with temperature quite well. In fact, it predicts the temperature at which responses decrease (therefore detachment of the electron) for most molecules whose responses actually decrease with increasing temperature. One can see that the response of azulene actually increases with temperature at low temperatures. The forward electron capture rate constant is assumed to be temperature independent for this program, however, and could not predict this increase in response. This temperature dependence will be discussed in greater detail in the next section.

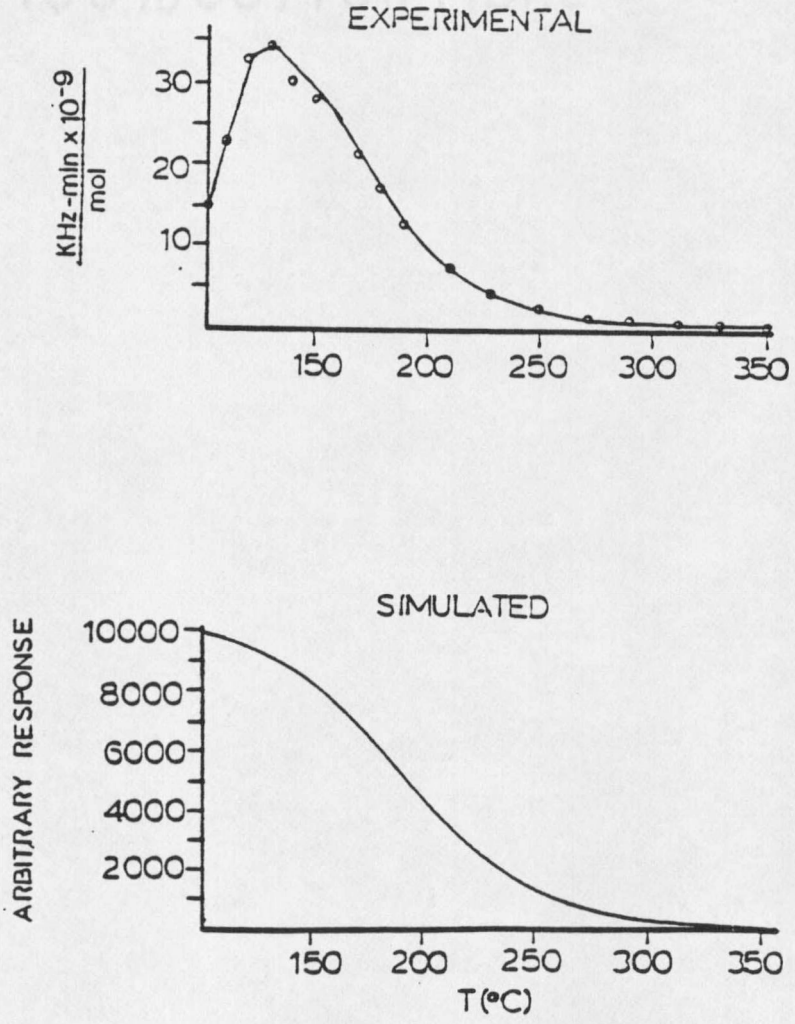


Figure 29. Experimentally determined ECD temperature dependent response curve and computer generated curve to 50 ng azulene. Forward attachment rate constant estimated to be 1.55×10^{-8} cc mol^{-1} sec^{-1} and temperature independent.

ECD Response Mechanisms and Temperature Dependence of Substituted Nitrobenzenes and Azulene

As was pointed out in Introduction, four possible ECD response mechanisms were proposed by Wentworth and coworkers (36, 37, 41). The first, designated mechanism I by these investigators, was shown as Reaction 4 in Introduction. This is a reversible, gas phase capture of an electron by the analyte molecule to form a molecular negative ion. Rate constants for this process vary widely from molecule to molecule, but can be as fast as 10^{-7} cc mol^{-1} sec^{-1} (62). Wentworth and Chen (43) concluded that the data of molecules reacting via this electron capture mechanism and having electron affinities of at least 18.5 kcal/mol would be in the beta region (Figure 2) and the responses would be temperature independent. The beta region corresponds to the kinetic relationship shown in Equation 2 where the recombination rate constant (k_+) is greater than the detachment rate constant (k_{-1}).

Nitrobenzene is a molecule that most certainly responds by forming a molecular negative ion. Its response decreases with the 200^o to 300^o C temperature increase indicating dissociative processes are not occurring, and its electron capture mass spectrum

(Figure 24) indicates only the molecular ion is formed in any abundance at the relatively high temperature of 300° C. Its electron affinity of 22.1 kcal/mol exceeds the 18.5 kcal/mol level where the response should be temperature independent and the data should lie in the beta region. The ECD response of 3.13 ng nitrobenzene was recorded by the author at a wide range of temperatures. This data is shown in Figure 30. Three distinct regions can be identified on this plot. The first is in the temperature range of 80° to 130° C where the response is significantly increasing. This data conflicts with conclusion of Wentworth and Chen (43) that the electron capture process should be temperature independent for this mechanism, and, in fact, disagrees with their data (37) for this molecule, shown in Figure 31. Their data were recorded using a tritium source, FFP-ECD, while the data here were obtained with the ^{63}Ni source, CCP-ECD previously described in Introduction and Experimental. The second region identified in Figure 30 is indeed one of temperature independence, occurring between 130° and 240° C. Any variations in response here are probably due to experimental and random errors. Up to the 240° C temperature level, the negative ions are undergoing recombination with positive ions before detachment of the

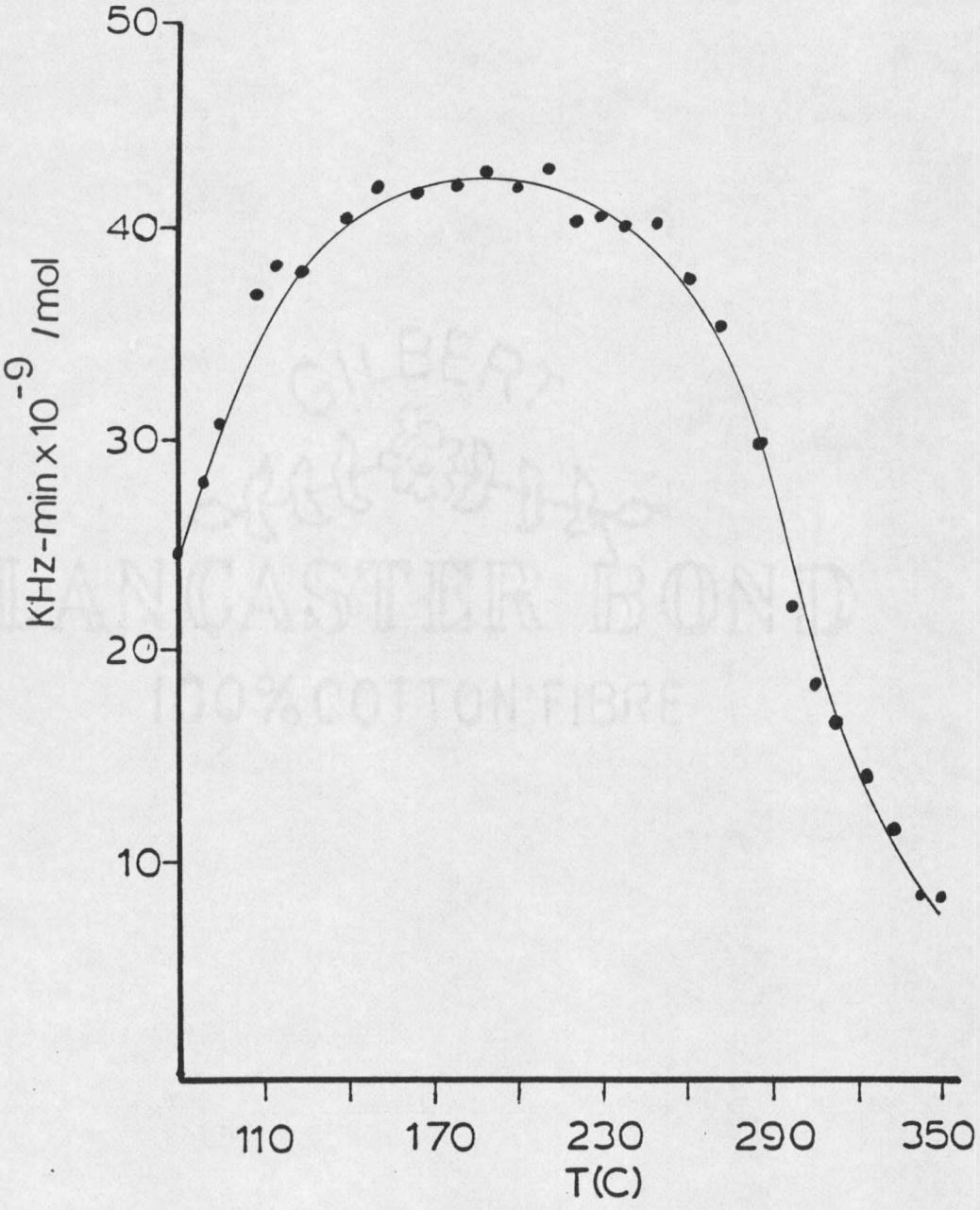


Figure 30. ECD temperature dependence response curve of 3.13 ng nitrobenzene.

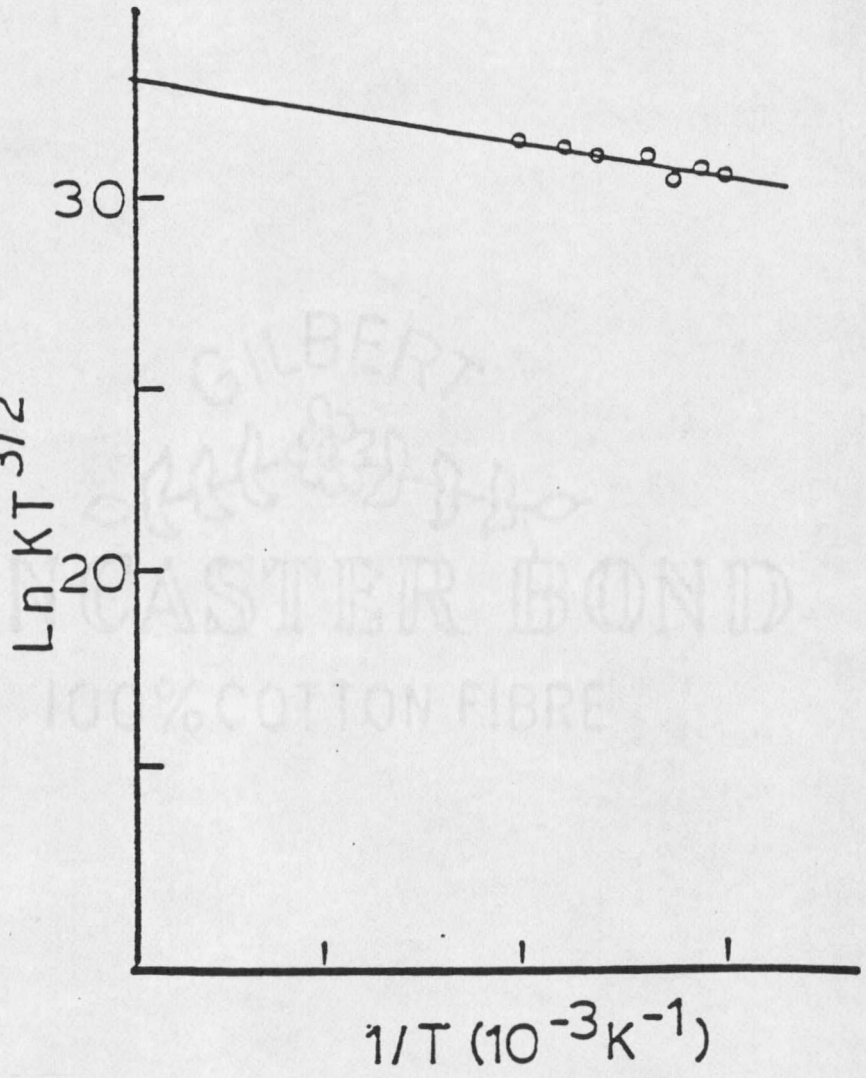


Figure 31. Ln $KT^{3/2}$ versus 1/T plot for ECD response of nitrobenzene obtained experimentally by Wentworth and Chen (37).

electron can occur. Finally, the third region in Figure 30 occurs between the temperatures of 240° and 350° C. The electron affinity of the molecule is not sufficiently high to prevent the electron from detaching to the original analyte molecule and electron at these temperatures. This detachment region corresponds to an alpha kinetic relationship (Figure 2 and Equation 9) where the detachment rate constant is larger than the recombination rate constant. A ln $KT^{3/2}$ versus 1/T plot for the author's data is shown in Figure 32, indicating the alpha detachment region absent from Wentworth and Chen's prediction and data. The detector that they used for their experiments and for formulating their mechanistic proposals had a maximum temperature limit of 250° C and it appears this is the temperature where detachment of the nitrobenzene negative ion begins.

Nitrobenzene was not the only molecule for which these results were obtained. Figure 33 shows the temperature dependence curves of the three isomers of nitrotoluene. All have a region of increasing response at low temperatures, followed by a temperature independent region and a region of response that decreases significantly with temperature. Again, the most interesting feature of this data is at the low temperature

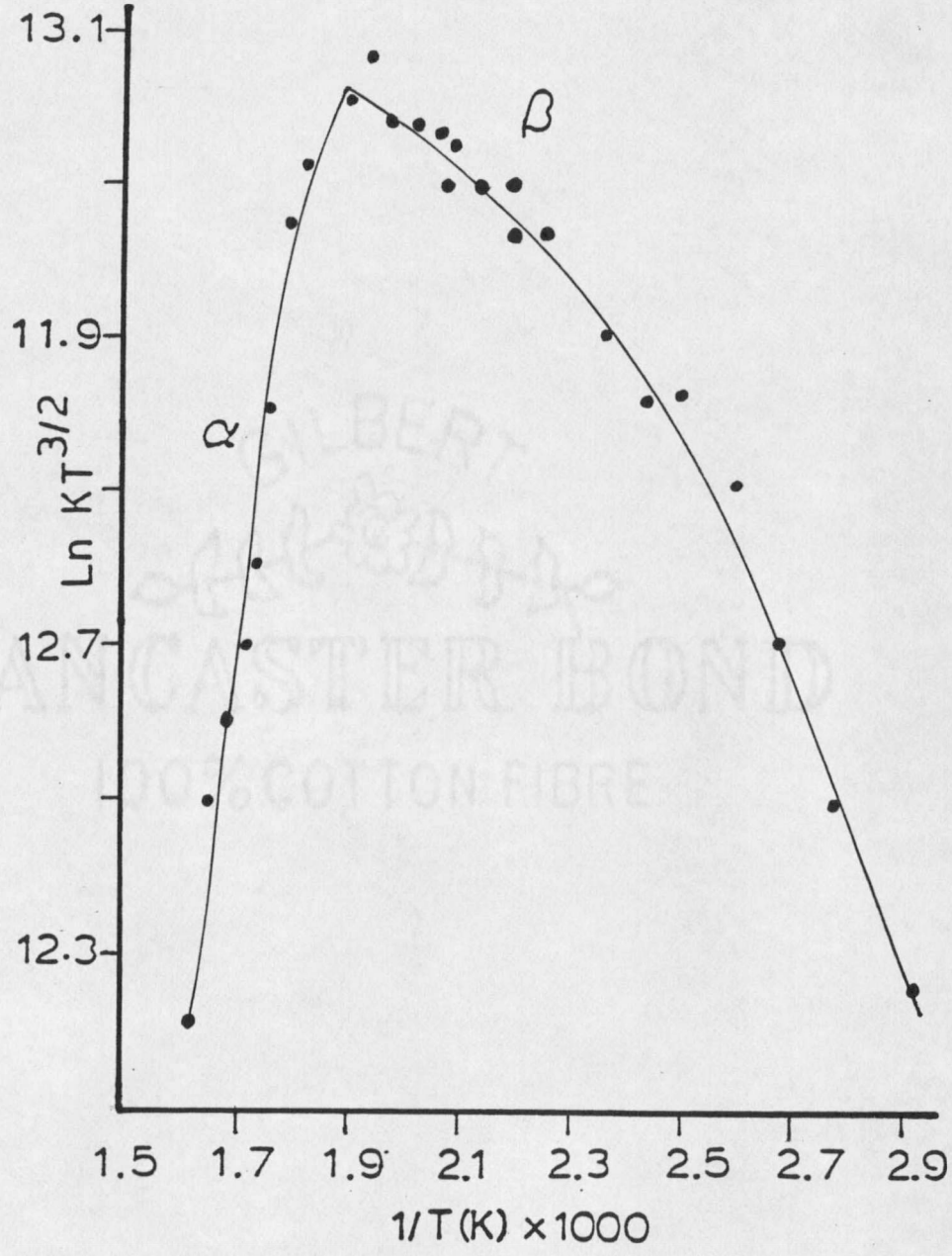


Figure 32. Ln $KT^{3/2}$ versus 1/T plot for ECD response of nitrobenzene, data obtained by author.

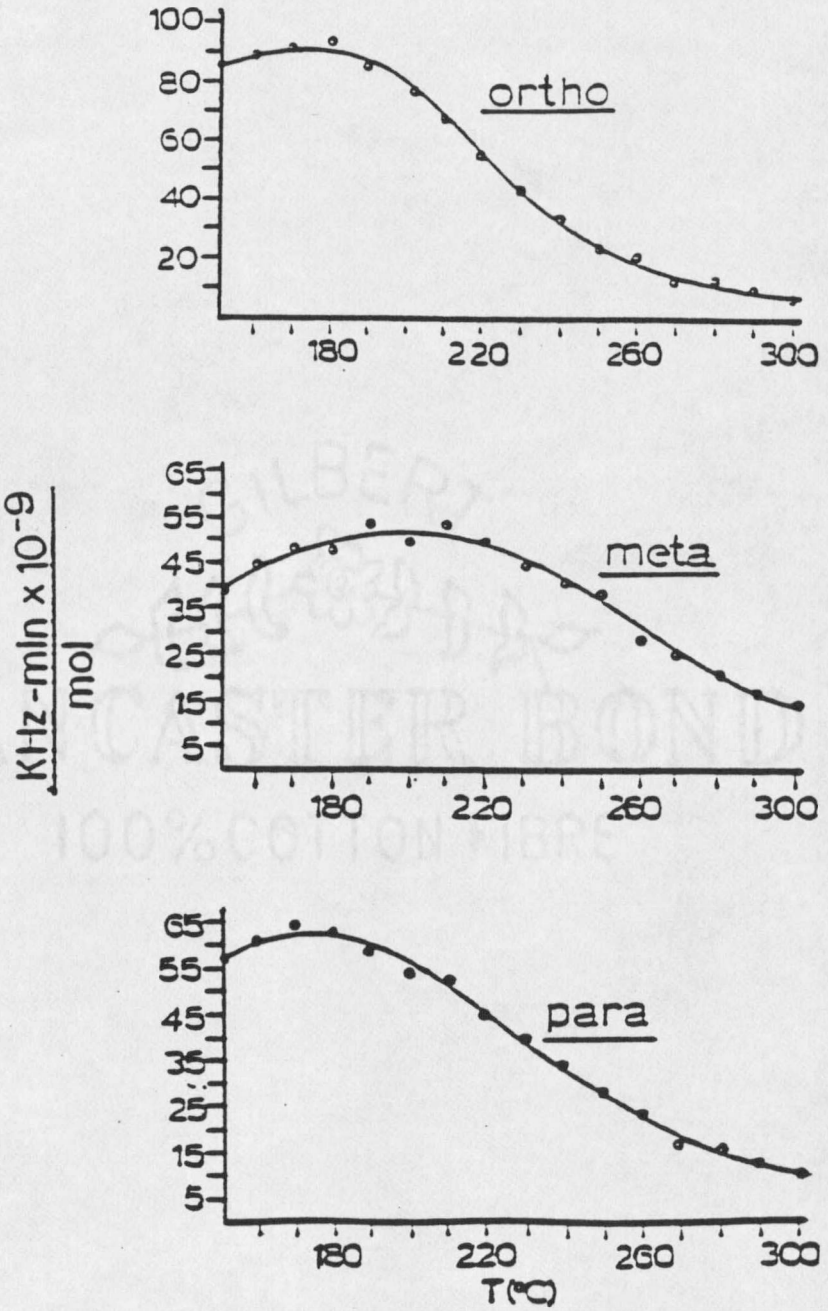


Figure 33. ECD temperature dependence curves for 100 pg o-nitrotoluene, 1 ng m-nitrotoluene, and 1 ng p-nitrotoluene.

levels where it is obvious that the electron capture process is not temperature independent.

The fluoronitrobenzenes provided an example of how isomeric variations can make a significant difference in the absolute ECD response and the response mechanism by which the analyte responds. Figure 34 shows the response as a function of temperature for each of the three isomers. The ortho isomer has a rather peculiar temperature dependence curve with four distinct regions. This molecule appears to be responding via response mechanism III or IV, whose potential energy and temperature dependence curves were shown in Figures 5-7. These two mechanisms involve formation of a molecular negative ion at low temperatures and a two-step dissociative ionization at high temperatures. The two mechanisms are very similar and cannot be differentiated by these experiments. The molecule's response is increasing from 150° to 200° C, again showing the forward electron capture rate constant is not temperature independent. Here, the recombination of the molecular negative ions with positive ions is occurring more rapidly than detachment. After a brief period of temperature independence, the response decreases, due to detachment, corresponding to the alpha detachment region of Figure 6.

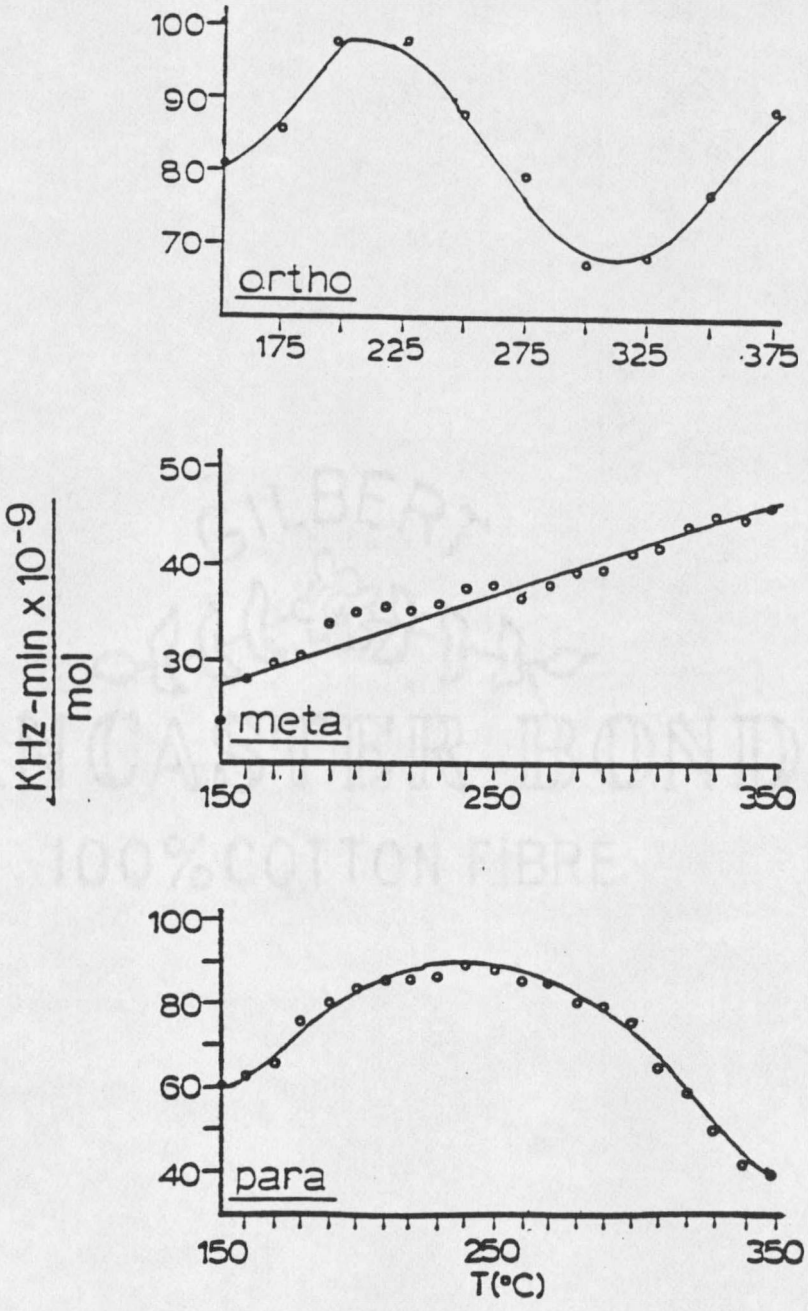


Figure 34. ECD temperature dependence curves for 4.53 ng o-fluoronitrobenzene, 2.67 ng m-fluoronitrobenzene, and 3.76 ng p-fluoronitrobenzene.

Here the detachment process is occurring more rapidly than both the recombination reaction and the dissociation reaction because the molecule's electron affinity (23.5 kcal/mol) is insufficient to retain the electron at temperatures of these magnitudes. Finally, at 300° C, the response begins to increase again with temperature. At this point the molecular negative ion AB^- is dissociating to form either A^- and $B^\cdot$ or B^- and $A^\cdot$. This dissociation corresponds to the gamma region of Figure 6 where the dissociation occurs more rapidly than the molecular negative ion - positive ion recombination. This mechanistic scheme is supported by the electron capture mass spectra for o-fluoronitrobenzene, shown in Figure 35. It can be seen from these spectra that at 200° C, the molecular negative ion (m/e=141) is formed in the greatest abundance, while at 300° C, the NO_2^- ion (m/e=46) dominates the spectrum. Therefore, the terminal ion formed in the ECD dissociative response mechanism is probably the NO_2^- ion. An alternative explanation for the increase of response beginning at 300° is that the molecule is now responding via mechanism II (Figures 3 and 4), which is a single, bimolecular dissociative electron capture reaction (Reaction 10) which does not involve the formation of a molecular negative ion.

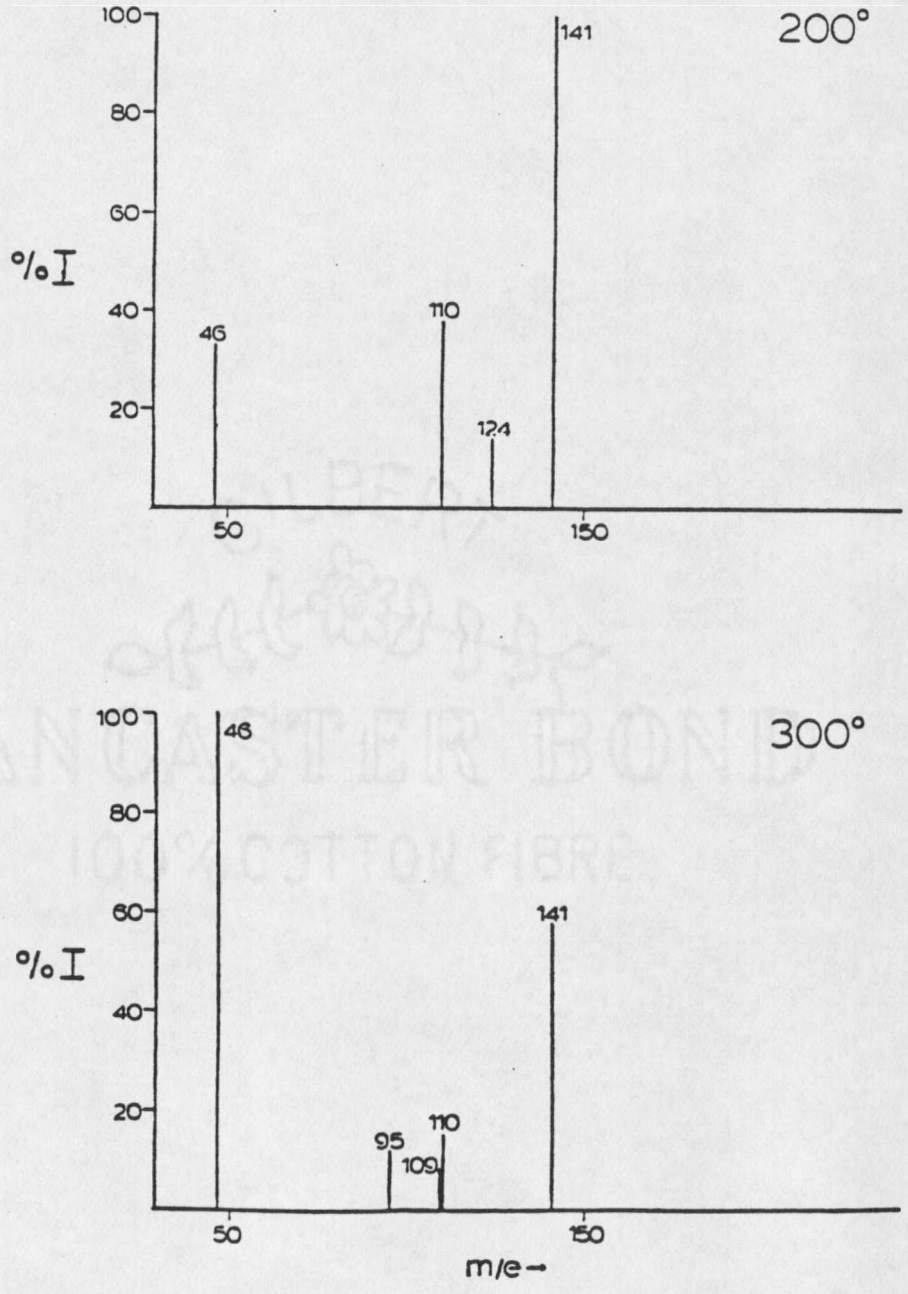


Figure 35. Electron capture mass spectra of 4.53 ng of o-fluoronitrobenzene at 200° and 300°.

The temperature dependence curve of m-fluoronitrobenzene, shown in Figure 34, increases continuously and relatively consistently with temperature. One might expect that the molecule is undergoing a dissociative electron capture process, as this is favored by higher temperatures. However, the electron capture mass spectra, shown in Figure 36 at 200° C and 300° C, lend evidence that something else is occurring. At 200° C the molecular ion (m/e=141) is the only ion of consequence. The 100° C temperature increase does increase the degree of fragmentation, but the molecular negative ion is still by far the most abundant. What must be happening here is that resonance electron capture (mechanism I) is occurring throughout the temperature range investigated, and the forward electron capture rate constant is not temperature independent but is increasing with temperature. The electron affinity is sufficiently high (27.5 kcal/mol) to prevent detachment even at 350° C.

The temperature dependence response curve for p-fluoronitrobenzene is also shown in Figure 34. The appearance of this curve is similar to that of nitrobenzene, with a section where response increases with temperature, a temperature independent region, and a region where responses decrease with temperature. The

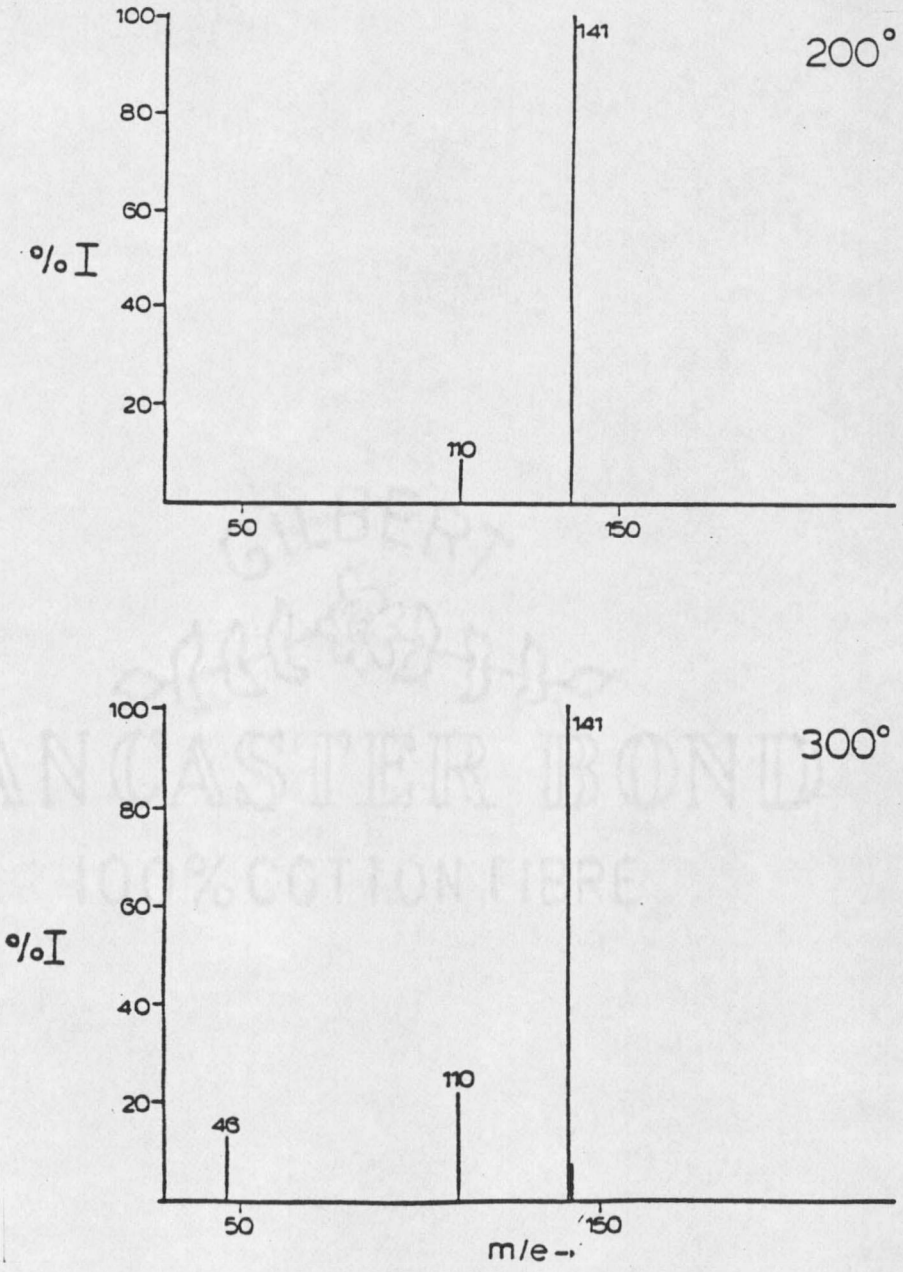


Figure 36. Electron capture mass spectra of 2.67 ng of m-fluoronitrobenzene at 200° and 300°.

difference between the temperature dependence of nitrobenzene and p-fluoronitrobenzene is that detachment commences at a higher temperature (300° C versus 200° C) for p-fluoronitrobenzene due to its higher electron affinity (24.3 kcal/mol versus 22.1 kcal/mol). This also explains the temperature dependence differences between the para and meta isomers of fluoronitrobenzene, therefore, the para isomer has the lower affinity (24.3 kcal/mol versus 27.5 kcal/mol) and detaches the election more readily at the higher temperatures. At this point it is fairly easy to predict the mass spectra of p-fluoronitrobenzene. One would expect the molecular anion (m/e=141) to be the most abundant ion at both 200° and 300° C, and this is in fact the case, as is shown in Figure 37. The para isomer also has a greater tendency toward fragmentation than does the meta isomer, as is evidenced by the greater abundance of the NO_2 ion in the mass spectrum of the para isomer.

Azulene, which has an electron affinity of 17.3 kcal/mol, is a molecule that should have data in the alpha and beta region, according to the conclusions reached by Wentworth and Chen (43) on electron capture mechanism I. The temperature dependence plot obtained by the author was shown previously in Figure 29. The response does indeed

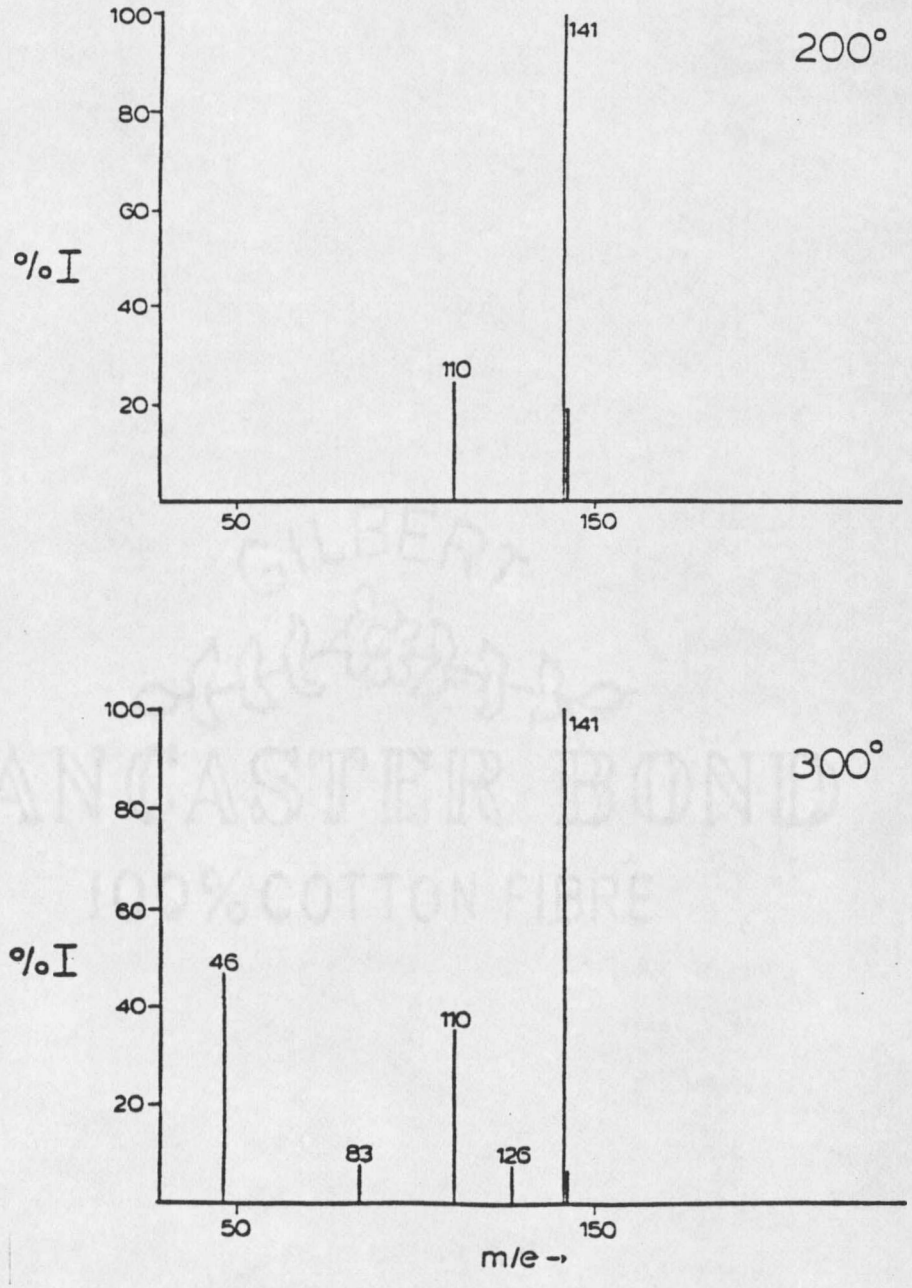


Figure 37. Electron capture mass spectra of 3.76 ng of p-fluoronitrobenzene at 200° and 300°.

decrease substantially once the detector temperature reaches 130° C, but no temperature independent region of response is observed. Again, the response is increasing until detachment begins, indicating that the forward resonance electron capture rate constant is not temperature independent but is increasing with temperature.

A molecule whose response increases with temperature, but for a different reason, is p-bromonitrobenzene. Figure 38 is the ECD response curve as a function of temperature. The curve is similar to that of m-fluoronitrobenzene, but a different mechanism is probably occurring. Electron capture mechanism II, previously described in Introduction, is a single, bimolecular electron attachment leading immediately to dissociation. The electron capture mass spectra of p-bromonitrobenzene, shown in Figure 39, seem to suggest that this mechanism is responsible for the ECD response and temperature dependence. The only ions observed are the two isotopes of the Br^- ion (m/e=79,81) at both 200° C and 300° C. These ions are observed in a nearly 50:50 ratio due to the nearly equal abundance of ^{79}Br and ^{81}Br. Some variations of this ratio appear in the mass spectrum due to a possible detector mass bias. The increase in ECD

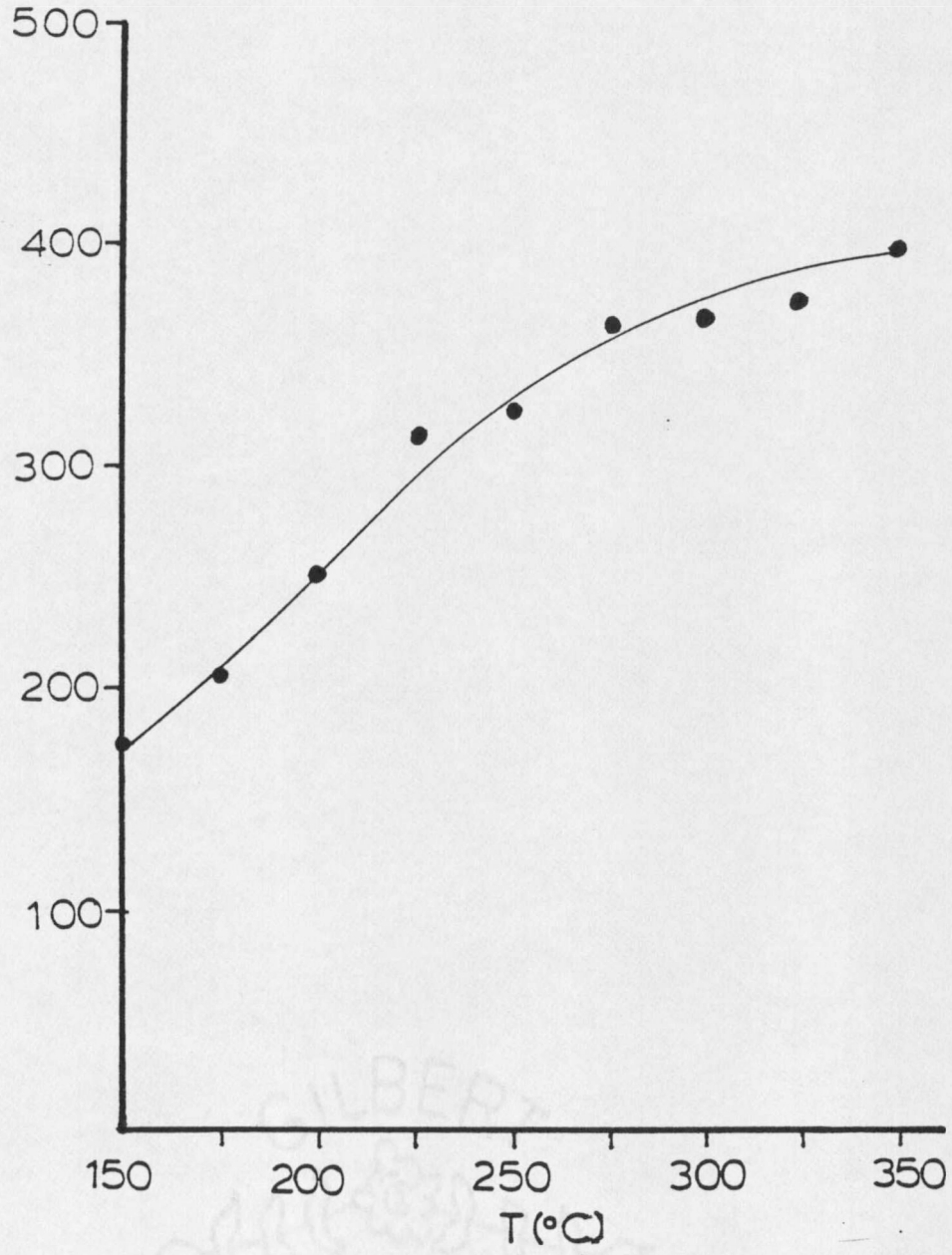


Figure 38. ECD temperature dependence response curve of 128 pg of p-bromonitrobenzene.

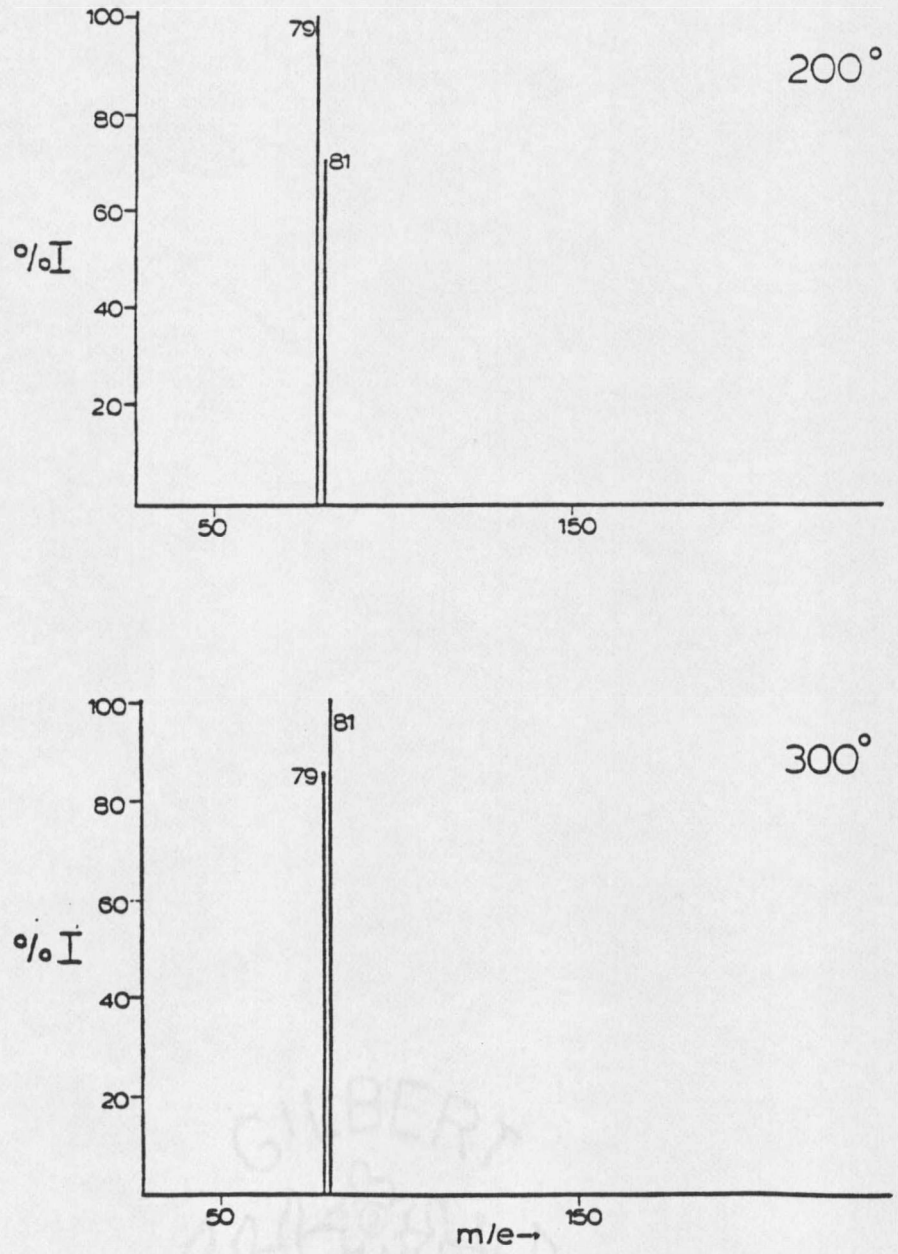


Figure 39. Electron capture mass spectra of 128 pg p-bromonitrobenzene at 200° C and 300° C.

response with temperature is expected because the dissociative process is favored by higher temperatures.

It appears then, that the forward resonance electron capture rate constant is not temperature independent, at least at low temperatures. It may, in fact, never be temperature independent. There are temperature ranges where the responses of nitrobenzene and other molecules are not affected by changes in detector temperature. This may be due, however, to a combination of attachment, detachment, and recombination rate constant magnitudes that produce unchanging responses, and not due to a constant attachment rate.

ECD Responses to Quinones and Electron Affinity Dependence of Responses

Three high electron affinity molecules whose responses were not determined in the TID-N_2 but were examined in the ECD are 1,4-benzoquinone (BQ), 2-methyl-1,4-benzoquinone (MBQ) and 1,4-naphthoquinone (NQ). The electron affinity of these molecules is 41.7, 40.4 and 39.5 kcal/mol, respectively (32). As was discussed in Introduction, Wentworth and Chen (37) deduced Equation 7 for the dependence of ECD response on a molecule's

electron affinity. According to this equation, a molecule with a high electron affinity should have a large ECD response, and therefore, a large electron capture rate constant.

By examining the structure of these quinones, one must conclude that these molecules would capture an electron non-dissociatively, as there are no electronegative functionalities that could readily detach from the molecule. Because the electron affinities of these molecules are so large, however, one would expect a large ECD response via resonance electron capture processes. A molecule of similar electron affinity, p-dinitrobenzene (43.6 kcal/mol), responds quite well in the ECD, producing a measurement of 456 KHz-min X 10^{-9}/ mol at 200^{o} C, as was shown in Table 3. Shown in Table 4 are the responses of the three quinones, and one can see that the responses of BQ and MBQ are nearly insignificant compared to that of p-dinitrobenzene.

The lowest electron affinity quinone, NQ, gives a reasonably large response, but still far smaller than p-dinitrobenzene. It is obvious from this data in Table 4 that a high electron affinity is not a guarantee for a

large ECD response. In fact, the order of response magnitude is reversed compared to the electron affinity values.

Table 4. ECD_{-9} responses (response per mole in KHz-min x 10^{-9}) of 20 ng 1,4-benzoquinone (BQ), 32 ng 2-methyl- 1,4-benzoquinone (MBQ) 1 ng 1,4-naphthoquinone (NQ).

BQ		MBQ		NQ	
200°C	300°C	200°C	300°C	200°C	300°C
.211	.344	.458	.729	75.2	116.6

There are several cases shown previously in Table 3 where strict dependence of response on molecular electron affinity does not exist. Shown in Table 5 are the responses of several molecules that are assumed to undergo resonance electron capture because their responses begin to decrease at higher temperatures, indicating detachment of the electron from the molecular negative ion. The responses listed were recorded at the temperature at which

Table 5. Maximum responses of resonance electron capture molecules and their calculated electron attachment rate constants.

Compound	Amt.*	EA**	T(max)***	Response****	k_1 *****
nitrobenzene	3.13	22.1	200	44.1	1.99×10^{-8}
o-nitrotoluene	1	20.0	170	69.3	3.13×10^{-8}
m-nitrotoluene	1	21.4	210	53.1	2.40×10^{-8}
p-nitrotoluene	1	2.05	170	64.3	2.90×10^{-8}
azulene	5.83	17.3	130	34.3	1.55×10^{-8}
1.4-benzoquinone	20	41.7	300	.333	1.5×10^{-10}
p-fluoronitrobenzene	3.76	24.3	240	89.1	4.03×10^{-8}
m-chloronitrobenzene	1.77	28.1	300	285	1.29×10^{-7}
o-dinitrobenzene	0.13	36.2	300	440	1.99×10^{-7}

* Nanograms
** Electron affinity in Kcal/mmol from ref. 32.
*** Temperature at which response is maximized
**** Molar response in KHz-min x 10^{-9}
***** Resonance electron capture rate constant in cc mol^{-1} sec^{-1}

the response is optimized. Also listed in Table 5 are the molecular electron affinities and the calculated forward electron capture rate constants. The rate constants were calculated using p-fluoronitrobenzene as the reference. The resonance electron attachment rate constant of p-fluoronitrobenzene was calculated from electron transfer equilibria of this molecule with C_7F_{14} (32), whose electron attachment rate constant is known (73). A plot of these calculated rate constants versus the molecular electron affinities is shown in Figure 40. One can see from this figure that a correlation between electron affinity and the forward electron capture rate coefficient is not necessarily observed. The temperature dependence curves of BQ, MBQ and NQ are shown in Figure 41. Significant decreases in ECD response are not observed with increasing temperatures, indicating that once the molecular negative ion is formed, it does not detach the electron due to the molecule's high electron affinity. This would seem to indicate that the ECD response is small due to a slow electron capture rate constant and not because of detachment.

The electron capture mass spectra of BQ, MBQ and NQ, shown in Figure 42, lend further evidence that the

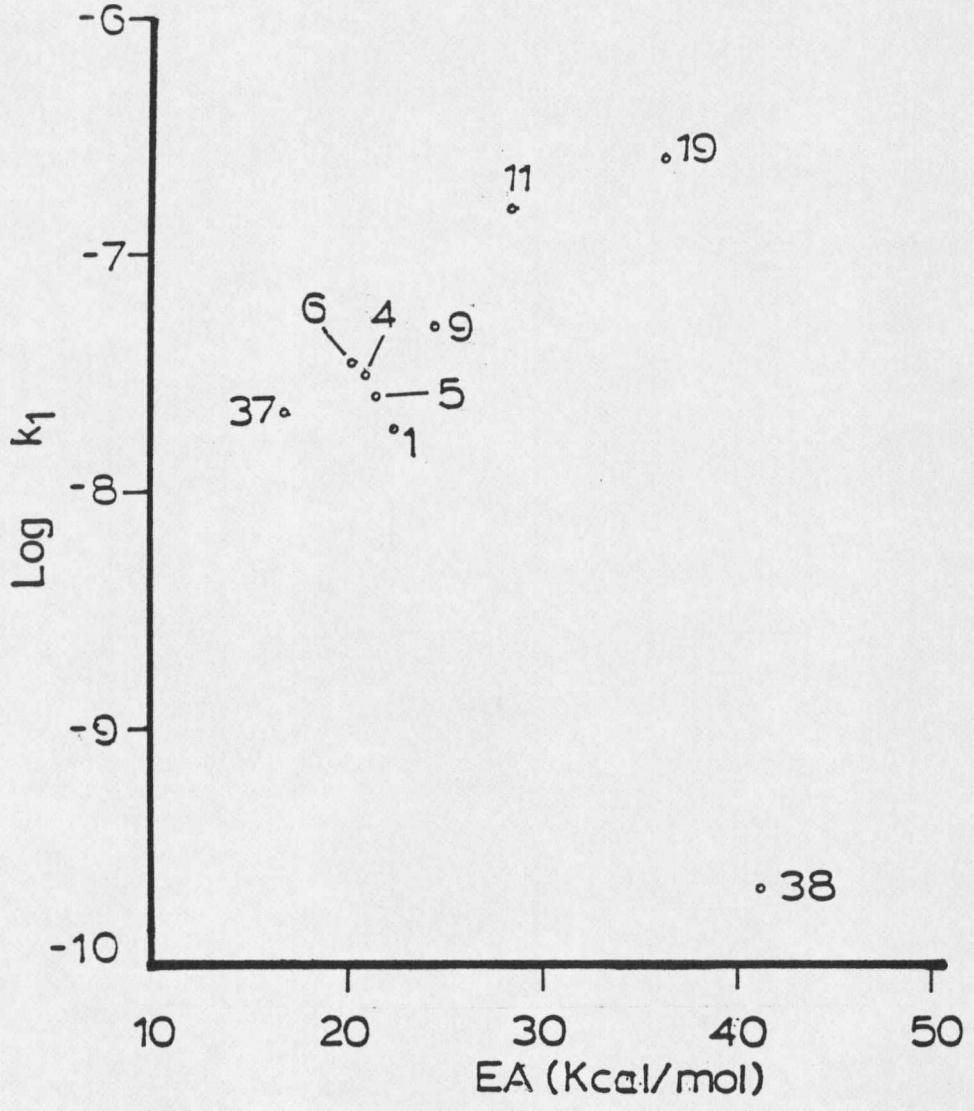


Figure 40. Plot of calculated resonance electron capture rate constants versus molecular electron affinity. Nitrobenzene = 1; o, m, p-nitrotoluene = 4, 5, 6, respectively; p-fluoronitrobenzene = 9; m-chloronitrobenzene = 11; o-dinitrobenzene = 19; azulene = 37; 1,4-benzoquinone = 38.

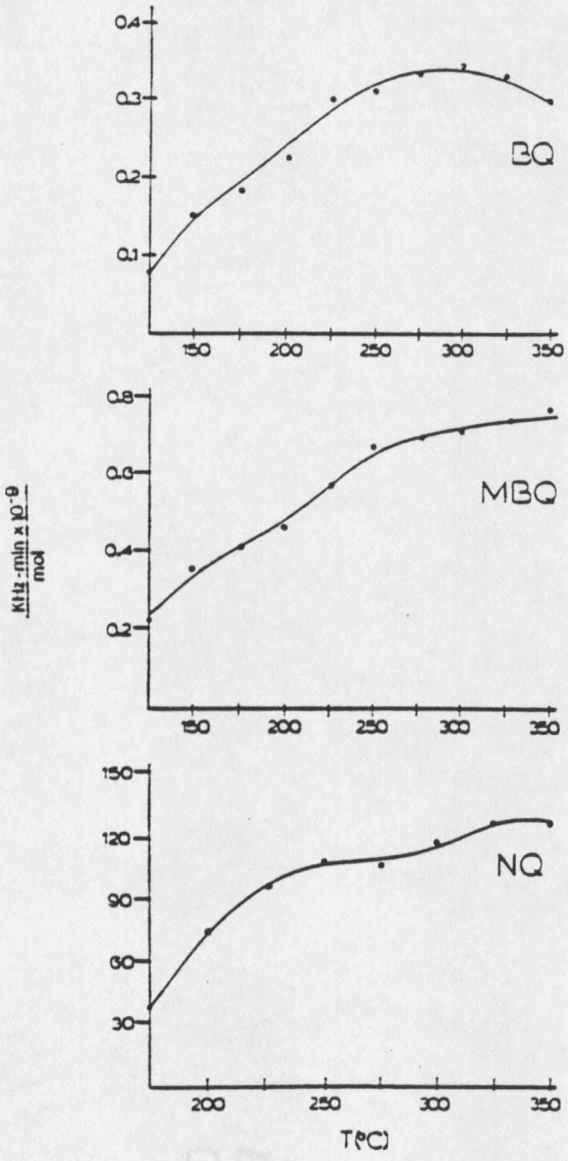


Figure 41. ECD temperature dependence response curves for 20 ng BQ, 32 ng MBQ, and 1 ng NQ.

electron attachment rate constants are small for the high electron affinity molecules BQ and MBQ. For a molecule undergoing resonance electron attachment, one would expect the molecular ion to be the base peak in the spectrum. The only one of the three quinones that produces the molecular negative ion as the base peak is NQ (m/e=158), which, incidentally, also generated the largest ECD response. In fact, the only ion of significance in the spectrum of NQ was the base peak. The spectra of BQ and MBQ are much more complex. Numerous ions, most of them greater in mass than the respective molecular ions (m/e=108,122) are seen in the negative ion mass spectra for these two molecules. It is obvious that some complex chemistry is occurring within the ion source, possibly on the source walls, when these two compounds enter the high temperature atmosphere of an ECMS source. At any rate, the electron attachment rate constant for formation of a molecular negative ion from BQ and MBQ must be relatively small, even though their electron affinities are quite large. The order of molecular ion abundance for the three quinones is the same as the ECD response magnitudes, and in reverse order of the molecular electron affinities.

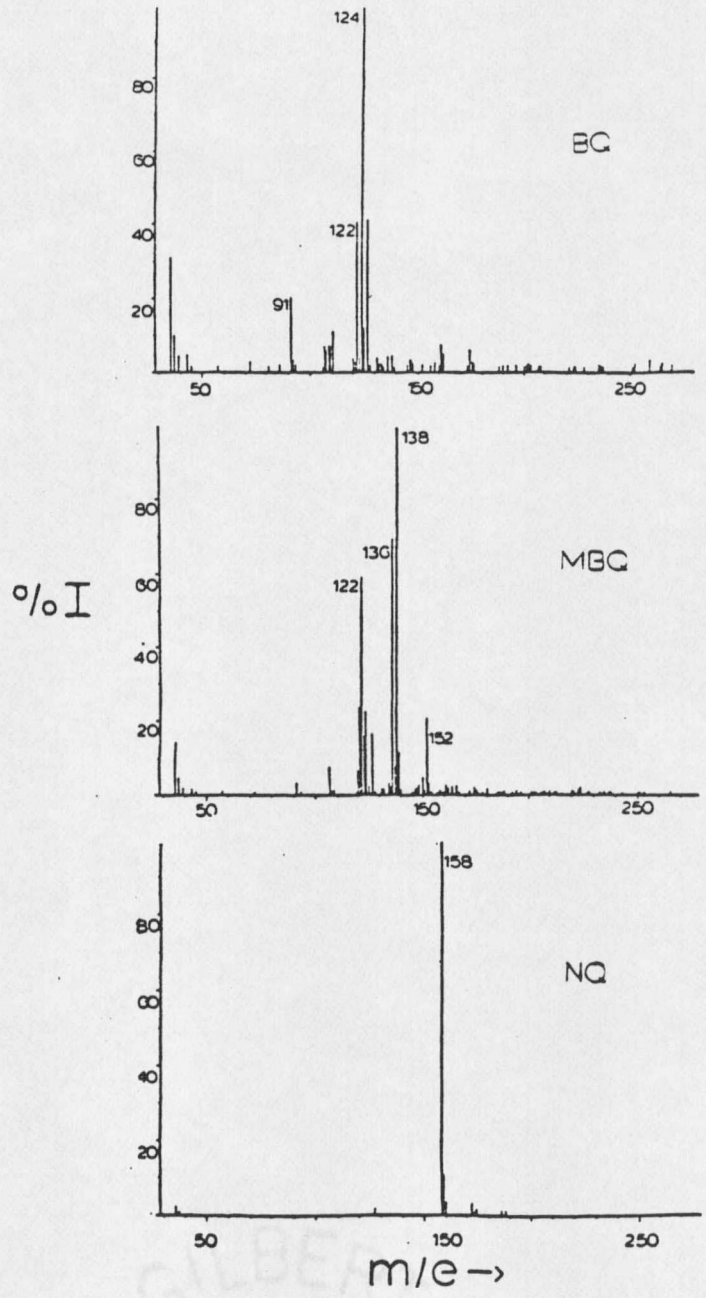


Figure 42. Electron capture mass spectra of 10 ng each BQ, MBQ, and NQ at 200° C.

From this data, it is obvious that just a high electron affinity is not a guarantee of a large ECD response. Another molecule that has a high electron affinity (53 kcal/mol) (31, 32) but a small electron capture rate constant (71) is NO_2. Possibly BQ and MBQ are rigid systems like NO_2, or may undergo large geometry changes during negative ionization leading to a small electron capture rate constant and hence small ECD response.

Comparison of the Detection Techniques

At first glance, the TID-N_2 and the ECD appear quite similar in that they both are selective to electronegative compounds and both generate an analytical signal by producing gas phase negative ions. The manner in which the ions are produced, however, is quite different, the ECD using beta radiation, the TID-N_2 employing a heated solid surface. One of the objects of this study was to find out if the TID-N_2 could be a non-radioactive substitute for the ECD. The conclusion at this point is that it is not, but can be applied more successfully than the ECD in certain situations.

For the molecules discussed here, most of them substituted nitrobenzenes, the ECD is the superior GC

detection device. The absolute detection limits are lower in the ECD for almost all the molecules except a few of the dinitro compounds. Response linearity varies widely from compound to compound in each detector and with the physical parameters of each. The TID-N_2 is a more selective device, responding very well to dinitro-organics and less well to halogenated compounds. Halogenated species are often-times contaminants in environmental samples, and for the selective detection of nitro compounds in a complex matrix, the TID-N_2 would be superior to the ECD.

The TID-N_2 has another advantage over the ECD, and that is it is less susceptible to carrier gas contaminants, especially oxygen. The data in Table 2 show that the TID-N_2 was not drastically affected by varying the detector gas atmosphere. Oxygen contamination is a serious problem in ECD-GC analyses (35, 63, 64) and removal of this gas from the system is critical. Trace amounts of oxygen in the TID-N_2-GC system is a trivial problem at worst.

It has also been noticed in this study that the use of chlorinated solvents is quite feasible during TID-N_2 analyses while nearly impossible for ECD experiments. By turning off the source heating current of a TID-N_2

during elution of the solvent, analyte signal interference and baseline disturbance are avoided. The ECD, however, responds so strongly to these solvents (CCl_4 and $CHCl_3$, for example) that the baseline may be unacceptable for long periods following injections, preventing accurate analysis of the analyte signal.

CONCLUSION

Both detectors have proven to be successful devices for the analyses of substituted nitrobenzenes. The ECD is the more universal of the two detectors, while the TID-N_2 is very selective to certain molecules. Neither detector displays a strict response dependence on the molecular electron affinity.

Little was known about the way a negative ion was generated in the TID-N_2 at the onset of the study. Six TID-N_2 candidate response mechanisms were considered. These varied from a simple electron transfer from the source to the analyte to more complex reactions involving inorganic species. Two response mechanisms, both involving thermal decomposition of the analyte followed by association with an emitted inorganic species provide the best explanations of the results. The differences between the two mechanisms are where association with inorganic species occurs (gas phase versus gas-solid interface) and when ionization occurs (before or after association with inorganic species). These mechanisms explain the anomalous responses of the nitrotoluenes, the observation of high mass ions in the APIMS, and the consistent plugging of the APIMS aperture. These two mechanisms are extensions of the second proposed mechanism, thermal

decomposition of the analyte followed by electron attachment, and are consistent with the results supporting that mechanism. The details of precisely what is occurring at the source surface when an analyte enters the detector cell are still not well understood. Perhaps a better explanation of the response dependence on the bias voltage would shed light on the fundamental processes occurring at the source surface. It appears at this point that increases in the field strength either assist in the ionization or the emission of ions. The response of the TID-N_2 definitely does not depend upon the analyte molecule's electron affinity, but a high electron affinity decomposition product, such as NO_2, most likely assists in the negative ionization process.

It was previously known that molecules responded in the ECD either dissociatively or non-dissociatively. By correlating the ECD response temperature dependence with the electron capture mass spectra of certain compounds, response mechanisms throughout the working temperature range of the detector were elucidated. It was found that molecules which respond via resonance electron capture do not have a temperature independent forward electron attachment rate constant, at least at low detector temperatures. The rate constant may never be constant

over the working temperature range of the detector, and the right combination of detachment, recombination, and attachment rate constant magnitudes may be responsible for temperature independent response curves. Molecular ions of molecules with electron affinities higher than 18.5 kcal/mol can indeed detach their electrons to re-form the original molecules and electrons. This may not have been observed before due to the low temperature limit of a tritium source ECD.

The response of the ECD does not bear a strict dependence on electron affinity, as the responses of the quinones clearly indicated. For these molecules, the ability to form a molecular negative ion correlated strongly with the magnitude of the ECD response. High electron affinity does not guarantee a large electron capture rate constant. Possibly molecular rigidity and geometry changes during ionization may deter the formation of a molecular negative ion.

Computer modeling of resonance electron capture processes showed that the forward attachment rate constant determines the magnitude of ECD response at low temperatures while the electron affinity determines response levels at high temperatures. Experimental data correlated well with simulated data for ions that detach

the electron at higher detector temperatures. Modeling predicted that ions of molecules with electron affinities higher than 30 kcal/mol should never detach throughout the working temperature range of an ECD.

While both detectors function by producing gas phase negative ions, they do not generate similar responses to the substituted nitrobenzenes. The TID-N_2 is very selective to dinitro compounds, while the ECD is the more universal device. The ECD is the superior device for the absolute detection of the substituted nitrobenzenes. In certain situations, the TID-N_2 is superior to the ECD, but it is not a replacement for the ECD.

LITERATURE CITED

1. A. J. James and A. J. P. Martin, Analyst, 77, 915 (1952).

2. A. Karmen, Anal. Chem., 36, 1461 (1964).

3. A. Karmen and L. Guiffrida, Nature (London), 201, 1204 (1964).

4. L. Guiffrida, J. Ass. Offic. Agr. Chem., 47, 293 (1964).

5. G. R. Verga and F. Poy, J. Chromatogr., 116, 17 (1976).

6. V. V. Brazhnikov and E. B. Schmidel, J. Chromatogr., 122, 527 (1976).

7. B. Kolb, M. Auer and P. Pospisil, J. Chromatogr. Sci., 15, 53 (1977).

8. P. L. Patterson, J. Chromatogr., 167, 381 (1978).

9. P. L. Patterson and R. L. Howe, J. Chromatogr. Sci., 16, 275 (1978).

10. G. R. Verga, J. Chromatogr., 279, 657 (1983).

11. D. R. Coahran, Bull. Envir. Contam. Toxicol., 1, 141 (1966).

12. E. Cremer, H. Moesta and K. Hablik, Chem. Ing. Tech., 38, 580 (1966).

13. P. L. Patterson, Chromatographia, 16, 107 (1982).

14. B. Kolb and J. Bischoff, J. Chromatogr. Sci., 12, 625 (1974).

15. Roy Greenhalgh, J. Chromatogr. Sci., 16, 9 (1978).

16. C. H. Burgett, D. H. Smith and H. B. Bente, J. Chromatogr., 134, 57 (1977).

17. P. L. Patterson, U.S. Patent 4,524,047. (1985).

18. P. L. Patterson, U. S. Patent 4,203,726. (1980).

19. B. J. Erlich, Ind. Res. Develop., 107, Apr, (1980).

20. I. B. Rubin and C. K. Bayne, Anal. Chem., 51, 541 (1979).

21. M. Thewlis (Editor), Encyclopaedic Dictionary of Physics, Vol. 7, Pergamon Press, New York, 1962, p. 252.

22. V. V. Brazhnikov, M. V. Gur'ev and K. I. Sakodynsky, Chromatogr. Rev., 12, 1 (1970).

23. D. J. David, Gas Chromatographic Detectors, Wiley, New York, 1974, Ch. 5.

24. J. Sevcik, Chromatographia 6, 139 (1973).

25. W. C. Michaels (Editor), The International Dictionary of Physics and Electronics, Van Nostrand, Princeton, New Jersey, 2nd ed., 1961.

26. P. L. Patterson, R. A. Gatten and C. Ontiveros, J. Chromatogr. Sci., 20, 97 (1982).

27. P. L. Patterson, J. Chromatogr. Sci., 24, 466 (1986).

28. P. L. Patterson, J. Chromatogr. Sci., 24, 41 (1986).

29. C. M. White, A. Robbat and M. H. Randall, Anal. Chem., 56, 232 (1984).

30. C. S. Jones and E. P. Grimsrud, J. Chromatogr., 387, 171 (1987).

31. E. Herbst, T. A. Patterson and W. C. Lineberger, J. Chem. Phys., 61, 1300 (1974).

32. E. P. Grimsrud, G. Caldwell, S. Chowdhury and P. Kabarle, J. Am. Chem. Soc., 107, 4627 (1985).

33. J. E. Lovelock, Institute Petroleum, Gas Chromatography Discussion Group, Oxford, England, May, 1957.

34. E. S. Goodwin, R. Goulden and J. G. Reynolds, Analyst, 86 (1961) 697.

35. J. E. Lovelock, Anal. Chem., 35, 474 (1963).

36. W. E. Wentworth, E. Chen and J. E. Lovelock, J. Phys. Chem., 70, 445 (1966).

37. W. E. Wentworth and E. J. Chen, J. Gas Chromatogr., 5, 170 (1967).

38. P. G. Simmonds, D. C. Fennimore, B. C. Pettit, J. E. Lovelock and A. Zlatkis, Anal. Chem., 39, 1428 (1967).

39. R. J. Maggs, P. L. Johnes, A. J. Davies and J. E. Lovelock, Anal. Chem., 43, 1966 (1971).

40. P. L. Patterson, J. Chromatogr., 134, 25 (1977).

41. R. S. Becker and W. E. Wentworth, J. Am. Chem. Soc., 84, 2210 (1963).

42. W. E. Wentworth and R. S. Becker, J. Am. Chem. Soc., 84, 4263 (1962).

43. W. E. Wentworth and E. C. M. Chen, in A. Zlatkis and C. F. Poole (Editors), Electron Capture Theory and Practice in Chromatography, Elsevier Scientific Publishing, New York, 1981, Ch. 3.

44. R. S. Becker and E. C. M. Chen, J. Chem. Phys., 45, 2403 (1966).

45. E. P. Grimsrud and S. W. Warden, Anal. Chem., 52, 1842 (1980).

46. E. P. Grimsrud, Anal. Chem., 50, 382 (1978).

47. E. P. Grimsrud, S. Chowdhury and P. Kebarle, Int. J. of Mass Spec. and Ion Proc., 68, 57 (1986).

48. K. Levson and H. Schwarz, Agnew. Chem. Int. Ed. Engl., 15, 509 (1976).

49. F. R. McDonald and U. Christian, Am. Lab., 97, Nov., (1976).

50. T. Fujii and H. Arimoto, J. Chromatogr., 355, 375 (1986).

51. J. A. Lubkowitz, J. L. Glajch, B. P. Semonian and L. B. Rogers, J. Chromatogr., 133, 37 (1977).

52. F. L. Bayer, J. Chromatogr. Sci., 15, 581 (1977).

53. D. F. McMillen and D. M. Golden, Annu. Rev. Phys. Chem., 33, 493 (1982).

54. Handbook of Chemistry and Physics, CRC Press, Boca Raton, Florida, 62nd edition, 1981, p. E-2.

55. W. Lindinger and D. L. Albritton, J. Chem. Phys., 62, 3517 (1975).

56. N. I. Shteinboc, The Application of Radioactive Radiation in Measurement Techniques, Moscow, USSR, 1960, p. 24.

57. D. Bombick, J. D. Pinkston and J. Allison, Anal. Chem., 56, 396 (1984).

58. J. J. Sullivan and C. A. Burgett, Chromatographia, 8, 176 (1975).

59. J. E. Lovelock and A. J. Watson, J. Chromatogr., 158, 123 (1978).

60. E. P. Grimsrud and W. B. Knighton, Anal. Chem., 54 565 (1982).

61. W. B. Knighton and E. P. Grimsrud, Anal. Chem., 55, 713 (1983).

62. L. G. Christophorou, Adv. Electron. Electron Phys., 46, 55 (1978).

63. G. G. Guilbault and C. Herrin, Anal. Chem. Acta, 36, 255 (1966).

64. F. W. Karasek and D. M. Kane, Anal. Chem., 45, 576 (1973).

65. E. P. Grimsrud, S. Chowdhury and P. Kebarle, J. Chem. Phys., 83, 3983 (1985).

66. F. Bruner, in A. Zlatkis and C. F. Poole (Editors), Electron Capture Theory and Practice in Chromatography, Elsevier Scientific Publishing, New York, 1981, Ch. 11.

67. J. E. Lovelock, Nature (London), 230, 379 (1971).

68. P. G. Simmonds, in A. Zlatkis and C. F. Poole (Editors), Electron Capture Theory and Practice in Chromatography, Elsevier Scientific Publishing, New York, 1981, Ch. 11.

69. A. Zlatkis and C. F. Poole (Editors), Electron Capture Theory and Practice in Chromatography, New York, 1981, p. XI.

70. J. Vessman, in A. Zlatkis and C. F. Poole (Editors), Electron Capture Theory and Practice in Chromatography. Elsevier Scientific Publishing, New York, 1981, Ch. 13.

71. H. Shimamori and H. Hott, J. Chem. Phys., 85, 4480 (1986).

72. E. W. McDaniel and E. A. Mason, The Mobility and Diffusion of Ions in Gases, Wiley, New York, 1973, p. 146.

73. E. Alge, N. G. Adams and D. Smith, J. Phys., 17, 3827 (1984).

MONTANA STATE UNIVERSITY LIBRARIES
3 1762 10113470 6